

# Brainstem circuits involved in skilled forelimb movements

**Inauguraldissertation**

zur

Erlangung der Würde eines Doktors der Philosophie

vorgelegt der

Philosophisch-Naturwissenschaftlichen Fakultät

der Universität Basel von

**Riccardo Schina**

Von Torino, Italien

2021

Original document stored on the publication server of the University of Basel

[edoc.unibas.ch](https://edoc.unibas.ch)



This work is licensed under a [Creative Commons Attribution 4.0 International License](https://creativecommons.org/licenses/by/4.0/).

Genehmigt von der Philosophisch-Naturwissenschaftlichen Facultät

Auf Antrag von

Faculty representative &

Thesis advisor: Prof. Dr. Silvia Arber

Co-Referee: Prof. Dr. Pico Caroni

Basel, 17.11.2020

Dekan: Prof. Dr. Martin Spiess

## Table of contents

Summary.....	5
1. The brainstem .....	7
2. Skilled forelimb movements.....	11
3. Brainstem centres controlling skilled movements .....	14
3.1 Reaching and Grasping .....	14
3.2 Grooming.....	17
3.3 Orofacial behaviors .....	21
4. Techniques for accessing the brainstem .....	24
4.1 Anatomical tracing and viral vectors.....	24
4.2 Single Unit Recordings .....	28
4.3 Fiber Photometry and calcium imaging .....	30
4.4 Optogenetics.....	33
4.5 Chemogenetics.....	36
4.6 Behavioral tracking and deep neural networks.....	39
Aim.....	43
5. A functional map for diverse forelimb actions within brainstem circuitry .....	45
5.1 Summary .....	46
5.2 Introduction .....	47
5.3 Results.....	48
LatRM neurons tuned to forelimb actions.....	48
Skilled forelimb behaviors require latRM .....	55
Projection targets divide latRM neurons .....	62
Functional tuning in latRM populations.....	68
LatRM neurons elicit forelimb behaviors.....	72
5.4 Discussion .....	78
5.5 Methods.....	80
5.6 Acknowledgements.....	103
5.7 Author Contributions .....	104
5.8 Author Information .....	104
6. Conclusions.....	105
6.1 Open questions and challenges.....	105
6.1 Skilled forelimb movements: the brainstem and beyond .....	106
6.2 Skilled forelimb movements and other motor behaviors .....	110
7. Acknowledgments .....	113
8. References.....	115



# Summary

Movement is the main output of the nervous system as well as the fundamental form of interaction animals have with their environment. Due to its function and scope, movement has to be characterized by both stability and flexibility. Such apparently conflicting attributes are reflected in the complex organization of the motor system, composed of a vast network of widely distributed circuits interacting with each other to generate an appropriate motor output. Different neuronal structures, located throughout the brain, are responsible for producing a broad spectrum of actions, ranging from simple locomotion to complex goal directed movements such as reaching for food or playing a musical instrument.

The brainstem is one of such structures, holding considerable importance in the generation of the motor output, but also largely unexplored, due to its less-than-accessible anatomic location, functional intricacies and the lack of appropriate techniques to investigate its complexity. Despite recent advances, a deeper understanding of the role of brainstem neuronal circuits in skilled movements is still missing.

In this dissertation, we investigated the involvement of the lateral rostral medulla (LatRM) in the construction of skilled forelimb behaviors. The focus of my work was centered on elucidating the anatomical and functional relationships between LatRM and the caudal brainstem, and specifically on the interactions with the medullary reticular formation, considering both its ventral (MdV) and dorsal subdivisions (MdD).

*In vivo* electrophysiology revealed that different sets of LatRM neurons are specifically tuned to forelimb-related actions such as reaching or handling but not to locomotion, a movement employing the same forelimb muscles but in a different fashion. Moreover, perturbation of LatRM neurons activity by means of DREADD revealed their necessity for the correct execution of skilled forelimb movements. Using combinatorial viral strategies, we therefore investigated the logic of intra-brainstem connectivity of LatRM neurons. By employing anterograde, synaptic-targeting viral vectors we revealed that LatRM has four main synaptic partners, namely the cervical spinal cord, the medullary reticular formation (MdV and MdD) and its contralateral twin nucleus.

We then took advantage of tracing viruses with retrograde potential to find out which cells in LatRM give rise to such projections and whether they might be segregated in distinct anatomical and functional groups. We found that neurons in the LatRM projecting

to the spinal cord occupy ventral positions, located just dorsal to the facial nucleus, while cells with direct connections to the MdD reside in a much more dorsal location. Moreover, cells projecting to the MdV appear to be more widely distributed along the dorsoventral axis of LatRM, nevertheless overlapping in part with the spinally-projecting population. Neurons connected to the contralateral LatRM are instead broadly distributed in a wide area centered in a rather medial location. Overall, we uncovered that cells projecting to these four main targets belong to largely non-overlapping populations of neurons, occupying adjacent and partially intermingled territories within LatRM.

Next, based on the knowledge that LatRM neurons are tuned to different skilled forelimb actions we hypothesized that neurons of the LatRM projecting to different targets might encode distinct phases of a skilled movement. To tackle this question, we employed fiber photometry coupled with an intersectional viral strategy, allowing us to express a calcium indicator either in spinally- or MdD-projecting neurons within LatRM and monitor their activity during a pellet reaching task. We found that neurons contacting the spinal cord are positively modulated during the reaching but not other phases of the task, while MdD-projecting neurons are silent during reaching but strongly upregulate their activity during the subsequent handling and eating phase.

This insight prompted us to test what behavior could be elicited by artificially activating LatRM neurons based on their projection specificity. We speculated that different projections might have the potential of driving unique actions or even separate aspects of the same movement. Optogenetic stimulation of spinally-projecting neurons produced simple reaching without any further involvement of the extremities, while MdV neurons drove a form of reaching which extended into finger grasping or tapping. Conversely, activation of LatRM neurons projecting to the MdD caused the extension of reaching into complex movements such as hand-to-mouth or grooming. In contrast, activation of contralateral-projecting neurons did not produce any apparent movement.

In summary, we reveal the existence of anatomically segregated subpopulations of neurons in the lower brainstem which encode different aspects of skilled forelimb movements. Moreover, we show that LatRM neurons are necessary for the correct execution of skilled motor programs and their activation produces complex coordinated actions. All this evidence suggests that LatRM may be a key orchestrator for skilled movements by functioning as integration center for upstream signals as well as coordinator by selecting the appropriate effectors in the lower medulla and the spinal cord.

# 1. The brainstem

From a purely anatomical standpoint, the brainstem is defined as the most posterior portion of the brain, located between the diencephalon and the spinal cord. Classically, it comprises three different sections: the Midbrain, Pons and Medulla oblongata.

The brainstem is the most ancient conserved structure in the brain, present in all vertebrates, from amphibians to mammals (Northcutt, 2002), and has been implicated in a number of autonomic functions such as breathing (Del Negro, Funk and Feldman, 2018), sleep (Weber and Dan, 2016), arousal and regulation of blood pressure (Ghali, 2017).

Importantly, the brainstem receives strong projections from cortical and subcortical areas (Figure 1.1) and innervates the spinal cord thanks to descending tracts that target directly motor neurons or interneurons (Kuypers and Brinkman, 1970, 1981; Kennedy, 1990; Palmer and Ashby, 1992; de Noordhout *et al.*, 1999; K uchler *et al.*, 2002; Isa *et al.*, 2007; Lemon, 2008; Esposito, Capelli and Arber, 2014).

For this reason, in the context of motor control, it was often thought of as a mere relay station for commands originating elsewhere. However, thanks to stimulation and lesion experiments, it was soon discovered that the brainstem has a much more active role in motor control than previously thought.

Transections of the neuraxis in the bullfrog (*Rana catesbeiana*) which leave the brainstem intact but eliminate all forebrain input (Roh, Cheung and Bizzi, 2011), were shown to have very limited effect on behavior and overall wellbeing: frogs lacking a forebrain could indeed still jump and swim normally. On the contrary, more caudal transections which maintain just the medulla had more dramatic effects (Roh, Cheung

and Bizzi, 2011), pointing in the direction of both sufficiency and necessity of the brainstem for generation of basic behavioral modules.

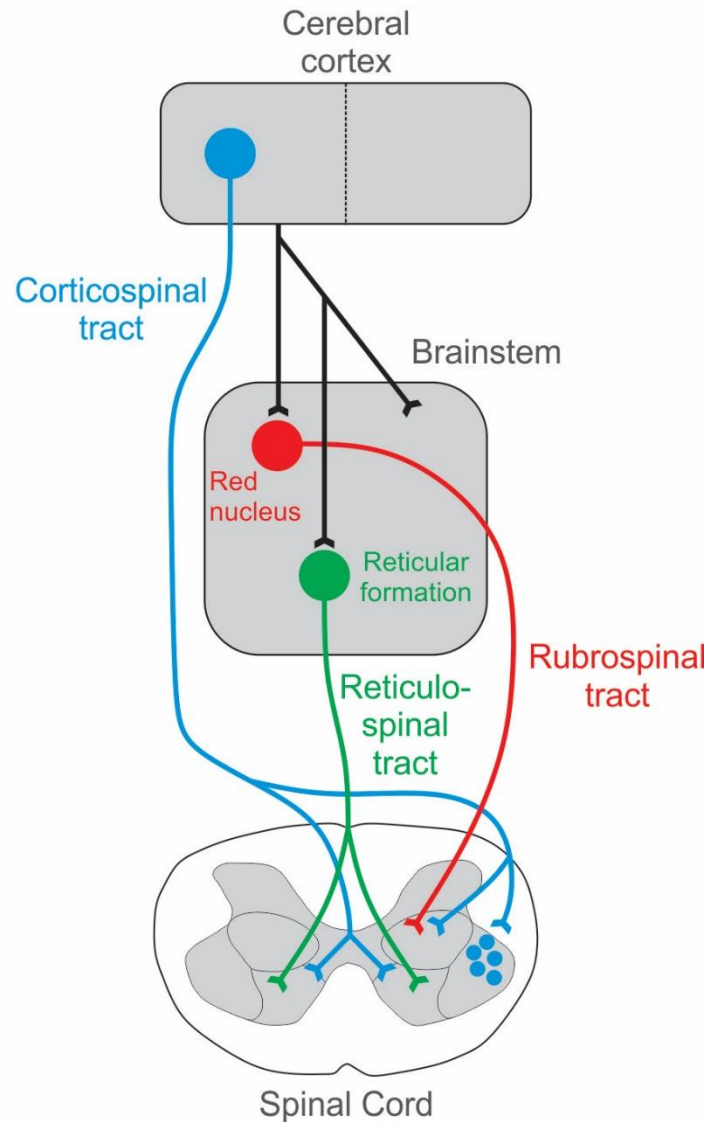


**Figure 1.1 Scheme of the classical view of descending motor pathways.** This scheme shows the distribution of various descending motor pathways, including the corticospinal- (blue), the rubrospinal- (red) and reticulospinal tract (green). Corticospinal fibers terminate mostly contralaterally on motor neurons, as well as in the ventromedial and dorsolateral intermediate zone. Note how the brainstem receive massive cortical innervation (black). Adapted from (Lemon, 2008)

In addition, cats deprived of the cerebral cortex in early postnatal stages appear normal in many respects, including basic vegetative functions, grooming and even sexual behavior (Bjursten, Norrsell and Norrsell, 1976). Rats with lesions producing complete transections at the level of the pons also appeared similar to controls in their demeanor including grooming (Berridge, 1989).

Electrical stimulation of several areas in the brainstem proved the existence of multiple sites from which movement can be produced (Ross and Sinnamon, 1984). Of those, the most studied and noteworthy is the Mesencephalic Locomotor Region (MLR). Unilateral stimulation of MLR is sufficient to elicit sustained quadrupedal locomotion (Garcia-Rill and Skinner, 1987; Takakusaki *et al.*, 2016) although which exact population and specific site is responsible for it is highly debated. In recent years, the uncertainty surrounding locomotion-inducing areas has been addressed with more advanced techniques such as viral tracing and optogenetics in mice, exposing an intricate network composed of different populations with unique effects on behavior depending on neurotransmitter identity and location within the MLR (Roseberry *et al.*, 2016; Caggiano *et al.*, 2018).

However, the MLR is not the only subcortical area involved in the control of locomotion, as there has been evidence that at least one control center exists in the lower brainstem. This was proved by experiments in which cooling the caudal brainstem produced a weakening of locomotion elicited by MLR stimulation (Shefchyk, Jell and Jordan, 1984; Orlovsky G.N., Deliagina T.G. and Grillner S., 1999).

Recent work has identified specific subpopulations in the medial medulla with opposite effects on the regulation of high speed locomotion (Capelli *et al.*, 2017). Here, excitatory neurons in the lateral paragigantocellular nucleus (LPGi) were shown to elicit high speed quadrupedal locomotion, while inhibitory neurons halted it without loss of muscle tone.

All these examples clearly point to a profound involvement of the brainstem in different aspects of motor behavior and to the importance of uncovering the connectivity and functions of its multiple intermingled neuronal pools.

## 2. Skilled forelimb movements

Besides being the main output of the nervous system, movement is essential for the survival of all animal species. Among the vast range of motor programs that can be generated, skilled forelimb movements are by far the most impressive and complex.

Skilled forelimb movements depend on the ability of the nervous system to activate a considerable number of muscles in specific definite patterns, usually aimed at reaching and manipulating food or other objects. Such motor programs need to be at the same time robust to allow for a successful execution and flexible enough to permit online adjustments and appropriate variations depending on the task.

Primates were for a long time thought to be the taxon in which skilled forelimb movements first appeared and developed into fairly complex sequences of actions (McNeilage, P.F, 1990), leading to the use of natural elements as rudimentary tools.

For example, orangutans were reported using tree branches to drive off insects (Biruté M. F. Galdikas, 1989) or obtain food (van Schaik, Fox and Sitompul, 1996); the same is true for the Chimpanzee (Nishida and Hiraiwa, 1982) and Capuchin monkeys (Falótico, Siqueira and Ottoni, 2017). In addition, various primate species have also shown the ability to prepare tools in advance for future use (Bräuer and Call, 2015).

It is in humans, however, that skilled forelimb movements assume their grandest expression, given that we can ascribe the rise of civilization and its greatest achievements, whether scientific, artistic and architectural to the mastering of this ability.

In later years, spontaneous tool usage has been reported in several other vertebrate species ranging from birds (Hunt, 1996; Fayet, Hansen and Biro, 2020), cetaceans (Mann *et al.*, 2008), otters (Hall and Schaller, 1964) and even rodents such as mole-rats

(*Heterocephalus glaber*) (Shuster and Sherman, 1998) and common rats (*Rattus Norvegicus*) (Nagano and Aoyama, 2017)

However, despite tool usage being the epitome of skilled forelimb movements, it is by no means the only one. The ability to reach for objects with hands and forepaws, to grasp them and manipulate them is a common and integral part of the behavioral repertoire of several tetrapod taxa. Skilled forelimb movements are thought to be an ancestral conserved feature that arose quite early in tetrapod evolution (Iwaniuk and Whishaw, 2000) and that feeding requirements shaped its refinement or, in some cases, its loss (Figure 2.1).

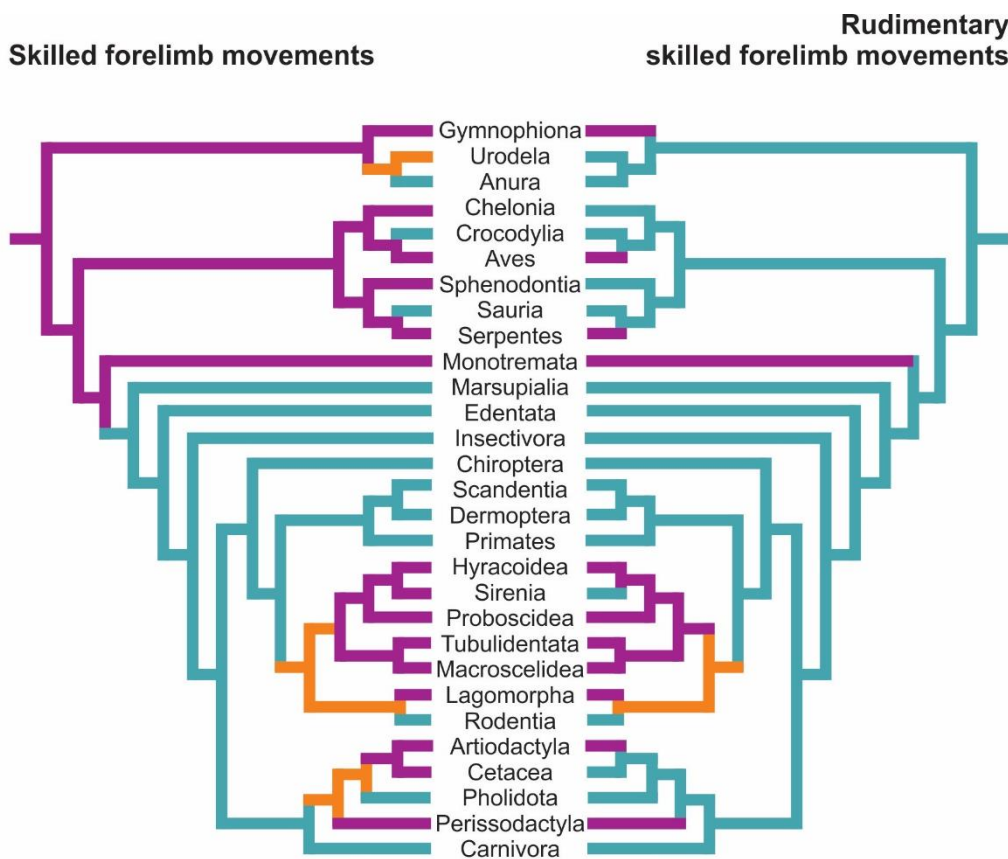


**Figure 2.1** The presence of skilled forelimb movements mapped onto the phylogeny of the major tetrapod taxa using maximum parsimony. Purple branches indicate absence, cyan indicates presence and the orange branches are equivocal. Note how the presence of skilled movements can be traced to very early evolutionary history in the tetrapod evolutionary tree. Adapted from (Iwaniuk and Whishaw, 2000).

The involvement of the brainstem in the generation and patterning of skilled movements has often been undervalued. The overshadowing idea that circuits responsible for reaching and grasping are located in the cerebral cortex and are directly relayed to the spinal cord by way of the corticospinal tract (CST) is an old one. Such idea stemmed from the observation that both the depth of penetration in the spinal cord and the length of CST tract fibers in different species are paralleled by a corresponding increase in dexterity (Bernhard, 1954; Heffner, 1983; Lemon *et al.*, 2004; Lemon, 2008).

However, although the importance of the corticospinal tract in humans and primates cannot be denied, it is important to keep in mind that many species with a limited CST, or even devoid of such feature show the inclusion of skilled forelimb movements in their behavioral repertoire (Iwaniuk and Whishaw, 2000). One key example of this is certainly the frog, which does not possess a cerebral cortex, yet it is known to use forelimbs to transport and manipulate prey during feeding. The use of forelimbs in a skilled way is a common characteristic of many *Anuran* taxa, and the arboreal frog subgroup has been shown to use grasping to capture prey (Gray, O'Reilly and Nishikawa, 1997).

The involvement of brainstem circuits in skilled movements will now be discussed more thoroughly in individual chapters dedicated to specific skilled movements of interest to this dissertation.

## 3. Brainstem centres controlling skilled movements

### 3.1 Reaching and Grasping

Many animal species utilize forelimbs and hands to reach, grasp and manipulate food for consumption. As we have seen in the previous chapter, food is not the only object of skilled movements but it is certainly one of great importance. Skilled reaching describes a movement in which a forelimb is first translated or transported towards an object, then by means of a hand with digits the object is grasped and finally transported towards the body for manipulation or the oral cavity for consumption.

Studying reaching in model animals is of great relevance, as many reports exist demonstrating the similarities of skilled reaching in rodents, monkeys and humans (Sacrey, Alaverdashvili and Whishaw, 2009), probably stemming from the similar morphology of the skeletal and muscular systems in these taxa. Conventionally, it is believed that reaching and grasping evolved from simpler actions as digging (Brácha, Zhuravin and Bureš, 1990), balancing on tree branches (Cartmill, 1974) or eating (Sustaita *et al.*, 2013).

In what are now considered to be fundamental classic experiments, Lawrence & Kuypers performed lesion experiments on Rhesus monkeys to clarify the involvement of different supraspinal descending pathways on different components of motor performance.

In a first series of experiments (Lawrence and Kuypers, 1968a), it was investigated the effect of a bilateral interruption of the pyramidal tract at the level of the caudal pons. Perhaps surprisingly, within days of the surgery monkey were able to run, climb and grip cage bars, even if they lacked the fluency of control individuals. Interestingly, although

clearly able to mechanically grasp, these monkeys were completely incapable of retrieving food with their hands and fingers. After a period of recovery however, reaching and grasping were somewhat restored, showing that subcortical structures, including the brainstem, could take over such functions to a certain extent.

In a second series of experiments (Lawrence and Kuypers, 1968b), monkeys that recovered from bilateral pyramidectomy were subjected to interruption of the descending brainstem pathways. Lesioning the ventromedial pathway produced severe impairments in posture, balance and locomotion but not to skilled reaching and grasping, while interrupting the lateral (rubrospinal) pathway created a total loss of control over the extremities and impossibility to perform dexterous movements such as reach and grasp.

Similar experiments have been performed in other species, such as rats (Whishaw, Gorny and Sarna, 1998). Here, lesions of either the pyramidal or the rubrospinal tract were shown to reduce success in a reaching/grasping assay. However, in both cases the animals were able to perform the task, and even a combined lesion of the two pathways did not abolish it completely. Moreover, after a stroke-like lesion of the motor cortex, rats were still able to reach and grasp a food pellet, although importantly, they lacked individual finger mobility (Alaverdashvili and Whishaw, 2008).

Such lesion experiments, together with mounting electrophysiological evidence (Schepens and Drew, 2004; Soteropoulos, Williams and Baker, 2012; Baker *et al.*, 2015), points to a strong involvement of the brainstem in reaching and grasping, an engagement which becomes more and more relevant once upstream forelimb centres fall out of the picture, possibly due to subcortical structures such as the red nucleus taking over and/or relaying of cortical signals to effectors in the spinal cord through alternative pathways (e.g. Rubrospinal tract (Mosberger *et al.*, 2017)).

Brainstem neurons project massively to the spinal cord, and lesions to the descending dorsolateral tract produces deficits in reaching and grasping in rats (Morris *et al.*, 2011). A study in mice showed that neuronal populations in specific brainstem nuclei form preferential connections with motor neurons innervating forelimb or hindlimb muscles (Figure 3.1) (Esposito, Capelli and Arber, 2014).

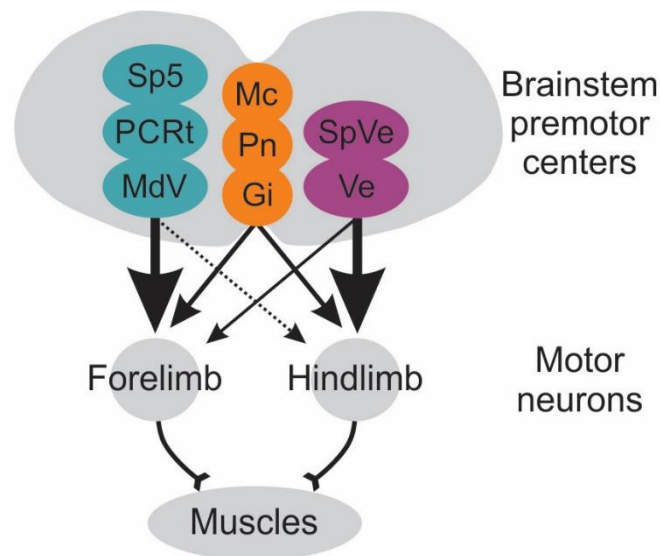


**Figure 3.1 Summary diagram of premotor centers in the brainstem with preferential connections to forelimb or hindlimb motor neurons.** Connections were uncovered using injections of trans-synaptic monosynaptic rabies virus in forelimb or hindlimb muscles. Note how some nuclei (i.e. MdV, PCRt) have preferential connections to one or the other limb, while others (i.e. Gi) project to both forelimbs and hindlimbs indiscriminately. Adapted from (Esposito, Capelli and Arber, 2014)

One such nucleus, the *medullary reticular formation, ventral part* (MdV) preferentially connects to forelimb-driving motor neurons and was shown to be essential for the correct performance of grasping within a forelimb reaching and pellet grasping task. Another brainstem nucleus preferentially connected to forelimb motor neurons is the *parvicellular reticular nucleus* PCRt, which is the main object of this dissertation and its involvement in reaching and grasping will be discussed in greater detail in chapter 5.

Finally, recent evidence coming from careful kinematic analysis of reaching and grooming has shown that these two seemingly different movements actually share a high percentage of similarity in the way they are executed (Naghizadeh, Mohajerani and Whishaw, 2020). Not only the execution of reaching and grooming shares the same body parts, but both the structure phases and relative joint positions during motion are shared. This evidence suggests new ideas about how reaching evolved, hinting at a possible reciprocal influence between reaching and grooming, or even at the possibility that skilled movements altogether emerged from the supposed more ancient act of grooming.

The evolution of grooming and its neural substrates will be discussed in detail in the next chapter.

## **3.2 Grooming**

Grooming is an essential part of animal behavior, existing in a wide range of vertebrate species and most probably as ancient as the root of the vertebrate tree itself. The main aim of grooming is a hygienic one, consisting in self-cleaning one's fur or skin from dirt, insects and parasites. In addition, grooming can have an important social significance, especially in primates (Dunbar, Robin, 1991), where it's used for strengthening social bonds between members of a community.

Grooming is an extremely conserved feature in rodents as well (Kent C. Berridge, 1990) and it has been observed that laboratory rats spend as much as 40% of their wake time grooming (Bolles, 1960). To discover the nervous substrates of such a widespread behavior has long been a topic of great interest in behavioral neuroscience.

Over the years, it became evident that grooming behavior is highly stereotyped, and tends to remain unchanged even in animals facing extreme constraints such as neonatal

forelimb amputation (Fentress, 1973), suggesting strong central control. Such stereotypy is first of all manifested by the cephalocaudal progression of the grooming in adult rats: starting from the nose, it progresses through eyes and ears to the lower body parts finally ending in the anogenital region (Gail Richmond and Benjamin D. Sachs, 1980). The cephalocaudal progression of the single grooming bout is beautifully mirroring the gradual development of the movement in neonate rats, which begins with nose wipes on post-natal days 2-3 and is gradually extended to more caudal regions until completed with the anogenital and tail areas on days 18-20 (Gail Richmond and Benjamin D. Sachs, 1980).

Most grooming bouts are made up by a mixture of licking, scratches and strokes performed in a rather flexible way. It was found, however, that rats periodically execute a much more rigid sequence, composed by the same single movements as common grooming bouts but highly stereotyped in order and time (Berridge, Fentress and Parr, 1987).

In this particular sequence a set of simple motor actions are linked together in a highly conserved "syntactic chain". In the highest degree shown, up to 25 different actions can be combined to form a highly univocal "structured transition between face and body grooming" with a natural occurrence 13.000 times above chance level (Berridge, Fentress and Parr, 1987). Although the syntactic chain represents a minority of the total grooming it has been used as a reference for grooming studies thanks to its extraordinary degree of stereotypy.

Syntactic grooming has four phases which always occur in a stable order: phase 1 consists of rapid elliptical strokes over the nose and phase 2 is made up by asymmetrical strokes of increased amplitude. Phase 3 consists of large bilateral strokes around the face and ears and phase 4 consists of postural and head movements, followed by body licking directed to the flanks and lower body (Figure 3.2).

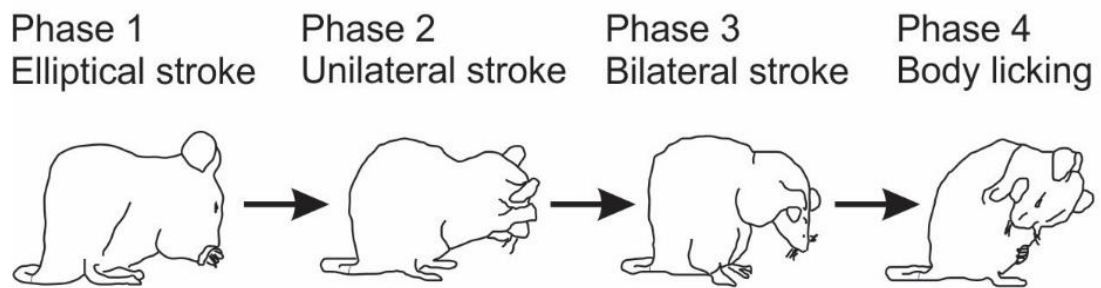


**Figure 3.2 The syntactic chain of grooming.** Mouse self-grooming has a complex structure that consists of repeated stereotyped movements known as syntactic chains, which proceed cephalocaudally from paw–head grooming to the rest of the body. Although chain grooming is noteworthy, note that the majority (approximately 90%) of self-grooming behaviour is represented by a more flexible, non-chain self-grooming behaviour. Adapted from (Kalueff *et al.*, 2016)

W.R. Hess was the first to elicit grooming-like movements with electrical stimulation of the cat diencephalon, showing that complex sequential behaviors could be generated by stimulation of definite areas of the brain. In the following years more reports have been published, extending Hess' findings in other species and areas of the brain (Berntson, 1973; Berntson, Jang and Ronca, 1988).

The search for the neural underpinnings of grooming made use of extremely interesting loss of function experiments that can be traced back at the study of JW Woods in the decerebrate rat (James W. Woods, 1964). In this study, rats were subjected to the removal of the whole forebrain with the exception of the hypothalamus and observed over several weeks. In accordance with previous studies in other species, the rats had become blind, anosmic and incapable of feeling touch, but surprisingly their overall motor capabilities quickly recovered. Strikingly, the author observed that just a few days after forebrain removal rats were again able to walk independently and most importantly perform grasping and self-grooming.

After the introduction of the syntactic chain concept (Berridge, Fentress and Parr, 1987), researchers had a useful reference to compare the effect of lesions to progressively caudal portions of the brain on grooming. In a series of seminal studies it was proven that damage to the striatal systems causes the syntactic chain to be initiated but frequently disrupted, due to incomplete sequences or to violations of the stereotypy (Berridge and Fentress, 1987). On the contrary, removal of the cerebral cortex had little or no effect on it, and that of cerebellum caused only temporary deficits (Berridge and Whishaw, 1992).

Moreover, looking to find out what is the minimal brain substrate necessary to generate the syntactic chain, three types of lesions were produced in rats: *Mesencephalic* (sparing Midbrain, pons, cerebellum and medulla), *Metencephalic* (sparing pons, cerebellum and medulla) and *Myelencephalic* (sparing the medulla only) (Berridge, 1989). Both Mesencephalic and Metencephalic rats were able to produce complete sequences linking up tens of actions organized in a syntactically correct order, although with much lower chain completion rate compared to controls. Myelencephalic rats never generated a complete sequence. However, it was possible for such animals to separately produce actions belonging to all four phases, even if the syntax was extremely irregular and fragmented (Berridge, 1989).

The results of this study are of utmost importance for the present dissertation, as they prove that the brainstem has in itself the capacity of generating a complex behavioral sequence such as the syntactic chain. Interestingly, the progressive degradation of the sequence happening with lesions of the striatum, and with consecutively more posterior lesions of the brainstem also suggests that no a single center is solely responsible for grooming, but rather it is a network of brain regions which concur to its generation contributing to its success in distinct ways.

### 3.3 Orofacial behaviors

The evolution of vertebrate species and their vital systems brought forward one important problem: how would different functions such as breathing, eating and a myriad other share the common space of the oropharyngeal space? This is an important question as already in rodents, breathing has to be coordinated with the most disparate behaviors: chewing, swallowing, whisking, sniffing and vocalizing. This is even more relevant in humans, where the airways are used for producing sounds associated to language generation and to usage of tools (e.g. musical instruments).

The cadence of breathing is controlled by neurons in the pre-Bötzinger complex, which generate the inspiration rhythm (Smith *et al.*, 1991; Tan *et al.*, 2008), as well as the Bötzinger complex and parafacial respiratory groups, all of which are located in the lower brainstem.

Another orofacial behavior, whisking, was also suggested to be regulated by brainstem centers, since it survives decortication (Semba and Komisaruk, 1984). Using sophisticated techniques, it was possible to show that the oscillatory phases of whisking and breathing are tightly locked to each other and that the rhythm of the whisking pattern generator, namely the intermediate reticular nucleus (IRt), is coordinated by the pre-Bötzinger complex (Moore *et al.*, 2013).

Orofacial motor programs extend much further than respiration and whisking. To bring one example forward, the act of eating is a complex sequence of muscle activations in which movements of the jaws, tongue, pharyngo–esophageal and of course respiration muscles have to be coordinated perfectly (Travers, DiNardo and Karimnamazi, 1997; Travers, DiNardo and Karimnamazi, 2000; Saito *et al.*, 2003).

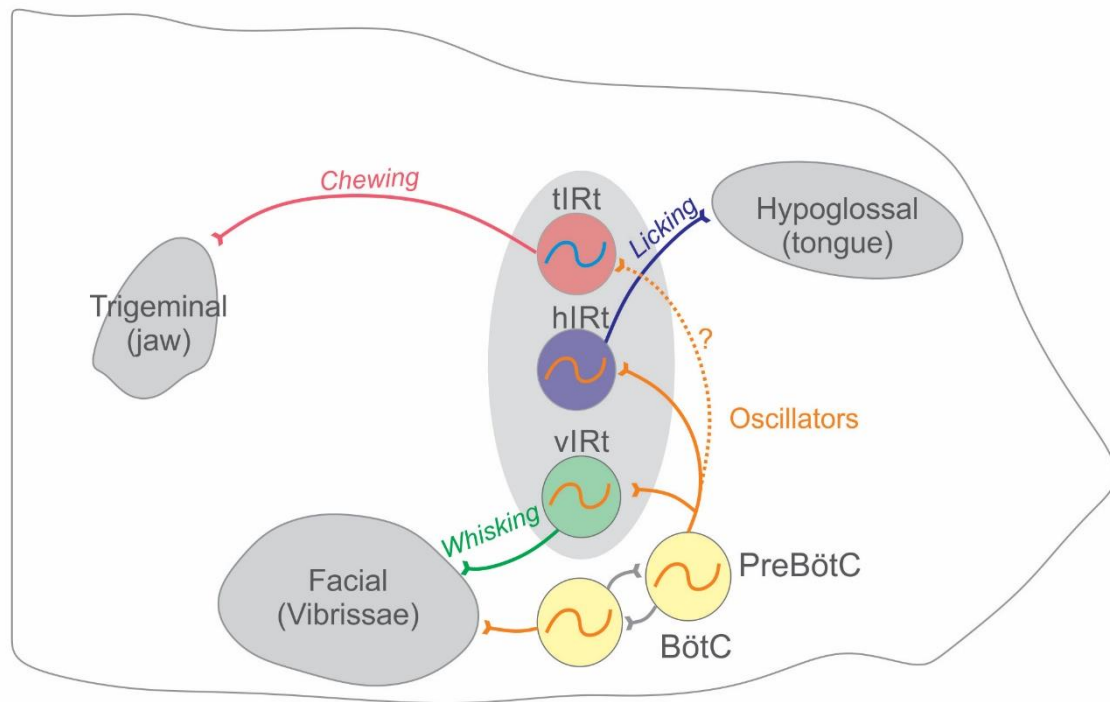


**Figure 3.3 Brainstem circuits controlling orofacial actions.** Sagittal view of the brainstem showing that shows the main cranial nerve nuclei controlling muscles involved in orofacial movements, as well as the putative neuronal oscillators that generate breathing rhythm (yellow), whisking (green), licking (blue) and chewing (pink). The oscillatory nature of a site is marked with a “~”. Abbreviations: vIRt, vibrissa IRt; hIRt, hypoglossal IRt; tIRt, trigeminal IRt; Adapted from (Moore *et al.*, 2013; Kleinfeld *et al.*, 2014a; Moore, Kleinfeld and Wang, 2014; McElvain *et al.*, 2018)

The muscles required to perform orofacial behavior are controlled by motor neurons situated in nuclei of the brainstem through cranial nerves. Several studies have revealed that premotor neurons giving input to such motor neurons are indeed located within the boundaries of the brainstem, and are often neighboring, if not intermingled with neurons controlling other orofacial behaviors, suggesting a complex interplay between them (Deschênes *et al.*, 2016; Kurnikova *et al.*, 2017; McElvain *et al.*, 2018; Kurnikova, Deschênes and Kleinfeld, 2019). Specific locations of the medial and lateral brainstem,

part of bigger areas labelled in the reference atlases as IRt and PCRt have been involved in multiple orofacial motor actions and are therefore considered possible hotspots for activity generation and coordination (Figure 3.3).

In this context, an open question of great importance remains about the neuronal underpinnings of the coordination between skilled forelimb movements and orofacial ones. Forelimb reaching and grasping have food retrieval and ingestion as their most prominent ethological purpose and during feeding behavior an exquisite concertation exists between the oral region and the rest of the body. It is therefore reasonable to assume that such coordination might have a reflection in the nervous system, and that the brainstem might be one of the regions of the brain in charge of it.

All in all, from this introductory chapters we have seen how the brainstem is not just a relay station for signals generated and regulated elsewhere, but a structure that can act as a command center as well as a coordinator of motor actions, perfectly integrated in the broader context of the motor systems. However, very little is known about the organization of such circuits, the identity of subpopulations and what is the involvement of the brainstem in building complex actions such as skilled movements.

## **4. Techniques for accessing the brainstem**

As I have described in the first part of this introduction, the brainstem is a complex structure, situated in one of the most inaccessible anatomical positions. Progress in its exploration and investigation by neuroscientists has been hindered by such constraints and it is only in the last decades that research in this part of the brain has been advancing at a faster pace. This is mostly due to technological breakthroughs that made it possible to access it and dissect it from multiple directions.

In the next chapters I will describe the main techniques that made this possible and how they contributed to new discoveries in the brainstem.

### **4.1 Anatomical tracing and viral vectors**

Anatomical tracing remains to this day one of the cornerstones of Neuroscience research.

For decades, before the advent of viral vectors, neuroscientists have used classical chemical methods to track neural connections. Until the development of the Horseradish Peroxidase (HRP) by Kristensson in 1971 (Kristensson and Olsson, 1971) most methods were based on lesioning the area of interest and detection of degenerate axons by means of complex stainings (Nauta and Gyax, 1951).

HRP was a revolutionary and extremely successful method due to its ease of use compared to predecessors, and many landmark anatomical discoveries can be ascribed to it. After application, usually by mechanical injection, this enzyme is passively internalized by neurons into endosomes and travels retrogradely towards the cell body where it gets degraded. This allowed extensive intra-brain connectivity tracing (Lavail

and Lavail, 1972; Mesulam M-M, 1982) which greatly advanced our knowledge of brain connectivity.

A second, landmark step for tracing was the introduction of the *Phaseolus vulgaris*-leucoagglutinin (PHA-L) (Gerfin and Sawchenko, 1985). Importantly, this tracer was transported anterogradely and its detection was based on immunohistochemistry, which permitted its combination with other antibodies and as a consequence the possibility of recognizing the identity and therefore the function of recipient neurons.

While HRP and PHA-L require more or less complex staining, inorganic fluorescent dyes provided a faster and easier way of visualizing connectivity. First described in 1979 (Bentivoglio *et al.*, 1979), the use of fluorescent tracers saw its golden age with the introduction of Fluoro-Gold (Schmued and Fallon, 1986), which gained fame due to its unique brightness, robustness and capacity of tracing extremely long connections (e.g. corticospinal neurons).

Ultimately, although chemical tracers are still used to some extent to this day, the biggest step forward in tracing technology was the introduction of viruses and the exploitation of their natural capacity of infecting neurons and travelling through the CNS (Nassi *et al.*, 2015; Lanciego and Wouterlood, 2020).

Initially, the *Herpes Simplex Virus* (HSV) was tested as an anatomical tracer with good results (Kristensson, Ghetti and Wiśniewski, 1974) and because of the virus capacity to cross synapses permitted for the first time to directly access second order neurons (Ugolini, Kuypers and Strick, 1989). Despite this obvious advantage, HSV had the caveat of traveling bidirectionally through neuronal circuits and presented clear health security issues due to its virulence towards humans.

For such reasons, and in particular its exquisite capacity of exclusively migrating retrogradely, the canine Rabies virus (RV) was tested (Ugolini, 1995) and rapidly adopted (Kelly and Strick, 2000). The wild-type rabies virus moves between neurons

through the synaptic junction (Iwasaki and Clark, 1975) in a time-dependent manner, so that its infectivity can be limited to connected neurons of the second-, third-, etc. order.

Because the only way to restrict the spreading of the RV is the termination of the experiment by euthanasia, results could be subject to errors and ambiguities. To tackle this problem the group of Edward Callaway developed mutant recombinant rabies viruses where the *Glycoprotein* gene was exchanged with eGFP (Ian R Wickersham *et al.*, 2007) Because such protein is not necessary for replication but only for trans-synaptic spreading, the virus will fill the infected neurons without spreading to presynaptic partners.

Supplying the Glycoprotein *in trans*, through another viral vector, produced a rabies virus that could spread to presynaptic neurons just one synapse away (Ian R. Wickersham *et al.*, 2007). However, because RV has evolved to spread centripetally from muscle fibers, it was necessary to optimize it so that it would infect any kind of starter cells, making it possible to trace from genetically defined populations. To this end, it was pseudotyped with EnvA, the envelope protein of the *subgroup A avian sarcoma and leukosis virus*. This permitted the infection of any cell expressing the cognate TVA viral receptor, found in birds but not in mammals. Therefore, the resulting RV, named SADΔG-EGFP(EnvA) could only infect starter cells supplied with TVA either genetically or by means of intersectional viral injections (Ian R. Wickersham *et al.*, 2007).

However, cytotoxicity hinders the capacity of RV to being used for long term studies since it produces changes to the physiology of infected neurons. A modified version of RV was developed that self-inactivates after infection, with no adverse effect on affected neurons (Ciabatti *et al.*, 2017).

Although the RV still holds a place of special interest, especially in tracing neuronal connectivity, Adeno-Associated Viruses (AAVs) are nowadays probably the most employed tool in Neuroscience. This stems from three reasons: first, their low toxicity

and low interference with normal cellular processes; second, the possibility of being used as conditional tools in combination with mouse transgenic lines expressing recombinases (e.g. *Cre* or *Flp*); third, the possibility of using them as delivery tools for functional proteins and not just as fluorescent tracers.

AAVs are single-stranded DNA viruses of the *Parvovirus* family which bind receptors on the cell surface, are internalized through endosomes and do not integrate in the host genome, but persist as stable episomes (Murlidharan, Samulski and Asokan, 2014). For this reason, AAVs are proving useful beyond neuroscience as the vector of choice for gene therapy due to their safety and low immune response (Li and Samulski, 2020).

Up to 12 different AAV serotypes have been identified, which present different tropism (Wu, Asokan and Samulski, 2006) and can be genetically engineered to achieve better delivery capacity to targets in the CNS and obtain enhanced transport capabilities (Sun and Schaffer, 2018). The capacity of AAVs to target specific genetically identified populations and induce the expression of functional proteins is of extreme interest in the context of the present dissertation, as it enables intersectional approaches making use of multiple viruses to access never-before studied subpopulations of neurons and makes long term studies of their neuronal activity possible for the first time.

Importantly, in the latest years a new AAV variant was developed (rAAV2-retro) which was engineered through in vivo directed evolution to allow for potent retrograde access to projection neurons with comparable efficiency to chemical retrograde tracers (Tervo *et al.*, 2016). This new variant can carry recombinases or functional proteins and as we show in the present work can be employed for anatomical and functional studies within the brainstem.

Viral vectors are one of the main drivers of new discoveries in the brainstem, since they allow access to specific sets of neurons not only based on their anatomic location, but also on their genetic identity or projection specificity. This is an extremely crucial

capability when studying intricate regions where intermingled subpopulations and subtypes of neurons exist, which are impossible to disentangle just by standard anatomic means.

## 4.2 Single Unit Recordings

Single unit recording is a method used for measuring the electrical activity of neurons employing microelectrodes. Of the many methods developed to record brain activity such as Electroencephalography (EEG) or functional magnetic resonance imaging (fMRI), single unit recordings is the only capable of reaching single neuron resolution.

The development of the first metal microelectrodes (Hubel, 1957) shifted the attention of neuroscientists from the brain as a whole to single neurons. This momentous trend has certainly delivered and brought us many of the classic notions we read in modern textbooks. The classic approach therefore consisted in making repeated measures of many neurons over different times, and inferring from such single behaviors theories about the activity of the whole network. However, to gain knowledge about the true dynamics of a neural network it is necessary to record the activity from several neurons at the same time.

Classic microelectrodes work by measuring the large transmembrane potentials produced by neurons during action potentials. If one or more neurons produce a spike in the vicinity of the electrode, they will all be recorded; because neurons of the same type produce identical action potentials, in order to isolate the signal of a single neuron the electrode must be placed in close proximity to its cell body, typically less than 20  $\mu\text{m}$  away. To record more than one single unit is therefore imperative to employ more than one electrode. Important steps in this direction were made with the development of the

stereotrode (McNaughton, O'Keefe and Barnes, 1983) and the optrode (O'Keefe and Recce, 1993; Mathew Wilson, Bruce McNaughton, 1995) which permitted the isolation of up to 15 neurons in the hippocampus (Wilson and McNaughton, 1993). The optrode has been the true workhorse of single unit recordings, thanks to their cheap and easy production, enhanced mechanical stability, allowing for long-term recordings in behaving animals, leading to breakthrough discoveries such as that of grid cells (Hafting *et al.*, 2005).

The development of silicon probes (Norlin *et al.*, 2002) has started a series of advancements that brought the number of parallel recording sites to double every 7 years over the last decades (Csicsvari *et al.*, 2003; Buzsáki, 2004; Stevenson and Kording, 2011). Silicon probes have several competitive advantages compared to tetrodes: they are standardized, have very low impedance, make for smaller implants both within the brain (producing less tissue damage and therefore less immune response) and outside (making the implant more bearable by the animal). In addition, the latest years saw the emergence of many innovative designs distributing recording electrodes either on multiple parallel shanks covering a larger planar area, or lined up on a longer shank, useful for example in the study of structures with columnar organization.

On one side, the greatest strength of single unit recordings is their high temporal resolution, essential to explore the subtleties of the motor system but on the other end, because it is only possible to record from tens of neurons at the same time, they lack the coverage needed to understand its complexity at the circuit level.

To begin tackle this issue, modern silicon probes have been developed that allow chronic recording from dozens of sites, producing a higher yield of units per session and per animal. Recently, these efforts resulted in a silicon-based probe capable of recording from almost a thousand electrodes spread over a 10mm shank (Jun *et al.*, 2017). Such probes have the advantage of allowing synchronous recording from a wide range of structures (e.g. cortical and subcortical) and therefore have enormous potential of

application in the forebrain, potentially creating a high temporal resolution alternative to optical techniques. However, its potential of use in the brainstem is limited by its ventral location and the presence of multiple small nuclei, composed of heterogeneous intermingled subpopulations, potentially having quite different properties and functions.

For all these reasons, understanding the intricate network of nuclei and neuronal populations of the motor brainstem necessitates the use of multiple techniques, often in combination, as we will see in chapter 5 of this dissertation.

### **4.3 Fiber Photometry and calcium imaging**

Every time a neuron fires, Calcium ions enter the pre-synaptic bouton, allowing the fusion of synaptic vesicles with the pre-synaptic membrane and the release of neurotransmitter in the synaptic cleft. Neuronal signaling therefore depends on local changes in  $Ca^{2+}$  concentration, and thanks to the development of calcium sensors or indicators (Cobbold and Rink, 1987) it has become possible to track the activity of neuronal populations in a semi-quantitative way (Yasuda *et al.*, 2004).

Fiber photometry or fluorometry was first proposed in the early nineties as a way to measure and study intracellular Calcium concentrations in the brain (Kudo *et al.*, 1992). The key innovation was the idea of simultaneously deliver and collect excitation and emission light through the same fiberoptic tether and optic fiber.

Since then, fiber photometry has evolved to accommodate new designs and calcium sensors, but at its core, a modern photometry system is still composed of the following four key components: a light source, usually a LED, capable of exciting the Calcium indicator, a detector (photoreceiver), sensitive to the sensor emission wavelength, a

fiberoptic tether, linking the system to the experimental subject, and a series of filters and dichroic mirrors (Figure 4.1).

As with photometry systems, Calcium indicators have also continued evolving steadily. A cornerstone of this evolution has been the invention of Genetically Encoded Calcium Indicators (GECIs) of which GCaMPs are the most prominent members.

Originally, traditional synthetic small molecule dyes had the advantage of being quite sensitive and having rapid kinetics, but such advantages came at a price: chemical calcium indicators involve invasive delivery methods, they are almost impossible to target at a specific population or cellular compartment, and most importantly, they are not feasible for chronic studies in vivo as they are progressively cleared. On the other hand, the first GCaMPs were not invasive and easily targeted to cell types or sub-cellular compartments but had slow kinetics and very limited sensitivity.

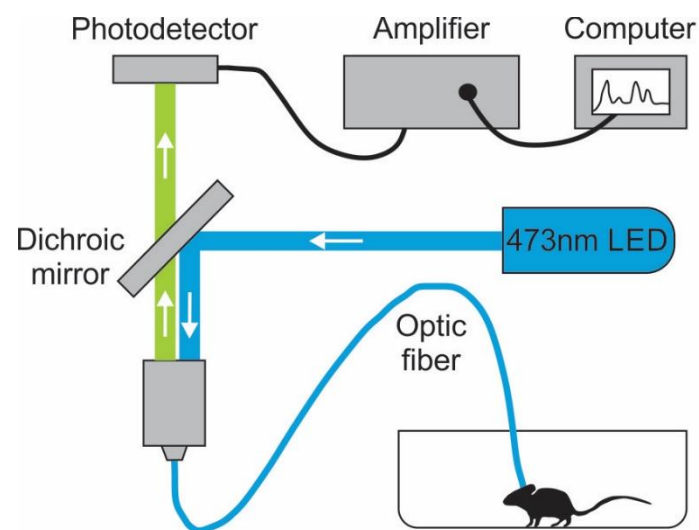


**Figure 4.1 Scheme of a fiber photometry experiment.** Shown are the main components of a fiber photometry apparatus, highlighting the simplicity of this technique and the possibility of easily adapting it to investigations in the behaving animal. Adapted from (Gunaydin *et al.*, 2014).

The evolution of GCaMPs is a perfect example of what modern techniques such as targeted mutagenesis and high throughput screening can achieve. The first GCaMP (Nakai, Ohkura and Imoto, 2001) was engineered linking the c-terminus of the eGFP molecule to Calmodulin CaM) and the n-terminus to the M13 fragment of myosin light chain kinase (MLCK), a target of CaM. In presence of  $\text{Ca}^{2+}$ , this would bind CaM, which would in turn connect to the MLCK fragment, causing a conformational change ultimately resulting in increased fluorescence by the eGFP molecule. The first GCaMP, now known as GCaMP1, had several issues, mostly due to instability of fluorescence above 30°C.

This molecule was later subjected to a process of random mutagenesis and some mutations were found to improve brightness. Moreover, the addition of a N-terminal 35-residue polyHis tail made it stable at body temperatures: GCaMP2 was born (Tallini *et al.*, 2006).

Through several rounds of targeted, structure-guided mutagenesis, scientists developed GCaMP3 (Tian *et al.*, 2009) which led to important studies on the activity of large populations in behaving mice (Dombeck *et al.*, 2010; O'Connor *et al.*, 2010). Following such breakthroughs, recent years have seen newer and better versions of GCaMP, each building up on the strengths of its predecessor and resolving its weaknesses, steadily reaching for faster kinetics and brighter emissions: GCaMP5 (Akerboom *et al.*, 2012), GCaMP6 (Chen *et al.*, 2013) and GCaMP7 (Dana *et al.*, 2019). The latest calcium indicators have also been created in several versions, each optimized for the kinetic requirements of a diverse range of applications, be it fiber photometry, GRIN lens or miniscope imaging.

Thanks to the improved GECIs, such a GCaMP6s and GCaMP7s, fiber photometry has reached new levels of precision and sensitivity, moving from sampling one brain region at any given time to multiple sites in parallel (Q. Guo *et al.*, 2015; Kim *et al.*, 2016), and

ultimately to arrays of optic fibers capable of surveying the activity of up to 48 brain regions (Sych *et al.*, 2019).

The clear advantage of fiber photometry stands on two properties: first, thanks to AAV vectors and mouse genetics, the calcium indicators can be delivered to the brain area and neuronal population of choice; second, it can potentially survey the overall average activity of a whole brain region, amounting to hundreds of neurons at the same time. Contrary to single unit recordings however, there is no information on single neurons and the temporal resolution is much lower. These two techniques, as we will see in chapter 5 can complement each other in a constructive way, each building on the strength of the other.

Fiber photometry is extremely useful in the context of brainstem studies, as it allows technically uncomplicated, direct access to the activity patterns of neuronal populations that are currently nearly impossible to survey with alternative calcium imaging techniques such as two-photon microscopy. The robustness of the technique and the stability of the implants means that it is possible to achieve high-quality, low-noise recordings of neural activity even from areas, such as the lower medulla, which are extremely unsteady due to respiratory motions, making it an invaluable tool for brainstem research.

## **4.4 Optogenetics**

Optogenetics is arguably the technique that has changed modern Neuroscience research more than any other. It solved the double problem of reliably controlling the activity of specific population of neurons without affecting others, and doing so with very fine temporal resolution. Being able to activate or disable certain neurons at the millisecond level is of paramount importance, especially in the field of motor control,

where sequences of muscle contractions happen at a rapid pace and tool matching such fast kinetics are necessary and decisive steps forward in comparison to pharmacological treatments.

At the same time, being capable of controlling specific, genetically identified sets of neurons is a key advantage when compared with previously used methodologies, such as electrical stimulation.

The history of how optogenetics came to be is a curious one, stemming from studies in Photochemistry. In 1971 a Rhodopsin-like protein was found for the first time outside of the retina of animals in *Halobacterium Halobium* (Oesterhelt and Stoeckenius, 1971). This *Bacteriorhodopsin* was found to act like a photo-activable ion channel. Soon, another of such proteins was identified, which had opposite effects compared to the one previously reported (Matsuno-Yagi and Mukohata, 1977). This second protein came to be known as *Halorodopsin* and was characterized as a light driven chloride pump (Bamberg, Tittor and Oesterhelt, 1993).

The turning point was in 2002, when a new opsin-related protein was found in the green alga *Chlamydomonas reinhardtii* (Nagel, 2002); this opsin, denominated *Channelrodopsin-1* (ChR1), was seen to be a composite photoreceptor and proton channel, with considerably faster photocurrents compared to Rhodopsins. Notably, in their 2002 work, the authors suggest that ChR1 could be “*a tool for measuring and/or manipulating electrical and proton gradients across cell membranes, simply by illumination*”. Soon, Channelrodopsin-2 was discovered by the same group (Nagel *et al.*, 2003), being a light-gated cation channel and showing inward currents in expressing cells just 50  $\mu$ s after a pulse of blue light at 473nm.

Finally, light activation of neurons was first obtained by expressing ChR2 in cultured hippocampal neurons, with minimal side effects (Boyden *et al.*, 2005). Activation of neurons *in vivo* was achieved soon after (Arenkiel *et al.*, 2007) thanks to transgenic

expression of ChR2-YFP under the *Thy1* promoter. At the same time an optical-neural interface was developed (Aravanis *et al.*, 2007), coupling a diode that could be controlled with millisecond precision to an optic fiber, delivering the necessary excitation light directly into a rat's brain.

Soon after such seminal discoveries, the newborn field of Optogenetics saw a tremendous expansion in both tools and scope. Rapidly, the first optogenetic inhibitor, derived from *Halorhodopsin* was described (Zhang *et al.*, 2007) and several variants of depolarizing opsins were sequentially developed (Lin *et al.*, 2009; Kleinlogel *et al.*, 2011), some allowing spike trains up to 200Hz (Gunaydin *et al.*, 2010; Klapoetke *et al.*, 2014). At the same time, various laboratories worked on the improvement of hyperpolarizing, inhibitory opsins, such as *ArchT* (Han *et al.*, 2011), *Jaws* (Chuong *et al.*, 2014), *GtACR* (Govorunova *et al.*, 2015)

One limitation of the classic ChR2 is the restricted excitation spectrum at which it can operate, between 450–545 nm. Because blue light is easily scattered by neural tissue, as well as absorbed by natural chromophores such as hemoglobin, ChR2 is not optimal for use in deep portions of the brain. The development of the red shifted variant ReaChR (Lin *et al.*, 2013) solved this issue allowing deep penetration in biological tissue, thanks to its excitation spectrum ranging from 470 to 650nm.

Optogenetics holds a promise for applications outside the nervous system, for example modulating the heart electrical function (Boyle, Karathanos and Trayanova, 2018), but it is in the field of neural circuit research that it has delivered the most.

Optogenetic has been used for the study of the motor system leading to the discovery of novel areas important for locomotion (Capelli *et al.*, 2017), defensive behavior (Tovote *et al.*, 2016) or even to create artificial memories (Vetere *et al.*, 2019).

The strength of optogenetics for neural circuit research lies not in itself, but in its combination with other powerful tools such as viral vectors and electrophysiological or

optical recordings of neuronal activity. Such combinations allow novel closed loop methods, where optogenetic stimulation is triggered by the readout of neuronal activity by means of calcium imaging or electrophysiology (Zhang *et al.*, 2018), or even by online tracking of mouse behavior (Kane *et al.*, 2020).

## 4.5 Chemogenetics

As discussed in chapter 4.4, the ability to activate or silence selected groups of neurons is of key importance in modern Neuroscience research. In this section will focus on Chemogenetics, a way of manipulating neuronal activity making use of genetically engineered receptors activated by small molecules.

The idea of genetically manipulating an existing receptor to make it insensitive to its natural ligand, but sensitive to others was first proposed in an influential work (Strader *et al.*, 1991) where the authors substituted one aminoacidic residue of the beta-adrenergic receptor. After the change, the mutant receptor unable to bind Adrenalin, its natural ligand, but was sensitive to previously inactive compounds such as catechol esters.

The research stemming from this first proof of concept focused mainly on the modification of other G protein-coupled receptors (GPCR) proteins. GPCRs make up a large group of related and evolutionarily conserved proteins in the eukaryotic lineage functioning as membrane receptors. Their ligands include hormones, neurotransmitters and other chemicals (e.g. odor sources); once the ligand has bound the receptor, a conformational change will follow, triggering a signal cascade with various end results.

The first step forward was the creation of RASSLs (receptor activated solely by a synthetic ligand) (Redfern *et al.*, 1999). Here, a novel protein (Ro1) based on the  $G_i$ -

coupled  $\kappa$  opioid receptor was expressed in cardiomyocytes, causing long-lasting bradycardia in mice when injected with the agonist *Spiradoline*.

Despite the innovation, various problems burdened RASSLs: first, the ligand had high affinity for the *wild-type* receptor, an obvious drawback when planning to use this tool *in vivo*; moreover, some RASSLs had a high level of constitutive activity, hindering the fine control needed by neuroscientists over neuronal activity.

The latest addition to the chemogenetic toolkit is DREADD (designer receptor exclusively activated by designer drug), which tackled these issues designing a receptor that could only be activated by a molecule with no other biologic activity (Armbruster *et al.*, 2007). The choice for the ligand fell on clozapine-N-oxide (CNO), which is mostly inert biologically, can be administered peripherally and was reported having a high penetrance in the nervous system (Bender, Holschbach and Stöcklin, 1994).

To create DREADDs, a human muscarinic M3 receptor was subjected to random mutagenesis, subsequently expressed in yeast cultures in presence of CNO. The yeast was engineered so that only colonies expressing a CNO sensitive M3 receptor would survive. The screening performed by the authors identified a mutant that fulfilled all conditions (sensitivity to CNO, insensitivity to acetylcholine and low constitutive activity).

The two mutations in this M3 receptor (Y149C, A239G) resulted in the creation of the first DREADD, now known as hM3Dq. Because such residues are common to all muscarinic receptors, the authors could engineer an entire family of DREADDs (Armbruster *et al.*, 2007), of which the most widely used in neuroscience are the original hM3Dq and hM4Di, derived from the M4 receptor.

Soon after, hM3Dq was reported to induce depolarization in pyramidal neurons of the hippocampus *in vivo* (Alexander *et al.*, 2009) through classical G protein signaling triggering  $\text{Ca}^{2+}$  influx. In contrast, hM4Di is known to reduce neuronal activity. Originally it was thought to provoke inhibition thanks to the aperture of inwardly rectifying potassium

channels, leading to hyperpolarization (Armbruster *et al.*, 2007), but it was later discovered that the main cause of inhibition is the suppression it exerts on synaptic transmission due to lower release probability (Stachniak, Ghosh and Sternson, 2014). This inhibitory DREADD has proven effective in silencing neurons *in vivo* (Ferguson *et al.*, 2011; Atasoy *et al.*, 2012).

Recently, one potential caveat of DREADD has emerged: it was found that instead of being solely activated by CNO, the DREADD receptors are potently bound and activated by Clozapine, the metabolic precursor of CNO (Gomez *et al.*, 2017). This is relevant because it is known that CNO can revert at least in part to Clozapine after *in vivo* administration, due to unspecified metabolic pathways in human and non-human primates (M. W. Jann, Y. W. Lam, W. H. Chang, 1994; Raper *et al.*, 2017). Moreover, it was further elucidated that CNO does not enter the brain and upon administration and it is converted Clozapine that is responsible for all cellular and behavioral effects of DREADDs (Gomez *et al.*, 2017).

While this has no effect on the overall efficacy of DREADDs on neuronal activation or silencing, it is cause of worry since Clozapine is an active molecule with several target receptors, and has been used to treat Schizophrenia for a long time (Wenthur and Lindsley, 2013) with reports of adverse effects in human patients, therefore limiting the therapeutic potentials of DREADDs.

The last innovation in the field of Chemogenetics is a new take on an older approach: Pharmacologically selective actuator modules (PSAMs), a tool based on the  $\alpha 7$  nicotinic acetylcholine receptor (nAChR), and activated by synthetic ligands (Magnus *et al.*, 2011). This approach had the disadvantage of short clearing times, making it less practical for addressing complex behavioral questions. New work from the Sternson group (Magnus *et al.*, 2019) has produced a new generation of “ultrapotent” chemogenetic tools. The PSAM<sup>4</sup> thus created was shown to strongly suppress the activity of cortical principal neurons *in vitro* and CA1 neurons *in vivo*. To complement this new PSAM, it was selected

a synthetic agonist with high CNS penetration and high activation rates at sub-nanomolar doses. (Magnus *et al.*, 2019).

## **4.6 Behavioral tracking and deep neural networks**

An accurate description and quantification of behavior is of paramount importance in modern neuroscience. Historically, scientists interested in studying behavior and movement in particular, have made use of existing or emerging technology to gain insight in the dynamics of animal and human motion. What amounted to recreational technology became for scientists a way to access what their eyes could not resolve: photography and videography were soon adopted thanks to their capacity of freezing motion and behavior, as well as enabling storage for future examination (Muybridge, E., 1887). These new media, photographs and videos, have been analyzed manually by researchers for decades, until a new technology emerged, paving the way to less labor-intensive ways to characterize behavior.

With the computer, photo-videography soon transitioned into digital form, and the exponential increase in computing power of CPUs allowed for a new standard to emerge: the combination of video recordings and reflective markers placed on discrete body parts of the experimental subject, allowing for precise and unbiased tracking and quantification of behavior (Johansson, 1975).

However, this approach, although innovative, had some caveats: first, it requires markers to be attached to the chosen body parts, potentially causing distress or distraction in animals; second, it lacks in flexibility, calling for an advanced decision on which body parts to track.

More recently, the coming of age of machine learning and computer vision gave steam to novel approaches based on segmentation (Nakamura *et al.*, 2016; Litjens *et al.*, 2017; Serre, 2019), but it was with the advance in *deep neural networks* that the field of pose estimation was definitely revolutionized.

In a classic artificial neural network (*ANN*), sets of *units* (also known as artificial neurons) are organized into layers and connected to each other by *edges*, the artificial equivalent of axons and synapses. Just as in their biological equivalent, artificial neurons receive multiple inputs and operate a computation in order to produce one output signal. In addition, *units* and *edges* also carry a specific *weight* in the network, which represent their relative importance which changes along with the training, strengthening specific connections and weakening others, therefore making certain parameters more influential. In a classic *ANN*, there is an input layer, a hidden layer and an output layer and information flows univocally from input to output.

*Deep neural networks* (*DNNs*) are simply *ANNs* in which multiple hidden layers are stacked in series. Therefore, where *ANNs* are networks capable of solving simple problems, *DNNs* are able to tackle complex problems by decomposing them into many simpler ones.

One of the most popular approaches in working with *DNNs* is supervised learning, where the network is fed a certain amount of annotated data (pairing inputs with desired outputs), which will be used to calibrate the weights of its connections.

*DNNs* have made possible the of creation of new tools based on computer vision that have the ability to track any body part without pre-defined physical markers. One of such tools is *DeepLabCut* (Mathis *et al.*, 2018), which is rapidly becoming the gold standard for pose estimation thanks to its ease of use and high reliability. The authors set out to create a *DNN* that would be robust and generalize well, while also reaching human levels of visual recognition. To do this they pre-trained their *DNN* on ImageNet, a vast database

of annotated images (Deng *et al.*, 2009), reducing in this way the amount of data needed for each training. The second step was to base the architecture of the algorithm on *DeeperCut* (Insafutdinov *et al.*, 2016), a previous algorithm optimized for human pose-estimation from photographs, which was found to generalize well to animal pose-estimation.

Thanks to this strategy, DeepLabCut provides high level tracking and labelling, while only requiring a minimum level of supervision: the authors found that a set of 200 training frames or images is enough to obtain a network capable of achieving human-like accuracy. In addition, it is able to track any number of body parts in parallel, even when multiple subjects are present in the video.

As shown in chapter 5 of this dissertation, DeepLabCut is able to reliably track skilled forelimb movements in behaving mice, making possible sophisticated kinematic analysis that was only achievable with head-fixation or complex instruments based on reflective markers placed on the body of the animal.

Importantly, recent developments of DeepLabCut have delivered a novel version of the software capable of delivering pose-estimation in real time with extremely low latency (15 ms at 100 fps) (Kane *et al.*, 2020). This advance is of great importance in the field of motor control and neuroscience in general, as it allows to automatize the control of a behavioral task or stimulation of neurons in real time based on what the animal is doing at any given time.



# Aim

The involvement of the brainstem in different aspects of movement, and in particular in skilled forelimb movements is still obscure. The aim of this dissertation was to gain an understanding of whether and how brainstem nuclei encode different sets of forelimb actions. To this end we recorded the activity of neurons in the rostral medulla while animals performed different skilled and non-skilled movements, revealing their tuning to specific actions. Moreover, we aimed to elucidate how brainstem nuclei interact with each other in order to generate and control complex skilled forelimb behaviors. We used state of the art viral tracing techniques to investigate the anatomical relationships between distinct neuronal populations, uncovering the logic of connectivity between the Lateral rostral medulla and its synaptic targets. Lastly, our goal was to probe the potential of brainstem circuits for generating skilled movements and to show that subcortical circuits are essential for the successful execution of complex behavioral actions. To address this point, we used optogenetic and chemogenetic tools, artificially activating or dampening the activity of specific identified sets of neurons in the rostral medulla, demonstrating them to be necessary for skilled forelimb movements and proving their activation sufficient for eliciting a diverse number of forelimb actions.



## **5. A functional map for diverse forelimb actions within brainstem circuitry**

Ludwig Ruder<sup>1,2</sup>, Riccardo Schina<sup>1,2</sup>, Harsh Kanodia<sup>1,2</sup>, Sara Valencia-Garcia<sup>1,2</sup>,  
Chiara Pivetta<sup>1,2</sup> and Silvia Arber<sup>1,2</sup>

<sup>1</sup>Biozentrum, Department of Cell Biology,  
University of Basel, 4056 Switzerland

<sup>2</sup>Friedrich Miescher Institute for Biomedical Research  
4058 Basel, Switzerland

## 5.1 Summary

The brainstem is a key center to control body movements. While the precise nature of brainstem cell types and circuits central to full-body locomotion are becoming known<sup>1-5</sup>, efforts to understand the neuronal underpinnings of skilled forelimb movements have focused predominantly on supra-brainstem centers and the spinal cord<sup>6-12</sup>. Here we define the logic of a functional map for skilled forelimb movements within the brainstem's lateral rostral medulla (latRM). Using *in vivo* electrophysiology in freely moving mice, we reveal a neuronal code with latRM populations tuned to distinct forelimb actions including reaching and food handling, behaviors both impaired by perturbation of excitatory latRM neurons. Combinatorial use of genetics and viral tracing demonstrates that excitatory latRM neurons segregate into distinct populations by axonal target, acting through the differential recruitment of intra-brainstem and spinal circuits. Probing the behavioral potential of projection-stratified latRM populations, we find that their optogenetic stimulation can elicit diverse forelimb movements, with each behavior stably expressed by individual mice. In summary, projection-stratified brainstem populations encode action phases and together serve as putative building blocks for regulating key features of complex forelimb movements, unraveling the brainstem's substrates for skilled forelimb behaviors.

## 5.2 Introduction

Understanding how diverse body movements are regulated necessitates the identification of neuronal circuit mechanisms central to this process. The brainstem represents a key integration and processing junction establishing links between upper motor centers involved in planning actions and circuits in the spinal cord required for execution of body movements (Grillner S., Georgopoulos A.P. and Jordan L.M., 1997; Grillner, 2006; Lemon, 2008; Kim *et al.*, 2017; Arber and Costa, 2018; Svoboda and Li, 2018; Klaus, Alves da Silva and Costa, 2019; Ruder and Arber, 2019). Specific neuronal circuits within the brainstem and their outputs to the spinal cord are dedicated to the regulation of locomotion (Bouvier *et al.*, 2015; Roseberry *et al.*, 2016; Capelli *et al.*, 2017; Caggiano *et al.*, 2018; Ferreira-Pinto *et al.*, 2018), a behavior requiring full-body coordination. Whether neuronal circuit modules devoted specifically to skilled forelimb movements exist within the brainstem, how they interact with spinal circuits and coordinate the construction of complex forelimb movements is poorly understood.

A major historical focus to understand how the nervous system regulates skilled forelimb movements has been on higher motor centers including motor cortex and basal ganglia (Georgopoulos *et al.*, 1982; Lemon, 2008; Alstermark and Isa, 2012; Klapoetke *et al.*, 2014; Peters, Liu and Komiyama, 2017; Wang *et al.*, 2017; Klaus, Alves da Silva and Costa, 2019). Yet, several lines of evidence suggest that the execution of skilled forelimb movements engages and is dependent on subcortical structures, especially the brainstem. Evolutionary analysis demonstrates that behavioral elements of skilled forelimb movements including reaching and food handling are already present in species without cortico-spinal tracts including frogs (Iwaniuk and Whishaw, 2000). In mice, ablation of specific excitatory neurons in the mouse caudal medulla impairs food grasping (Esposito, Capelli and Arber, 2014). The brainstem's medulla and pons also

harbor neurons recruited during forelimb reaching in cats (Schepens and Drew, 2006; Schepens, Stapley and Drew, 2008) and digit movements in monkeys (Soteropoulos, Williams and Baker, 2012). Monkeys with lesions of the cortico-spinal tract compensate all aspects of skilled forelimb movements except the use of single digits (Lawrence and Kuypers, 1968a; Lemon *et al.*, 2012). Strikingly, an additional specific lesion of the lateral but not the medial lower brainstem entirely abrogates these behavioral compensations (Lawrence and Kuypers, 1968b; Lemon *et al.*, 2012). Lastly, systematic electrical microstimulation experiments in these regions, albeit focused on locomotion as read-out, identified sites within the lateral medulla, whose stimulation elicited specifically forelimb movements with no effects on hindlimbs (Ross and Sinnamon, 1984). Together, these findings point to the existence of important, yet uncharacterized neuronal substrates in the lateral medulla, required for the execution of skilled forelimb movements.

## 5.3 Results

### LatRM neurons tuned to forelimb actions

To assess the activity of neurons in the latRM, we performed *in vivo* recordings using chronic silicon probe implants in the brainstem. We centered the implant in the parvicellular reticular nucleus (PCRt) (Franklin K.B. and Paxinos G., 2007) at the rostro-caudal level of the facial nucleus (7N) (Fig. 5.2a, b), a brainstem region in which we had observed neurons specifically premotor to motor neurons innervating forelimb muscles (Esposito, Capelli and Arber, 2014). This allowed us to monitor the activity of single neurons while freely-moving mice performed different behavioral tasks (Fig. 5.1; Fig. 5.2). We trained mice on a food pellet reaching and retrieval task (pellet task) to specifically engage in unilateral forelimb reaching and subsequent food handling (Xu *et al.*, 2009). As a distinct but behaviorally similar forelimb-engaging task, we trained mice

to reach for and press a lever (lever task), the successful execution of which allowed them to retrieve a reward (Jin and Costa, 2010). To contrast these mostly forelimb-engaging behaviors, we assessed latRM neuron activity during full body locomotion, a behavior also strongly engaging forelimb muscles but in a very different context

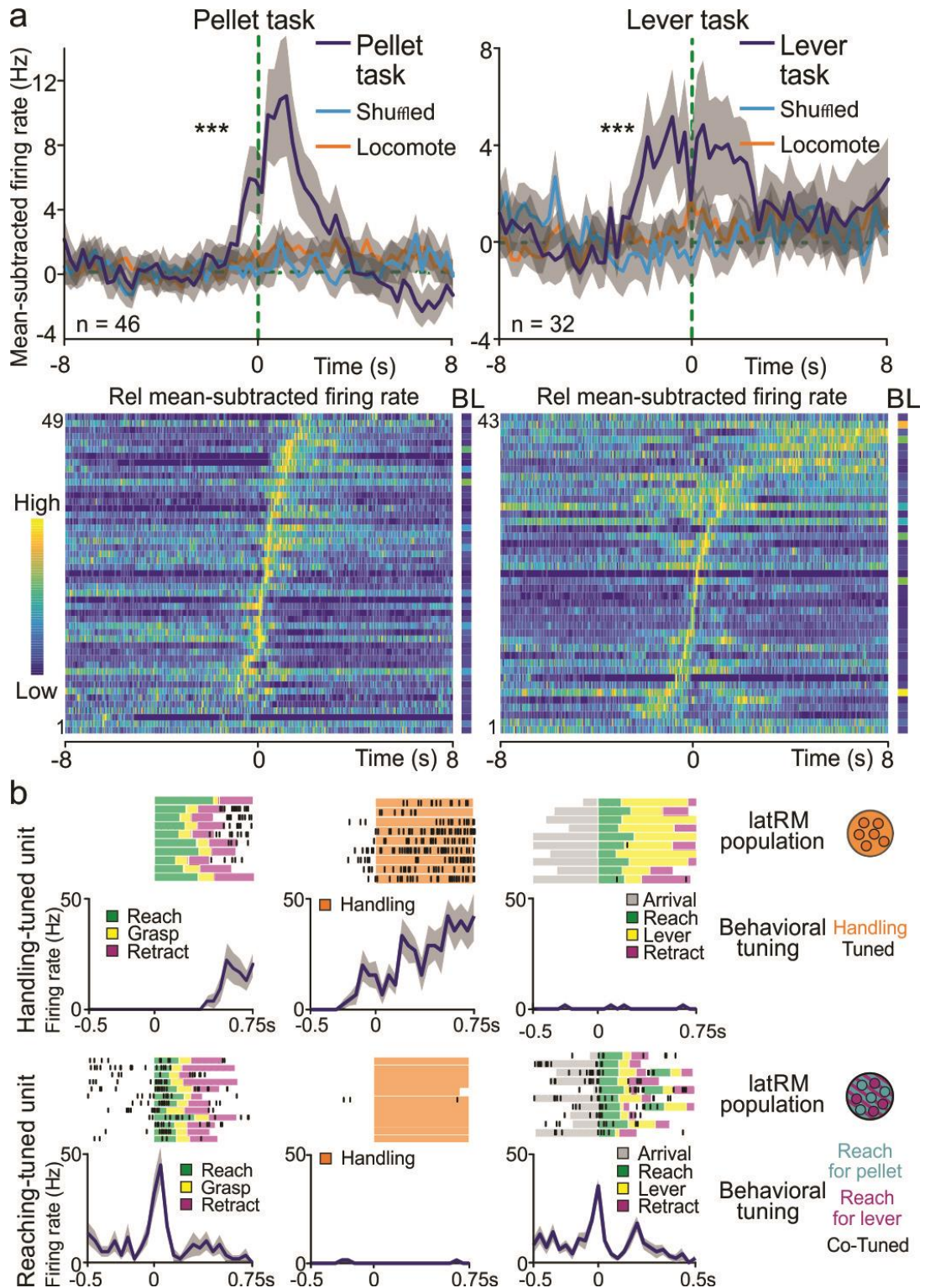


### Figure 5.1 Brainstem neurons specifically tuned to forelimb behaviors

(a) Mean subtracted firing rate of all task-tuned latRM neurons analyzed for pellet (left) and lever task (right), depicting average over all neurons (top; recorded also in locomotion) or individual neurons sorted by time of maximal relative mean subtracted firing rate (bottom, recorded in shown task; color scale: Low (0) to High (1) for relative mean subtracted firing rate and Low (0Hz) to High (100Hz) for BL, baseline firing rate), with time 0 representing reaching onset. Also displayed in top graphs are average of mean subtracted firing rate of these neurons during onset of locomotion trials (locomote), or shuffled data (n=5 mice; n = 46 neurons assessed during both pellet reaching and locomotion, n = 32 for neurons assessed during both lever pressing and locomotion, see Methods).

(b) Examples for two latRM neurons during pellet task (left), food handling (middle), and lever task (right). Behavioral phases are marked in color for all trials and summary schemes shown on the right. Example unit on the top displays tuning preference for handling over other behavioral phases, the bottom one for reaching (for lever or pellet) over handling (average firing rate (Hz) is shown below single trials; n=1 example neuron each).

Grey shade:  $\pm$ SEM; \*\*\*P<0.00033; Wilcoxon signed rank test. Bonferroni correction was applied to account for multiple comparisons.

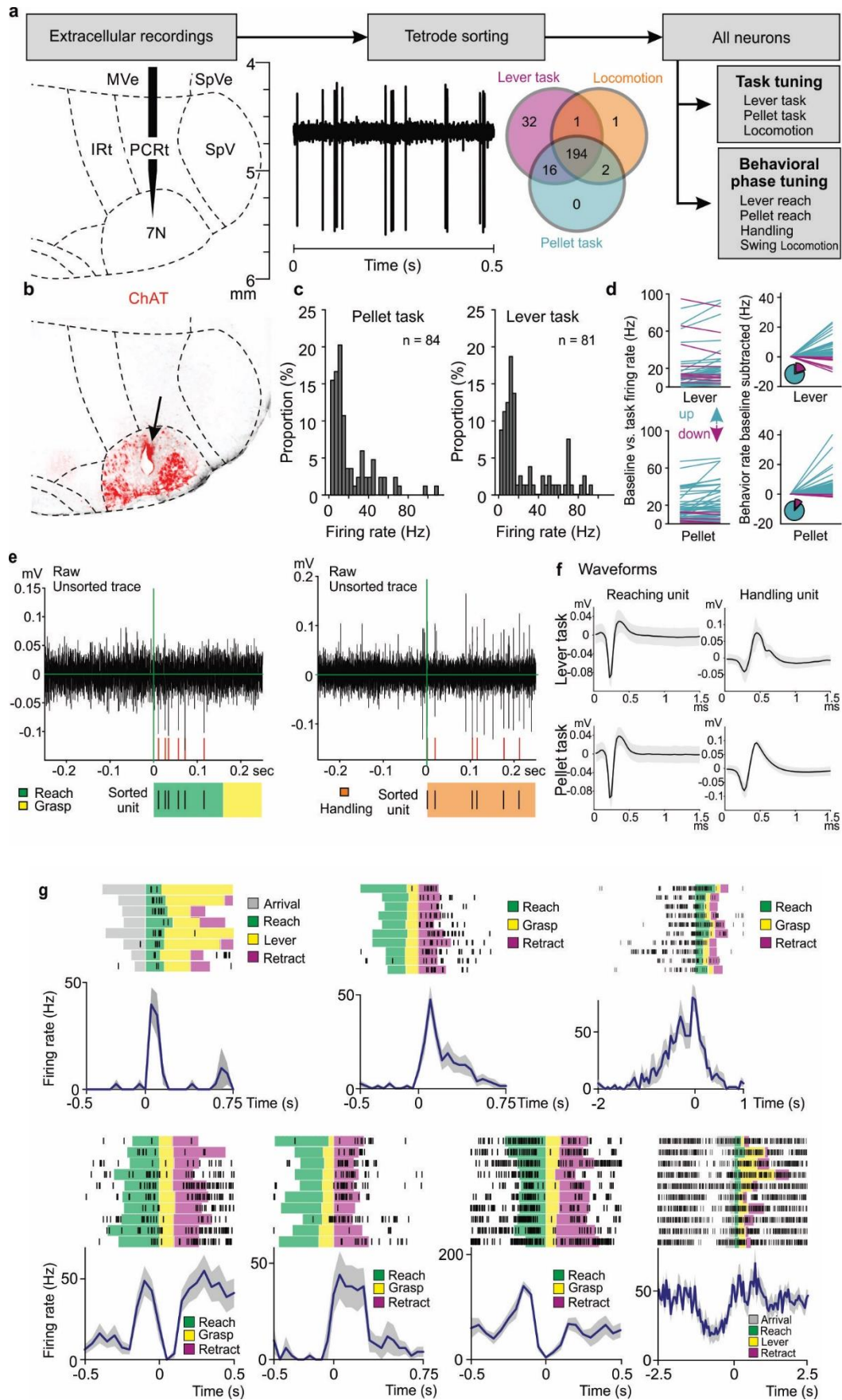


## Figure 5.2 Methodological approaches and firing properties of latRM neurons

(a) Scheme outlining experimental setup and analysis pipeline for single unit recordings of latRM neurons. A total of 194 neurons were recorded in lever task, pellet task and open field assay.

(b) Representative latRM section from mouse undergoing single unit recordings, depicting end point of silicon probe trajectory, visualized through electrical lesion (arrow) performed at the end of all recording sessions, counterstained for ChAT to visualize 7N neurons.

(c) Analysis of average firing rates of behaviorally-relevant neurons for pellet (left,  $n = 84$  neurons) and lever (right,  $n = 81$  neurons) task, demonstrating that most neurons fire at relatively low rates.

(d) Analysis of changes in firing rate of task-tuned neurons comparing baseline to behavior. Note that the large majority of neurons upregulate their firing rate, while only few downregulate it ( $n = 43$  neurons for lever task,  $n = 49$  neurons for pellet task).

(e, f) Two examples of raw unsorted traces (e), aligned to reaching (left) or handling (right) onset, depicting the spiking pattern of the subsequently sorted unit below with indication of behavioral time windows. Waveforms for these two units are shown for lever and pellet task which were carried out sequentially.

(g) Recordings from seven example LatRM neurons during lever or pellet task, displaying single trials aligned to behavioral phases (spikes shown as lines) as well as average firing rate (Hz) below single trials ( $n=1$  neuron each); grey shade:  $\pm$ SEM.

To get an overview of activity changes of latRM neurons during a task, we analyzed the mean-subtracted firing rate of all neurons tuned to one of the two forelimb tasks. We observed a striking overall increase in firing rate during each of the forelimb tasks (pellet and lever tasks) but not during locomotion or when analyzing shuffled data from the same neurons (Fig. 5.1a). For both forelimb tasks, individual neurons contributed to the overall curve by tiling the behavioral space from preparation to execution (Fig. 5.1a), and a large majority of neurons upregulated their firing rate (Fig. 5.2c, d). Analysis of the firing profile changes revealed diversity, with selectivity to particular time windows (Fig. 5.1a; Fig. 5.2e-g).

We next addressed the question of whether latRM neuron populations are tuned to specific behavioral phases. We analyzed neuronal activity changes during sharp behaviorally-defined time windows (see Methods). We identified neurons tuned to the reaching phase of the pellet or lever task (relatively similar forelimb actions), and compared these to neurons tuned to food handling, an action phase behaviorally distinct from reaching (Fig. 5.1b). At the population level, action ensemble co-tuning for both reaching phases was significant, while we observed no significant co-tuning or anticorrelation for either of these behaviors and food handling ( Fig. 5.3a-f). In contrast, we found that the handling-tuned latRM population is not recruited during the lever task or locomotion swing phases (Fig. 5.1b; Fig. 5.3a). However, it is recruited with delay during the pellet task, where reaching is followed by food handling. Thus, the handling-tuned latRM population is engaged during skilled forelimb behaviors involving food handling. In agreement with the interpretation of action-specific tuning, the latRM population tuned to lever-reaching was also recruited during pellet-reaching, but not during handling or locomotion swing phases (Fig. 5.3b). These findings demonstrate that latRM neurons fractionate into distinct ensembles, displaying behavior-specific tuning

within the forelimb action space (Fig. 5.1b, Fig. 5.3f), and are unlikely recruited exclusively according to a muscular or receptive field map (Schepens and Drew, 2006).

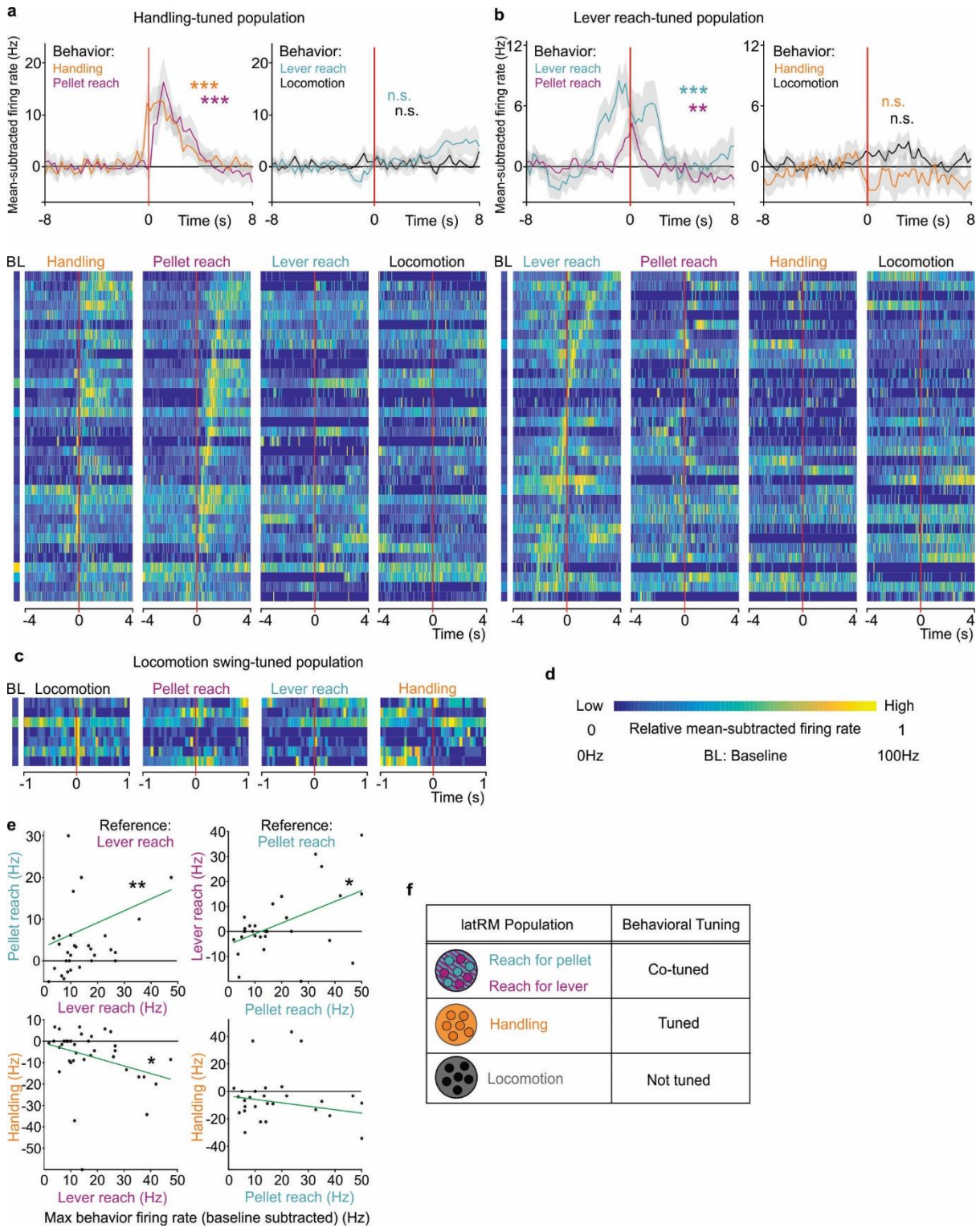


### Figure 5.3. Behavioral tuning properties of latRM neurons

(a-d) Analysis of handling-tuned (a) and lever-reach-tuned (b) latRM populations (n=34 neurons each), depicting response properties of all respective neurons aligned to behavioral onset of handling, pellet reach, lever reach or locomotion swing phase (top: average of all neurons, bottom: raster plot for individual neurons ordered by peak time of pellet-reach (a) or lever-reach (b)). Data in (c) depicts raster plots for the small number of latRM neurons making up a locomotion swing-phased tuned latRM population. Color scale in (d) depicts Low (0) to High (1) for relative mean subtracted firing rate and Low (0Hz) to High (100Hz) for BL, baseline firing rate.

(e) Correlation analysis of behavioral tuning of all units analyzed in lever, pellet and handling task (n=5 mice; n = 38 neurons for lever reach tuned population, n = 30 neurons for pellet reach tuned population, also see Methods).

(f) Summary scheme displaying population co-tuning for latRM neurons during lever reaching and pellet reaching. In contrast, the handling-tuned latRM population is not engaged in reaching. Note also that analyzed neurons are not tuned to locomotion (swing phase).

Grey shades:  $\pm$ SEM; \*\*P<0.0025; \*\*\*P<0.00025; Wilcoxon non-parametric signed rank test. Bonferroni correction was applied to account for multiple comparisons. (a, b); \*\*P<0.01; \*\*\*P<0.001; Spearman's rank correlation test (e).

### Skilled forelimb behaviors require latRM

To determine whether and which aspects of forelimb behaviors require latRM neurons for execution, we used loss-of-function tools in mice trained in forelimb reaching or food handling, two behaviors recruiting distinct latRM populations. We expressed the inhibitory designer receptor exclusively activated by designer drugs (DREADD) hM4Di whose activity can be regulated by systemic Clozapine N-oxide (CNO) injection (Roth, 2016) or as a second tool Diphtheria toxin receptor (DTR) whose expression leads to neuronal ablation upon systemic injection of Diphtheria toxin (Esposito, Capelli and Arber, 2014) in the latRM of *vGlut2<sup>Cre</sup>* mice (Fig. 5.5a).

We found no difference in open field locomotor activity comparing conditions with or without CNO (Fig. 5.5b). In contrast, forelimb reaching and food handling were severely affected in mice with chemogenetically silenced or ablated excitatory latRM neurons (Fig. 5.4). First, we evaluated mice for their performance in the pellet task. We found a highly significant and reversible decline in the success rate to retrieve food pellets to the mouth over baseline with CNO injections in latRM-hM4Di-vGlut2 mice (Fig. 5.4b). The drop in success rate reflected a significant increase in the miss rate of the pellet by the forepaw during the reach in CNO-injected latRM-hM4Di-vGlut2 mice (Fig. 5.4c). Reconstructions of the point of maximal extension of reaching trajectories showed that these mice consistently over-reached the pellet position and displayed significantly higher variability in end point position (Fig. 5.4d; Fig. 5.5c-e). Recording from latRM neurons during a two-choice reaching assay demonstrated that reaching-task-tuned latRM neurons line up along a spectrum of differential firing rate changes comparing medial to lateral reaches (Fig. 5.5f, g). Our findings demonstrate that excitatory latRM neurons are essential during forelimb reaching for endpoint targeting, and that some neurons exhibit signatures of reaching directionality, a property previously observed in the cortex of monkeys and mice (Georgopoulos *et al.*, 1982; Galiñanes, Bonardi and Huber, 2018).

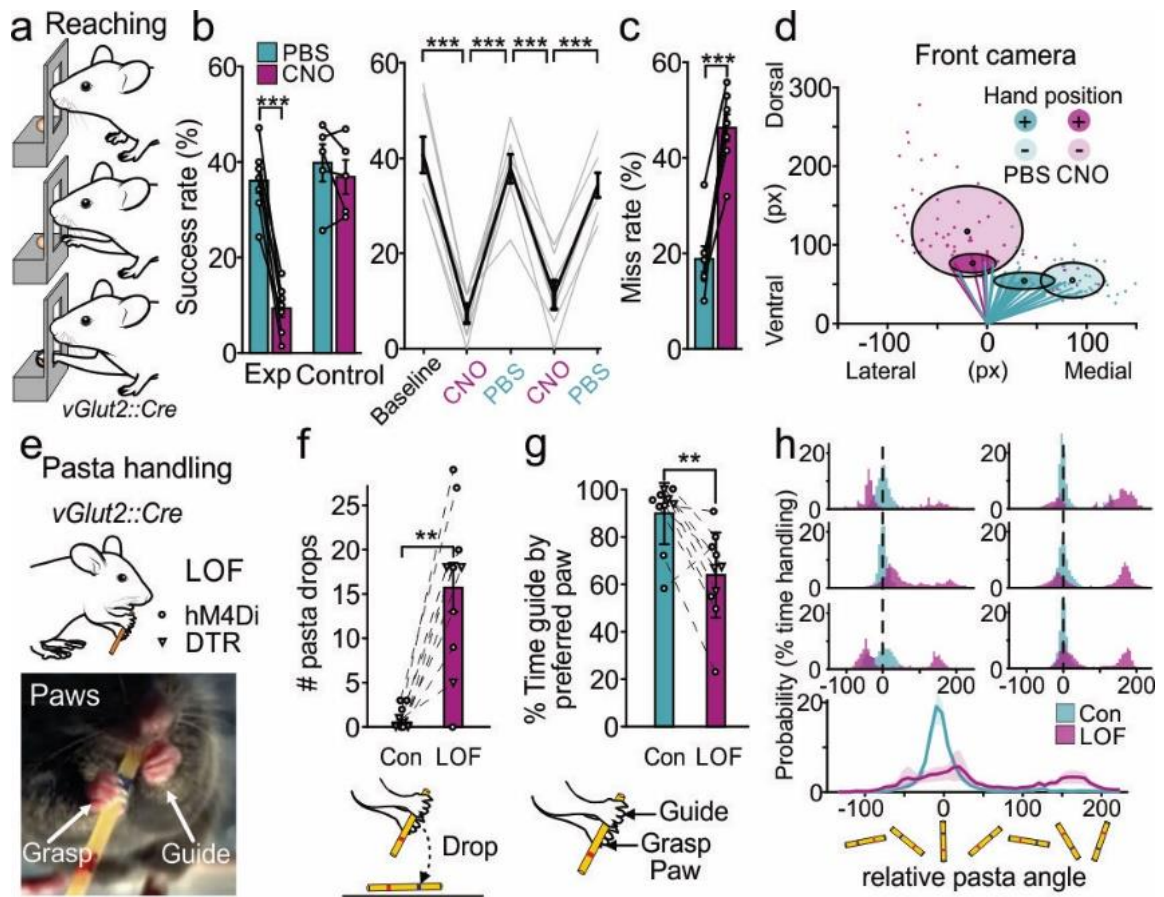


**Figure 5.4. Excitatory latRM neurons are required for reaching and handling**

(a) Experimental design for food pellet reaching assay, displaying mouse before reaching onset, during reaching, and at target.

(b) Success rate for same group of experimental mice trained on pellet task (Exp:  $n = 7$  mice, Control:  $n = 5$  mice), displaying overall success rate (left,) and success rate separately displayed by baseline recording day as well as two days each with the injection of CNO or PBS (right).

(c) Increased food pellet targeting miss rate upon CNO injections in latRM-hM4Di-vGlut2 mice ( $n=7$  mice).

(d) Point of maximal extension for reaching trajectories (solid circles: average position of trials not missing the target; transparent circles: same measure for missed trials; each on days with PBS or CNO injection respectively).

(e) Illustration of pasta handling assay, displaying guide and grasp forepaw used in the handling task and the markings on pasta used for tracking of pasta position.

(f) Quantification of the number of pasta drops per behavioral session for latRM-hM4Di/DTR-vGlut2 mice without (Con) or with (LOF; loss of function) perturbation of excitatory latRM neurons (n=7 mice hM4Di and n=3 mice DTR).

(g) Quantification of percentage of time during which preferred paw as defined for the control condition is used as guide paw (n=7 mice hM4Di and n=3 mice DTR).

(h) Fraction of time spent handling pasta at a given angle, relative to the preferred pasta angle for each mouse defined in the control session (set to 0 degree; see Methods) shown for 6 representative mice (top) and average of all analysed (bottom; n=7 mice hM4Di and n=3 mice DTR).

Data are mean  $\pm$ SEM (b, c) and mean  $\pm$ SD (f, g); Shades around mean:  $\pm$ SD; \*\*P<0.01 \*\*\*P<0.001; two-sided paired t-test (b, c), Wilcoxon signed rank test (f, g).

We next assayed the performance of latRM-hM4Di/DTR-vGlut2 mice in pasta handling, a well-established paradigm to determine and quantify the ability of rodents to manipulate food with their forepaws (Tennant *et al.*, 2010; Whishaw *et al.*, 2017). Rodents rarely drop the pasta piece and employ stereotypical handling patterns, using a constant forepaw to guide the pasta into the mouth (guide paw), while the second paw grasps the pasta piece further away to stabilize it (grasp paw), together allowing for a relatively stable angle of the pasta (Fig. 5.4e). latRM-hM4Di/DTR-vGlut2 mice exhibited severe pasta handling defects, dropping pasta pieces significantly more frequently than during control sessions (Fig. 5.4f). We also found that latRM-hM4Di/DTR-vGlut2 mice frequently switched hands during handling (Fig. 5.4g), and pasta angle stability was severely affected, leading to an overall broadening of the pasta angle tuning curve due

to handling instability and hand switching (Fig. 5.4h; Fig. 5.6a). Despite these striking defects in pasta handling however, latRM-hM4Di/DTR-vGlut2 mice were not deficient in grip strength (Fig. 5.6b), suggesting that the forelimb behavioral defects relate to the orchestrated use of forepaws in manipulation. Together, these experiments demonstrate that excitatory latRM neurons are required for various aspects of skilled forelimb movements, as shown here for reaching and food handling.

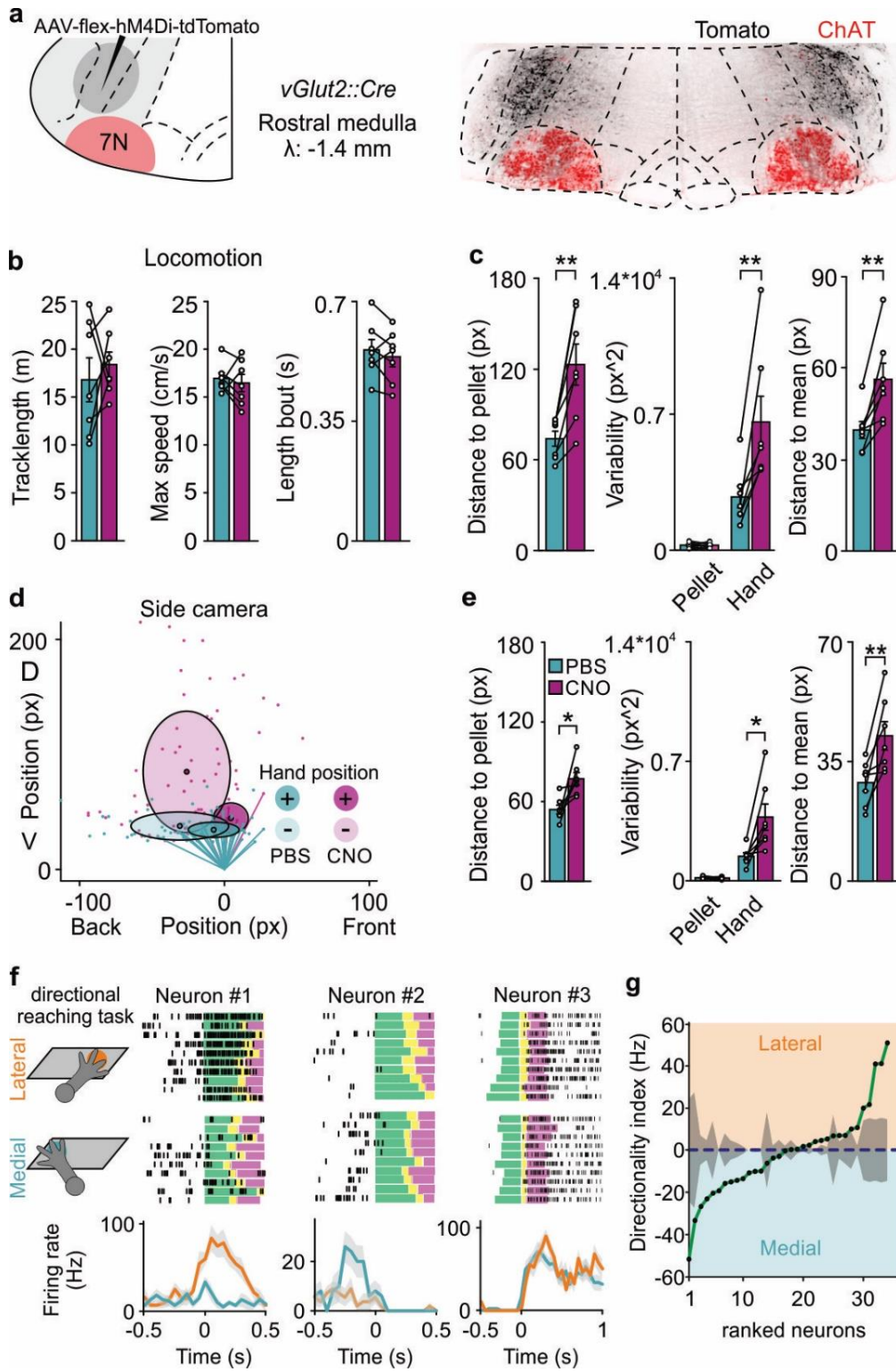


**Figure 5.5. Excitatory latRM neurons are required for precise directional reaching**

(a) Experimental scheme for injection of AAV-flex-hM4Di to the latRM of *vGlut2::Cre* mice and representative picture of targeting specificity for behavioral experiments, counterstained for ChAT.

(b) Attenuation of excitatory latRM neurons does not lead to defects in open field locomotion (track length, maximal speed, length of locomotor bouts), comparing PBS or CNO trials respectively (n=7 mice).

(c) Quantitative analysis of distance to food pellet, variability and distance to mean, separately shown for PBS and CNO trial days (front camera analysis, same mice as in Fig. 2; n=7 mice).

(d) Analysis of point of maximal extension for reaching trajectories using a side camera for recordings (dark colored circles: average position of trials not missing the target; light colored circles: same measure for missed trials; each on days with PBS or CNO injection respectively).

(e) Quantitative analysis of distance to food pellet, variability and distance to mean, separately shown for PBS and CNO trial days (side camera analysis; n=7 mice).

(f) Experimental design for two-choice directional reaching task with lateral and medial reaching positions (left), 3 examples for recorded latRM neurons (right; n=1 neuron each), each displaying single trials aligned to behavioral phases (green: reach; yellow: grasp; magenta: retract), spikes shown as lines (top), as well as average firing rates for lateral vs medial recorded trials (bottom).

(g) Quantification of directionality index (sorted from medial to lateral in ascending order, n = 34 neurons) for latRM neurons recorded during the two-choice directional reaching task.

Data are mean  $\pm$ SEM; grey shades:  $\pm$ SEM; \*P<0.05; \*\*P<0.01; two-sided paired t-test.

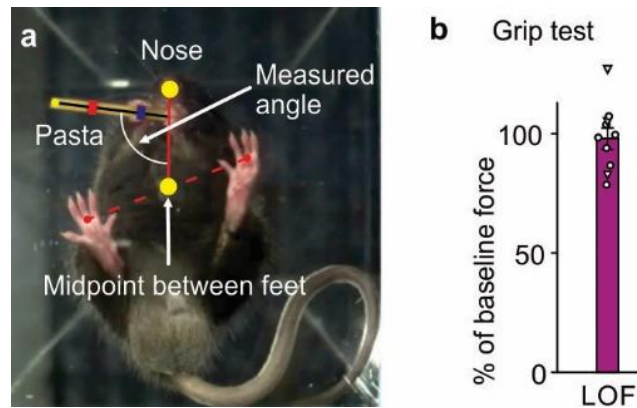


**Figure 5.6 Excitatory latRM neurons are required for pasta handling but not grip strength**

(a) Scheme explaining the approach to quantify pasta angle during handling.

(b) latRM-hM4Di/DTR-vGlut2 mice do not display defects in grip strength (n=7 mice hM4Di and n=3 mice DTR; data are mean  $\pm$ SEM).

### Projection targets divide latRM neurons

The behavioral requirement and differential recruitment of excitatory latRM neurons in distinct phases of skilled forelimb movements raises the question of whether latRM neurons can be meaningfully stratified using anatomical and genetic approaches. We employed anterograde tracing approaches with latRM-centered injections of AAV-flex-SynTag viruses into *vGlut2<sup>Cre</sup>* mice (Fig. 5.8) to select three major termination regions for further analysis. These were the cervical spinal cord, the caudal medulla at the level of 10/12N (vagus/hypoglossal) motor neurons, and the contralateral latRM (Fig. 5.8). We injected AAVs with retrograde targeting potential<sup>36</sup> conditionally expressing nuclear tags (retAAV-flex-nTag) into these downstream regions of *vGlut2<sup>Cre</sup>* mice and mapped distribution of neurons retrogradely marked in the RM (Fig. 5.7a; Fig. 5.9). We subdivided caudal medulla injections into medially (MdV: medullary reticular formation, ventral part) and laterally (MdD: medullary reticular formation, dorsal part) centered positions (Fig. 5.7a).

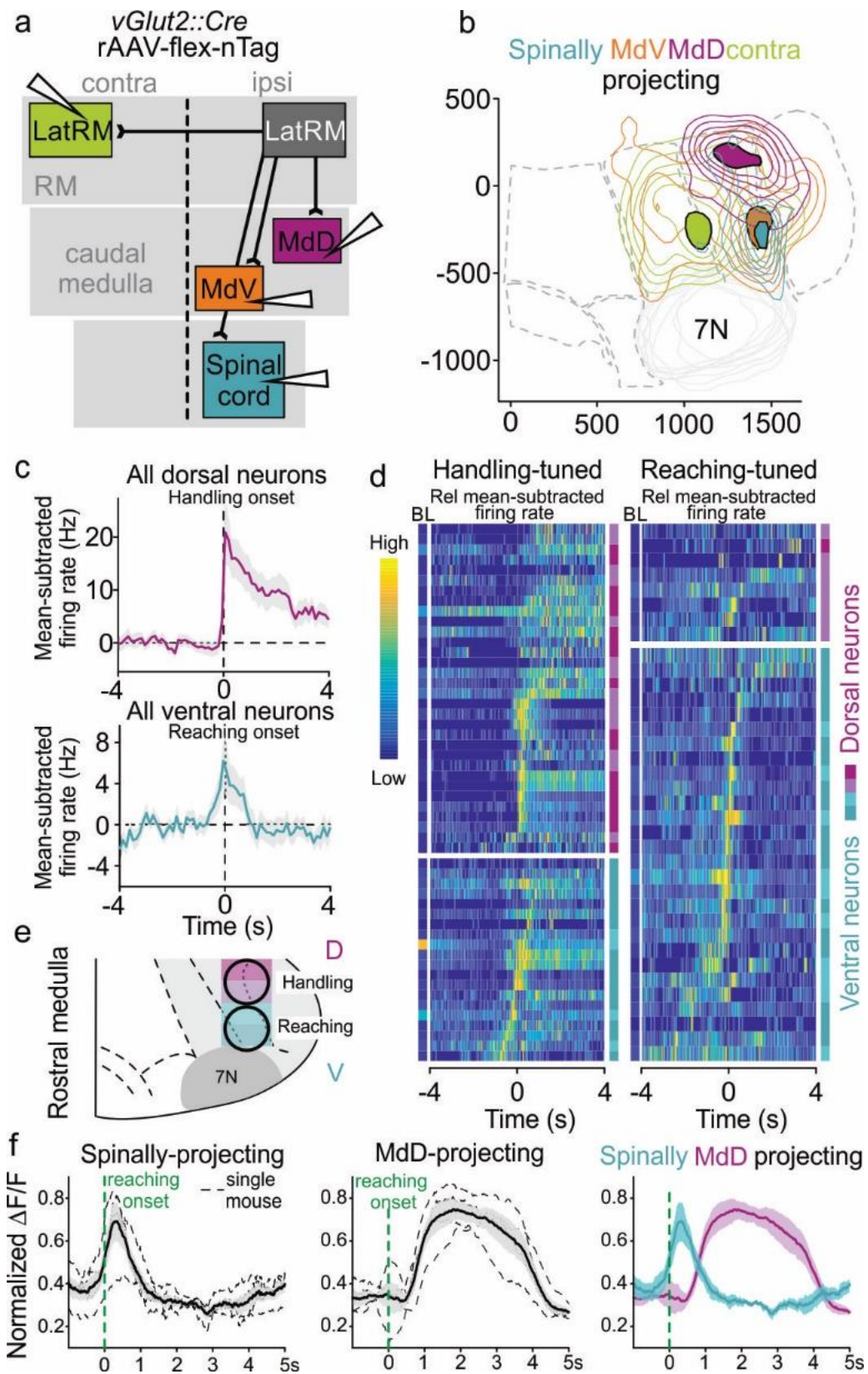


### Figure 5.7 Differential tuning of latRM subpopulation to forelimb behaviors

(a) Experimental design to analyze neuronal distribution of excitatory latRM neurons with projections to cervical spinal cord, the caudal medulla regions centered to MdV and MdD, and contralateral latRM in *vGlut2<sup>Cre</sup>* mice.

(b) Density analysis of retrogradely marked neuronal cell bodies within latRM upon injection in the four different downstream regions. Solid area marks the sites of highest 6<sup>th</sup> of density.

(c, d) Mean subtracted firing rate of behaviorally-tuned latRM neurons divided by dorsal (2 shades of magenta) and ventral (2 shades of cyan) recording sites during pellet task. Data in (c) depicts average over all dorsal (top; aligned to handling onset) or all ventral (bottom; aligned to reaching onset) behaviorally-tuned neurons (neurons: n = 37 dorsal, n = 43 ventral). Raster plot in (d) depicts individual neurons tuned to handling (left; aligned to handling onset; n=52) or reaching (right; aligned to reaching onset; n=36), sorted by time of maximal relative mean subtracted firing rate (color scale on the left depicts Low (0) to High (1) for relative mean subtracted firing rate and Low (0Hz) to High (100Hz) for BL, baseline firing rate).

(e) Summary diagram to illustrate that dorsal recording sites encompass preferentially latRM neurons active during handling, while ventral sites encompass latRM neurons active already during or before forelimb reaching.

(f) Fiber photometry data analyzing the dynamics of calcium activity in excitatory latRM neurons retrogradely targeted from the cervical spinal cord (left, n = 4 mice), from MdD centered injections (middle, n = 4 mice), or overlay thereafter. Shades around mean:  $\pm$ SEM.

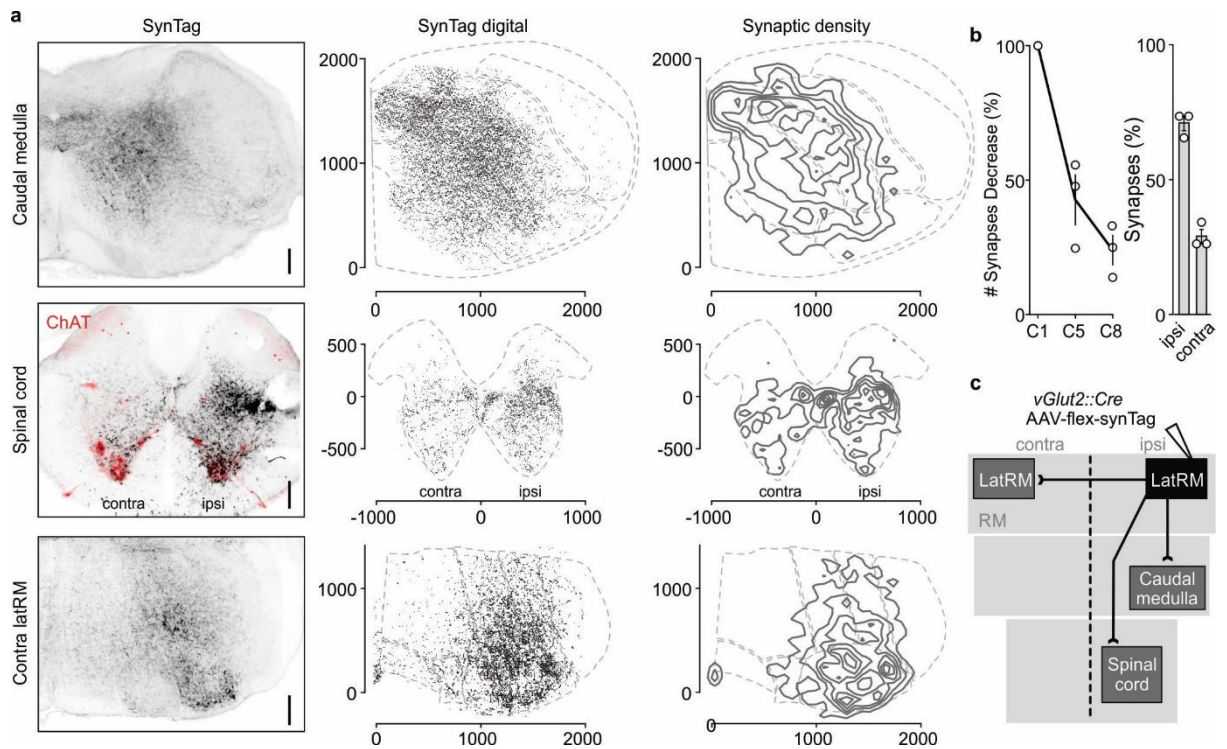


**Figure 5.8 Major synaptic targeting regions of excitatory latRM neurons**

(a) Analysis of synaptic output derived from excitatory latRM neurons in *vGlut2-Cre* mice to the cervical spinal cord, caudal medulla and contralateral latRM. Shown are representative pictures (left; from one of three mice use for quantification in b) and reconstructions (middle) of SynTag puncta and synaptic density (right) plots for these output structures (scale bar = 250 $\mu$ m).

(b) Quantification of synaptic numbers along the rostro-caudal axis of the cervical spinal cord (C1, C5, C8). Note the decrease in synapses between rostral and caudal cervical spinal cord segments, demonstrating that spinally projecting excitatory latRM neurons terminate more strongly in rostral cervical spinal cord segments compared to caudal counterparts (n=3 mice, data are mean  $\pm$ SEM).

(c) Summary scheme of main synaptic output areas by excitatory latRM neurons.

We first compared neuronal distribution between medial (med) RM and latRM. For spinally- or MdV-projecting populations, ~80% of neurons were located within medRM, with a high level of overlap between these populations (Fig. 5.9). MdD-projecting neurons showed the opposite distribution profile with ~80% residing in the latRM. Neurons projecting to the contralateral latRM were also dominant within the latRM (Fig. 5.9). We next assessed the distribution patterns of the four retrogradely marked populations within the latRM. We observed a striking difference between spinally- and MdD-projecting excitatory latRM neurons, with the first population showing a dominant neuronal cluster immediately dorsal to 7N neurons within the ventral PCRt, and the latter exhibiting a dorsally shifted cluster split between PCRt and the adjacent spinal trigeminal nucleus (SpV) (Fig. 5.7b; Fig. 5.9). MdV-projecting neurons were more evenly distributed within the latRM, but the highest neuronal density coincided with the spinally-projecting population. Contralaterally-projecting excitatory latRM neurons were also broadly distributed but with a more medial location of the highest density (Fig. 5.7b, Fig. 5.9). We determined the extent of overlap between spinally-, MdV- and contra-projecting excitatory latRM neurons and found that the majority was anatomically separate (Fig. 5.9b). Much higher overlap was found within the medRM for spinally- and MdV-projecting excitatory neurons, or when two retrograde viruses were co-injected into single target sites (Fig. 5.9c). Together, these findings demonstrate that within the latRM, anatomically largely distinct populations with different projection targets share a tight space, yet exhibiting spatial organization. Whereas spinally-projecting latRM neurons reside most ventrally and MdD-projecting latRM neurons locate towards the dorsal pole, MdV- and contralaterally projecting latRM neurons distribute more broadly throughout the territory (Fig. 5.7b; Fig. 5.9).

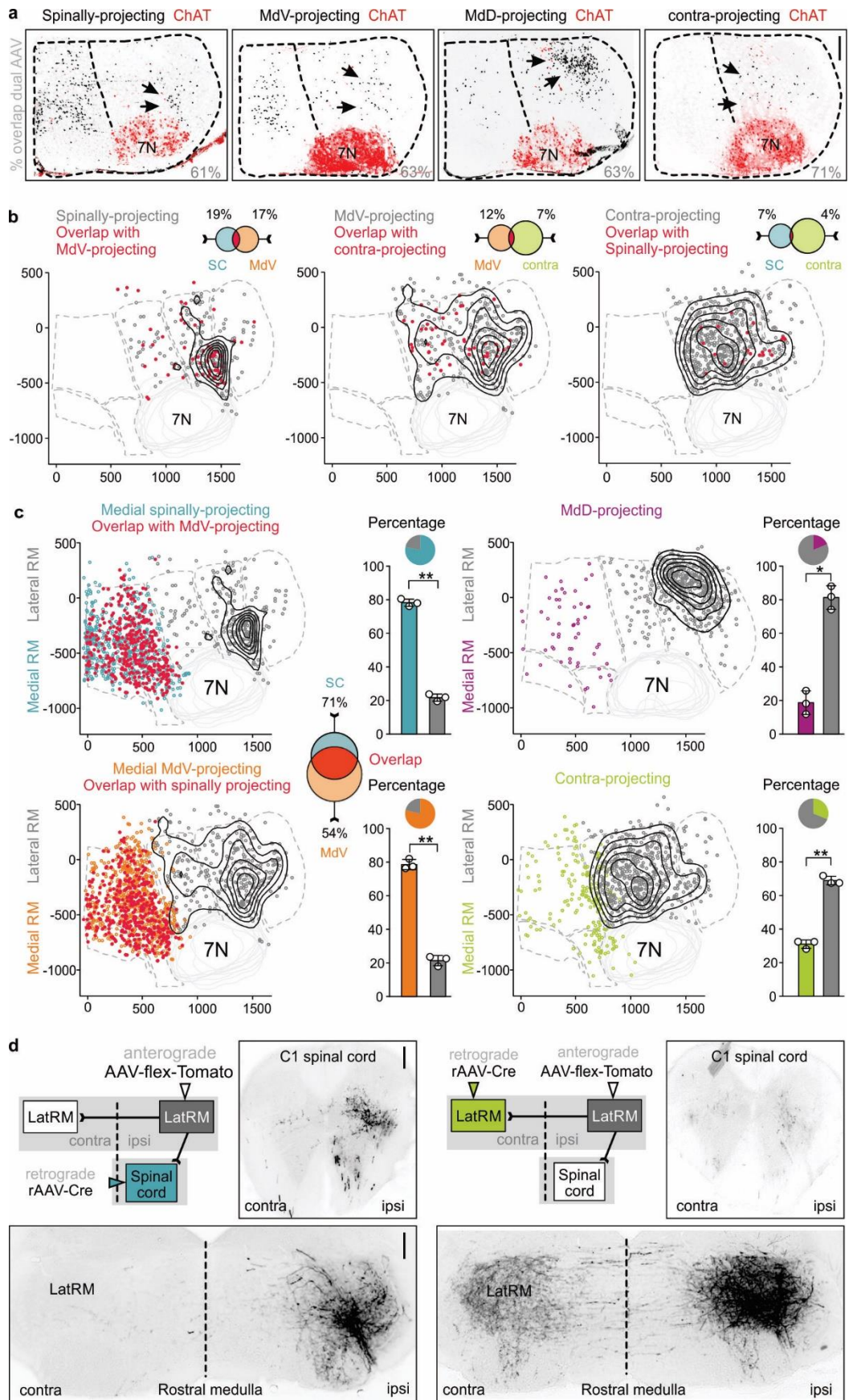


## Figure 5.9. Anatomical dissection of RM neurons based on projections

(a) Example pictures of retrogradely targeted excitatory latRM neurons from cervical spinal cord (from n=3), MdV- (from n=2), MdD- (from n=2) or contralateral (from n=3) latRM-centric injections counterstained with ChAT (red). Arrows point to cluster of neurons within the latRM, dotted vertical line depicts division between medRM and latRM. Numbers in grey shown in bottom right corner depict percentage overlap for co-injection of two retrograde AAVs into the corresponding output structure; scale bar = 250 $\mu$ m.

(b) Cellular overlap in excitatory latRM neurons retrogradely marked from triple injections in the cervical spinal cord, centered in MdV and in contralateral latRM, representative example shown. Note minor overlap between the three populations as indicated by the Venn diagrams (n = 3 mice; dots: position of individual neurons; red dots: overlap with other displayed population; contour lines: density for distribution).

(c) Analysis of fractions of excitatory RM neurons residing in medRM vs latRM for 4 analyzed populations shown in different colors (color code see Fig. 3, n = 3 mice from triple injections in the spinal cord, MdV-centric and contra latRM, n = 3 mice from MdD-centric), as well as overlap between excitatory medRM neurons retrogradely labeled from the cervical spinal cord and MdV-centric injections (red).

(d) Experiment combining retrograde targeting of latRM neurons with rAAV-Cre from the spinal cord (left; from n=3 independent replicates) or contralateral latRM (right; from n=2 independent replicates) with anterograde injections of AAV-flex-Tomato into ipsilateral latRM. Pictures demonstrate sparse projections of spinally-projecting latRM neurons to contralateral latRM (left), and sparse projections of contralaterally projecting latRM neurons to the spinal cord (right), visualizing Tomato immunofluorescence. Scale bar = 250 $\mu$ m.

Data are mean  $\pm$ SEM; \*P<0.05; \*\*P<0.01; two-sided paired t-test.

## Functional tuning in latRM populations

To determine whether excitatory neurons in the dorsal and ventral latRM exhibit differential neuronal activities during forelimb tasks, we acquired single unit data along different dorso-ventral latRM positions (Fig. 5.7c-e; Fig. 5.10). Aligning behaviorally-

defined windows with neuronal activity, we found that reaching-tuned neurons were much more prevalent for ventral than dorsal latRM recordings sessions. Conversely, latRM neurons from dorsal recording positions exhibited a significant bias towards handling-tuning compared to reaching (Fig. 5.7c-e; Fig. 5.10).

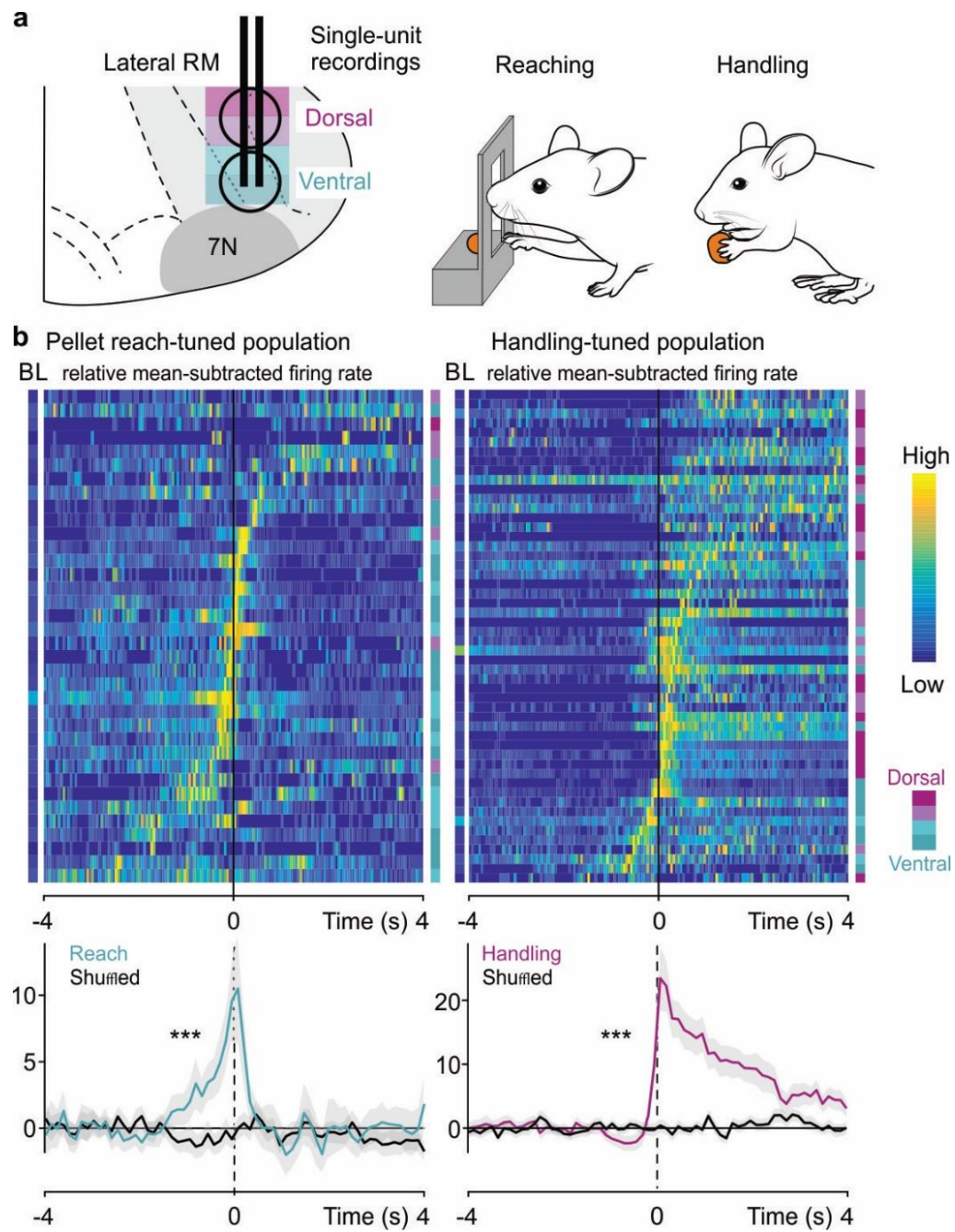


### **Figure 5.10 Analysis of activity along the dorso-ventral axis in latRM**

(a) Experimental scheme depicting recording in dorsal vs ventral latRM during pellet task, with the focus on reaching vs food handling as behaviors (magenta shades: dorsal recording sites; cyan shades: ventral recording sites).

(b) Pellet-reach tuned (left; n=36) and handling tuned (right; n=52) latRM population ordered by peak time of respective behavior onset. Dorso-ventral recording position (4 depth) are indicated to the right of plot by a color code. Bottom plots show average responses of all neurons as well as corresponding shuffled data. Color scale depicts Low (0) to High (1) for relative mean subtracted firing rate and Low (0Hz) to High (100Hz) for BL, baseline firing rate; grey shades:  $\pm$ SEM; \*\*\*P<0.001; Wilcoxon non-parametric signed rank test. Bonferroni correction was applied to account for multiple comparisons.

We next determined whether differential functional signatures in the dorsal and ventral latRM coincide to the activity of different populations stratified by axonal projection. We employed retrograde viral injections to selectively target the expression of GCamp7s to excitatory latRM neurons projecting either to the spinal cord or the MdD, residing in mostly ventral or dorsal latRM positions respectively (Fig. 5.7f; Fig. 5.11). We found that while the signal of spinally-projecting latRM neurons was upregulated preceding reaching, MdD-projecting populations showed preferential upregulation during handling after reaching (Fig. 5.7f; Fig. 5.11). These findings demonstrate that within the latRM, neurons tuned to the distinct forelimb-subfunctions reaching and handling map onto a dorso-ventral axis aligned with their axonal projections.

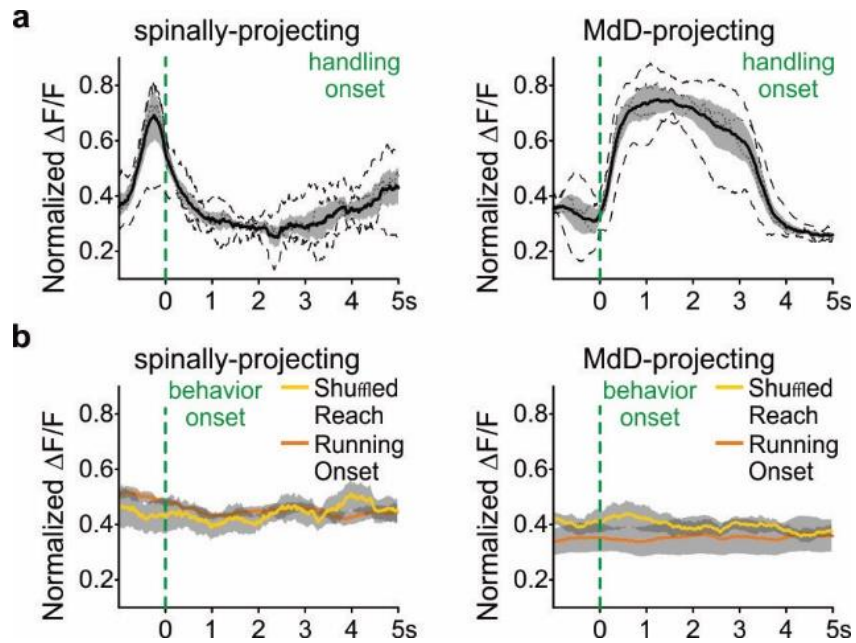


**Figure 5.11 Monitoring calcium activity from spinally- and MdD-projecting latRM neurons**

(a) Fiber photometry data analyzing the dynamics of calcium activity in excitatory latRM neurons retrogradely targeted from the cervical spinal cord ( $n = 4$  mice) and from MdD-centered injections ( $n = 4$  mice). Traces are aligned relative to handling onset (dotted line). Shades around mean of individual mice:  $\pm$ SEM.

(b) Average of mean dynamics of calcium activity for neurons shown in (a) during onset of locomotion trials (running,  $n = 4$  mice MdD-centered projections,  $n = 3$  mice spinal cord projections), or shuffled data (aligned to reaching onset,  $n = 4$  mice MdD centered projections,  $n = 4$  mice spinal cord projections). Shades around mean of individual mice:  $\pm$ SEM.

## LatRM neurons elicit forelimb behaviors

We next asked whether and what kind of behavior can be induced by optogenetic stimulation of excitatory latRM neuron populations identified by axonal targets. To contrast these latRM-centered experiments, we also probed spinally-projecting medRM neurons. We targeted RM neurons retrogradely using retAAV-(flex)-FLP-V5 injections in the different downstream targets of *vGlut2<sup>Cre</sup>* mice and injected a dual-recombinase activated AAV (Fenno *et al.*, 2014) expressing ReaChR into the RM with optic fiber placement dorsal to the mapped highest neuronal density location (Fig. 5.12a; Fig. 5.13a). To quantify the repertoire of behaviors elicited in these optogenetic stimulation experiments, we charted their nature and reliability for individual mice (Fig. 5.12b-d). We found that individual mice express stable behavioral phenotypes at high reliabilities (Fig. 5.12d). Moreover, the nature of the expressed phenotype was linked to the identity of the downstream target of the studied neuronal population, but we observed further behavioral diversity for experiments targeting MdV or MdD-projecting latRM neurons.

Optogenetic stimulation of spinally-projecting excitatory latRM neurons induced unilateral forelimb reaching, but not more complex forelimb movements involving digit flexure (Fig. 5.12b-d; Fig. 5.13). Electromyographic (EMG) recordings from biceps and triceps forelimb muscles showed that the same muscle activation sequence occurred during naturally-executed and optogenetically-induced forelimb reaching, albeit the latter at a faster time scale (Fig. 5.14) (Yakovenko, Krouchev and Drew, 2011). Moreover, although challenging due to the freely moving nature of our experiments, analysis of reaching trajectory endpoints showed higher similarity between trials of one mouse than to the trials of other mice (Fig. 5.12c; Fig. 5.13b), possibly indicating that the precise composition of the optogenetically-targeted ensemble is instrumental for behavioral nuances between animals. Stimulation of MdV-projecting latRM neurons elicited ipsilateral reach-to-grasp movements in a fraction of mice, characterized by the

supplementation of induced reaches by digit flexing/grasping, or ipsilateral forelimb tapping movements in the remaining mice of this category (Fig. 5.12b-d; Fig. 5.13b). In contrast, stimulation of MdD-projecting latRM neurons produced hand-to-mouth movements or grooming (Fig. 5.12b-d; Fig. 5.13). Stimulation of contralaterally-projecting excitatory latRM neurons did not induce obvious movements (Fig. 5.12d; Fig. 5.13). Strikingly, while behaviors elicited by latRM subpopulation stimulation all involved forelimb use, stimulation of medially-located spinally-projecting medRM neurons induced head-turning ipsilateral to implantation (Fig. 5.12d). These findings suggest a medio-lateral segregation of neuronal substrates for head-turning and forelimb movements within the RM in mice, perhaps distinct from cats where both elements seem to be located rather medially (Drew and Rossignol, 1990). Lastly, optogenetic stimulations of excitatory latRM neurons targeted by direct injection into the latRM elicited only simple ipsilateral forelimb movements including reaching and tapping-like behaviors. Thus, the successful production of behavioral diversity by latRM neurons is critically dependent on the specific latRM ensemble targeted for optogenetic stimulation experiments through their distinct axonal projections. Whether these latRM populations also exhibit differential roles in the execution of natural forelimb behaviors awaits the generation of viral tools for more complete retrograde targeting than currently possible.

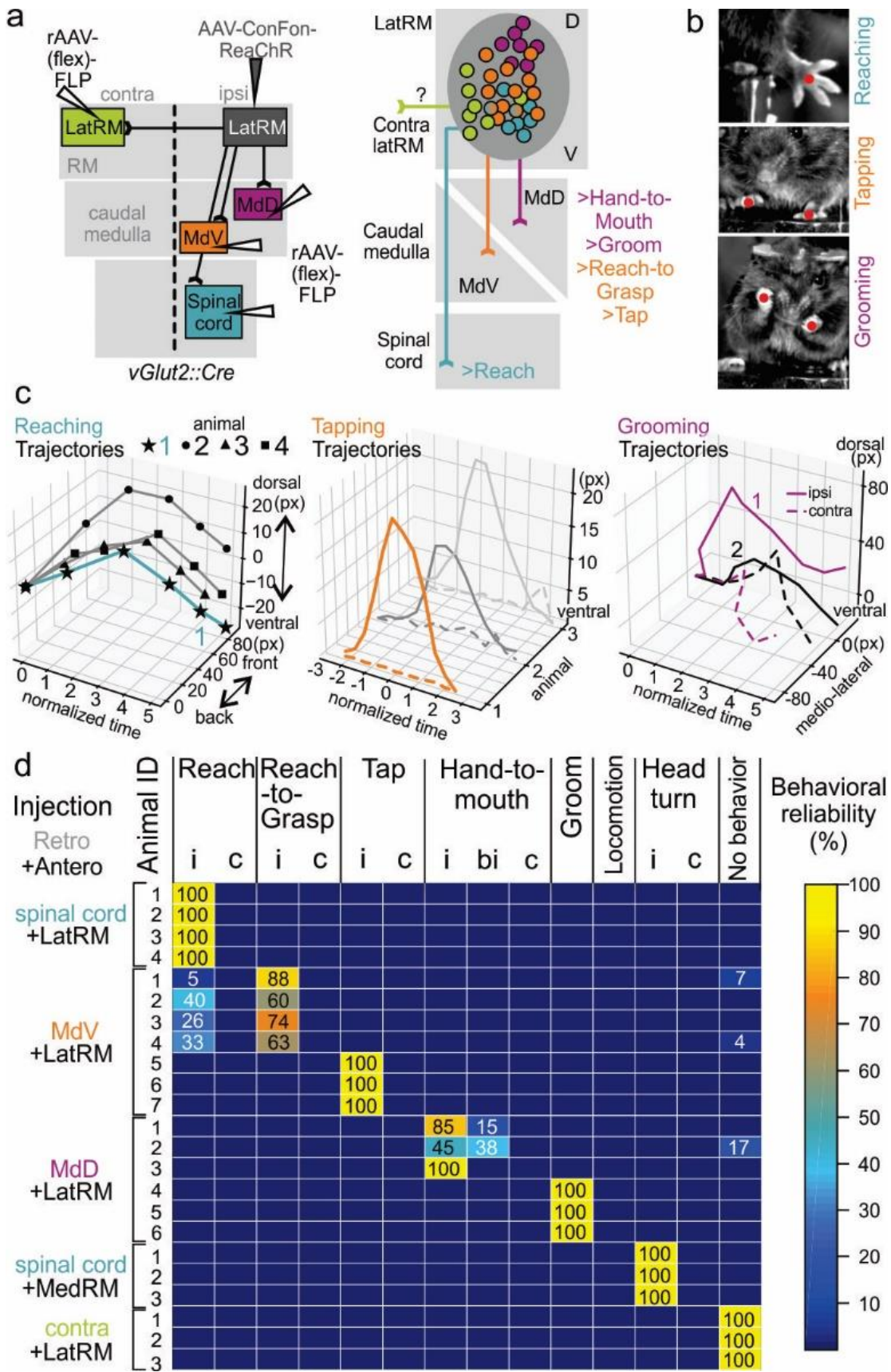


### Figure 5.12 Stimulation of latRM populations elicits specific forelimb movements

(a) Injection scheme for experimental design to optogenetically stimulate excitatory latRM neurons projecting to different downstream targets (left). Neurons were retrogradely targeted through spinal cord injections, MdV- or MdD-centered injections in the caudal medulla, or contralateral latRM-centered injections with rAAV-(flex)FLP in *vGlut2<sup>Cre</sup>* mice, combined with ipsilateral latRM-centered AAV-ConFon-ReaChR injections to target latRM neurons co-expressing Cre and FLP. (right) Summary diagram displays the alignment between identity of excitatory latRM neuron population by projection target and observed behaviors. Stimulation of latRM neurons engaging circuits in the caudal medulla elicit more complex forelimb movements involving digits than stimulation of excitatory latRM neurons directly engaging spinal circuits.

(b) Spatio-temporal analysis of optogenetically-induced movements using DeepLabCut. Data depicts example pictures from movies of different behaviors as indicated, including DeepLabCut tracked positions (red dots).

(c) Average trajectories of DeepLabCut-tracked, optogenetically-induced reaching (left, n=4 mice), tapping (middle, n=3 mice) and grooming (right, n=2 mice; solid and dotted lines indicate the trajectory of ipsi- and contralateral forelimb during grooming respectively).

(d) Chart displaying behavioral repertoire of mice included in the optogenetic stimulation dataset. Animal ID on the left is stratified by injection sites for retrograde (rAAV-(flex)FLP) and anterograde (AAV-ConFon-ReaChR) AAVs. Vertical columns depict observed behaviors, using a color scale for behavioral reliability (0-100%), summing up to 100% for all columns.

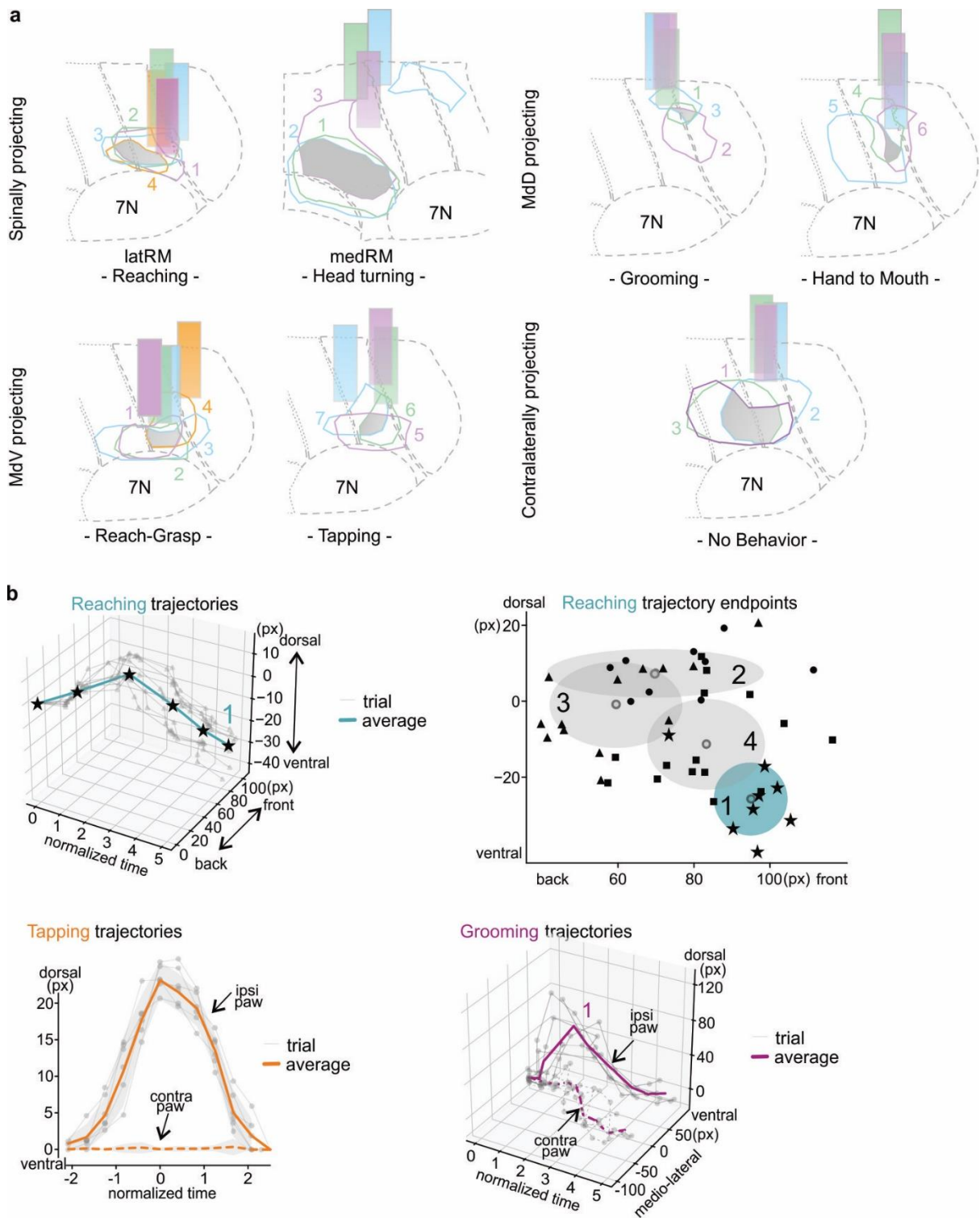


**Figure 5.13 Optogenetic activation of RM subpopulations**

(a) Reconstruction of fiber placements and local virus expression sites at the RM level. Each color corresponds to one mouse included in the analysis shown in Fig. 4 (code corresponds to mouse ID number shown in Fig. 4d).

(b) Spatio-temporal analysis of optogenetically-induced movements using DeepLabCut. Data depicts reaching trajectories (top, left) of different stimulation trials (grey lines) in one mouse (average: cyan), and the lateral view of the trajectory endpoints of reaching mice shown in Fig. 4c using a side-camera (top, right; see methods for details). Also shown are trajectories of different stimulation trials reconstructed for forepaws ipsi- and contralateral to stimulation during optogenetically-induced tapping (bottom left; average: orange; grey shade:  $\pm$ SD) or grooming (bottom right; average: purple).

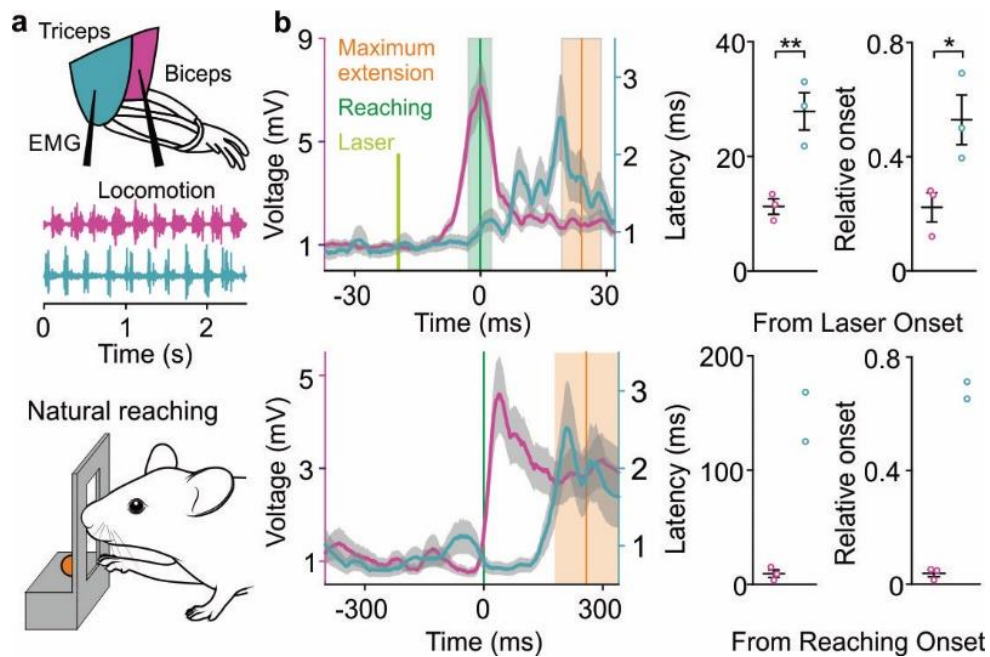


**Figure 5.14 Stimulation of spinally-projecting excitatory latRM neurons recruits forelimb muscles in a sequence resembling natural reaching**

(a) Scheme depicting implantation of EMGs into forelimb biceps and triceps muscles, and below raw signal demonstrating that these muscles are active in alternation during natural locomotion, according to their flexor (biceps) and extensor (triceps) function.

(b) EMG recordings and quantification (latency, relative onset) for biceps and triceps recordings during optogenetically induced reaching by stimulation of spinally-projecting excitatory latRM neurons (top; n=3 mice for biceps and triceps) or natural reaching (bottom; 0=reaching onset; n = 3 mice for biceps and n = 2 mice for triceps).

Grey shades:  $\pm$ SEM; \*P<0.05; \*\*P<0.01; two-sided paired t-test.

## 5.4 Discussion

Our work describes the brainstem's latRM as a critical orchestrator for the execution of skilled forelimb movements. Here we discuss models of how complex skilled forelimb movements may be regulated by combinatorial usage of specific brainstem-to-spinal cord and intra-brainstem circuits. We found that latRM neurons divide into at least four anatomically distinct populations by axonal targets. Initiation of most skilled forelimb movements requires the transport of one or both hands to the site of action, commonly referred to as forelimb reaching. Optogenetic stimulation of the spinally-projecting latRM subpopulation elicits unilateral reaching. In agreement, latRM neurons exhibit preferential projections to the ipsilateral rostral cervical spinal cord, harboring circuits for proximal forelimb muscle control. Strikingly, latRM neurons with direct spinal projections are not sufficient to elicit more complex forelimb movements than reaching. Excitatory latRM neurons projecting to the caudal medulla signal and can generate diverse complex forelimb movements, involving digit use during grasping and/or action bilateralization during grooming or hand-to-mouth movements. These diverse forelimb behaviors are stably expressed in individual mice in a "winner-take-it-all" fashion, likely due to targeting of specific neuronal ensembles through retrograde axonal infection, instrumental to obtain behavioral diversity through optogenetic probing. Caudal medullary neurons then establish functional links to the caudal cervical spinal cord essential to generate distal forelimb movements (Esposito, Capelli and Arber, 2014), likely involving propriospinal neurons with direct connections to motor neurons (Alstermark and Isa, 2012; Pivetta *et al.*, 2014).

Our work uncovers the existence and organization of brainstem circuits encompassing task- and action phase selective neuronal ensembles in the rostral medulla. Notably, shared latRM neuronal ensembles are engaged during related forelimb actions (i.e.

reaching in different forelimb behaviors), while distinct ensembles are used for dissimilar forelimb movements (i.e. reaching vs food handling). No significant encoding in the latRM is observed for locomotion. The here-described circuit elements are therefore non-overlapping with pathways implementing full-body movements including locomotion (Shik and Orlovsky, 1976; Roseberry *et al.*, 2016; Capelli *et al.*, 2017; Caggiano *et al.*, 2018), engaging the same muscles but in an entirely different task and context. These findings resonate with recent work in the striatum, where closer actions are also encoded by overlapping neuronal ensembles, while distant actions engage distinct ensembles (Barbera *et al.*, 2016; Klaus *et al.*, 2017; Parker *et al.*, 2018). In the striatum, these ensembles are found in common overall space, while our findings demonstrate that anatomical de-mixing of signals for locomotion and skilled forelimb movements has occurred within brainstem circuits. The here identified brainstem neuronal populations are in a prime position to integrate cortical and other brain-wide directional signals and transmit them for precise forelimb execution to the spinal cord. Even beyond its role in execution of forelimb movements, the lateral brainstem is a complex integration hub for higher motor centers also engaged in regulating orofacial behaviors (Han *et al.*, 2017; Svoboda and Li, 2018; Mercer Lindsay *et al.*, 2019; Petersen, 2019; Ruder and Arber, 2019), suggesting additional integration and coordination in this area. The discovery that neuronal segregation by task-specificity in action space exists in the most caudal part of the brain, and that identified brainstem neurons together are needed to implement different aspects of skilled forelimb movements provides a deep understanding of how body actions employing limbs are regulated through the use of dedicated neuronal circuits.

## 5.5 Methods

### Mice

We used *vGlut2<sup>Cre</sup>* mice (RRID: IMSR\_JAX:028863) (Vong *et al.*, 2011)<sup>48</sup> maintained on a mixed genetic background (129/C57Bl6). Experimental mice originating from different litters were used in individual experiments. No criteria were applied to allocate mice to experimental groups, and mice had marks for unique identification. For all behavioral experiments, we used 2-4 month-old heterozygous males, backcrossed to C57Bl6. For anatomical experiments, both male and female mice were used. Mice were maintained on a 12 hours light-dark cycle in a temperature (22±1°C) and humidity controlled (45-65%) environment. Housing, surgery procedures, behavioral experiments and euthanasia were performed in compliance with the Swiss Veterinary Law guidelines.

### Virus production, injections and implantations

We used the following, previously described adeno-associated viruses (AAV), all based on a backbone derived from Allen Brain (AAV-CAG-flex-tdTomato-WPRE-bGH): AAV-flex-SynGFP and AAV-flex-SynMyc, referred to as AAV-flex-SynTag, AAV-flex-DTR as well as AAV-flex-Flp-H2B-V5 and AAV-H2B-10xMyc (Esposito, Capelli and Arber, 2014; Pivetta *et al.*, 2014; Takeoka *et al.*, 2014; Capelli *et al.*, 2017). Not previously reported viral constructs were designed in analogy to above constructs: AAV-flex-H2B-GFP, AAV-flex-H2B-TdTomato, AAV-flex-H2B-V5 (referred to as AAV-flex-nTag), AAV-flex-hM4Di-Tomato, AAV-flex-GCaMP7s (Dana *et al.*, 2019) and AAV-Flp-H2B-V5. The AAV-ConFon-ReaChR-Citrine-YFP construct was created using a previously described strategy (Fenno *et al.*, 2014). To infect neuronal cell bodies but not axons, a serotype plasmid 2.9 was used as in previous studies (Esposito, Capelli and Arber, 2014; Pivetta *et al.*, 2014; Basaldella *et al.*, 2015). For retrograde labeling by means of axonal infection,

a rAAV2-retro capsid plasmid (Tervo *et al.*, 2016) was used for coating as described before (Capelli *et al.*, 2017). AAVs used in this study were of genomic titers  $>1 \times 10^{13}$  and produced following standard protocols.

Viruses were injected into the brainstem with high precision stereotaxic instruments (Kopf Instruments, Model 1900) under isoflurane anesthesia as previously described (Esposito, Capelli and Arber, 2014; Capelli *et al.*, 2017). Viral injections in the spinal cord were targeted to the cervical spinal cord comprising spinal segments C1-C5 (approximate injection volume: 300-500nl). The following coordinates were used to target the investigated brainstem regions referenced with lambda as the point of origin for anterior-posterior (AP), medio-lateral (ML) and dorso-ventral (DV) axis (AP; ML; DV; in mm; approximate injection volumes: 50-100nl): latRM (-1.4;  $\pm 1.55$ ; -4.8); MdV (-3.0;  $\pm 0.6$ ; -5.5); MdD (-3.0;  $\pm 1.4$ ; -5.3); latRM dorsal (-1.4;  $\pm 1.55$ ; -4.3); medRM (-1.4;  $\pm 0.5$ ; -4.8). To map output projections of excitatory latRM neurons, we injected AAV-flex-SynTag and waited  $>2$  weeks for expression. Retrograde tracings of latRM outputs using retro-flex-nTag viruses were carried out by injections in the spinal cord before brainstem injections. After the last injection, we waited for  $>10$  days. Triple injections were performed for the combination of spinal cord, MdV and contralateral latRM. MdD injections were performed in separate experiments. For co-injections into single target regions, viruses were mixed before injection. Injections to bilaterally target excitatory latRM neurons for loss-of-function experiments were carried out  $>2$  weeks before baseline reaching success rates were assessed or handling proficiency was assayed, to allow for sufficient time for expression of hM4Di. CNO (Tocris, Cat. No. 4936) was injected intraperitoneally at 10 mg/kg body weight in PBS to initiate attenuation of neuronal firing upon interaction with the hM4Di receptor (Armbruster *et al.*, 2007; Caggiano *et al.*, 2018). For mice expressing DTR in excitatory latRM neurons, diphtheria toxin (Sigma D0564) was administered intraperitoneally (100 ng per g body weight) after

baseline behaviors were recorded. For optogenetic activation of selected neuronal subpopulations, injections involving the cervical spinal cord were conducted first, as described above and using retro-(flex)-Flp-H2B-V5. Subsequently, the latRM was injected unilaterally with AAV-ConFon-ReaChR-Citrine-YFP and an optic fiber was implanted 200 $\mu$ m above the injection site (diameter: 200 $\mu$ m: MFC\_200/230-0.48\_6mm\_ZF1.25\_FLT Mono Fiberoptic Cannula; Doric lenses). For all other subpopulations stratified by projections involving targets in the brainstem (contralateral latRM, MdV, MdD), injections and implantations were only targeted to the brainstem. For fiber photometry experiments, the optic fiber was implanted 100 $\mu$ m above the neuronal population of interest (diameter: 200 $\mu$ m: MFC\_200/230-0.48\_6mm\_ZF1.25\_FLT Mono Fiberoptic Cannula; Doric lenses). For electrophysiological recordings, single-shank chronic 16-channel or dual-shank chronic 32-channel silicon probes were implanted (Cambridge NeuroTech Inc., P-series, 6mm length). These were mounted on a nanodrive (Cambridge NeuroTech Inc.) allowing for sequential recordings at different depths and implanted in the latRM (AP and ML coordinates as for virus injections) at a dorsal-ventral depth of around -3.0 mm using light curable cement (Relyx Unicem 2, 3M Inc.). Stimulation experiments were started >2 weeks after injection and implantation. We assessed injection sites after termination of experiments by using ChAT immunohistochemistry (see immunohistochemistry and microscopy section) to visualize motor nuclei. For electrophysiological recordings, we also visualized the site of electrical lesion at the end of the recordings to confirm correct probe placement. The mouse brain atlas was used as reference for determining the spatial injection specificity of the viral labeling<sup>29</sup>. For optogenetic activation experiments with latRM and medRM subpopulations, we mapped fiber placement as well as the extent of targeted neurons at injection sites. Only mice with confirmed anatomical precision were included in the subsequent analysis. The region here referred to as latRM combines sites of the brainstem regions indicated as IRt, PCRt and SpV in the rostral part of the medulla

spanning the rostro-caudal extent of the facial motor nucleus (7N). The rostro-caudally aligned region medial to latRM is referred to as medRM. For MdV and MdD nomenclature, we followed the boundaries delineated in the mouse brain atlas (Franklin K.B. and Paxinos G., 2007).

### **Electrophysiological recordings**

Following surgery (see virus production, injections and implantations), the probe was lowered during subsequent days to the starting position in the latRM. After every recording session, the probe was lowered by 100-200 $\mu$ m to record along the dorso-ventral axis of the latRM to finally reach the position in the facial nucleus (7N, DV: -5.0 mm from the brain surface) on the last experimental day. For recordings specifically focusing on DV position analysis, the electrode was lowered in steps of 200 $\mu$ m, spanning the LatRM DV axis in four steps (the first two grouped as dorsal indicated by shades of magenta and second two grouped as ventral indicated by shades of cyan in the corresponding Figure panels). Electrical lesions (3s at 200  $\mu$ A) shortly before perfusions were performed to confirm recording locations (see Fig. 5.2) using an electrical stimulator (WPI Inc., Stimulus isolator A360). The extracellular signal was amplified and acquired at 40 kHz using a commercially available soft- and hardware recording system (OmniPlex, Plexon Inc.). Filtered, continuous data from each recording session consisting of all behavioral tasks carried out within this session was grouped into adjacent, fictive tetrodes and sorted manually in tetrode mode, using commercially available software (Offline Sorter v3.3.5, Plexon Inc.). Autocorrelation, high-relative signal to noise-ratios as well as waveform comparison were used to ensure high-quality data using commercially available software (NeuroExplorer v5, Plexon Inc.) (Fig. 5.2e). Further cross-correlation between channels ensured the elimination of units recorded at multiple recording sites. For recordings comparing multiple behaviors (see behavioral experiments section), we recorded a total of 243 neurons in the lever task, 212 neurons

during pellet reaching and handling and 198 neurons during open field behavior, totaling 246 neurons across all behaviors and 194 neurons that were stable and reliably present across all behaviors in 5 mice (see Fig. 5.2a). For recordings assessing differential encoding along the dorso-ventral axis and distinct response properties depending on medio-lateral reaching direction (see behavioral experiments section), we recorded a total of 144 neurons in 2 mice. Sorted, single-unit data and spiking timepoints were used for further analysis on other freely moving behaviors (see behavioral experiment and analysis section).

### **Electromyographic recordings**

For electromyographic (EMG) recordings during stimulation of spinally-projecting latRM neurons, injections and fiber implantation were conducted as described (see virus production, injections and implantations). Cable preparation and EMG implantation of the biceps and triceps muscle were conducted as previously reported (Miri *et al.*, 2017). Acquisition was carried out either in response to optogenetic stimulation (see optogenetic activation experiments) or during pellet reaching (see pellet reaching task). The signal was amplified and bandpass filtered (A-M systems 1700, gain 100, bandpass 100-1000 Hz) and acquired using a plexon recording system (Omniplex, Plexon Inc.) at 5000 Hz. We subsequently applied a mean subtraction to correct for the DC offset.

### **Photometry recordings**

Recordings of calcium activity started two weeks after surgery, employing a Multi Fiber Photometry system (CineLyzer, Plexon Inc.). Implants were connected to the system through a customized patch cord (Doric Lenses) to simultaneously allow for delivery of excitation light (470nm Plexon Inc.) and collection of GCaMP emission at 60 Hz. A continuous excitation intensity of 30–40  $\mu$ W was used for all experiments, measured as

described (see optogenetic activation experiments). Experimental sessions were repeated to collect at least 10 successful, first reaching trials (see behavioral experiments, pellet task).

### **Immunohistochemistry and microscopy**

Immunohistochemistry to visualize virally expressed transgenes was performed on all mice used in this study. This included mice from anatomical and behavioral experiments. Mice were anesthetized using a Ketamine-Xylazine solution before trans-cardial perfusion with cold phosphate buffer saline (PBS) and subsequent fixation using a 4% paraformaldehyde (PFA) solution (Sigma). Brains and spinal cords were carefully dissected and post-fixated with PFA for >8 hours following perfusion. To cryopreserve the tissue, we incubated brains and spinal cord in a 30% sucrose w/vol/PBS solution for at least one day. We cut 80µm thick slices on a cryostat, collected sections sequentially into individual wells (coronally for brain tissue and transversely for spinal cord). Following a one-hour incubation in blocking solution (1% BSA/0.2% TritonX100/PBS), we added primary antibodies diluted in blocking solution for 1-3 days of incubation at 4°C. Secondary antibodies coupled to standard fluorophores (Jackson or Invitrogen) were used for one-day incubations at 4°C, after extensive washing of tissue sections. After final washing, we mounted sections on glass slides with anti-bleach preservative medium in sequential order along the rostro-caudal axis. Primary antibodies used in this study were: chicken anti-GFP (Invitrogen, 1:2000), chicken anti-Myc (Invitrogen, 1:5000), goat anti-ChAT (Millipore, 1:500), mouse anti-Myc (ATCC, 1:100), mouse anti-V5 (Invitrogen, 1:1000) and rabbit anti-RFP (Rockland, 1:5000). Secondary antibodies used were: Alexa Fluor 488 donkey anti chicken IgY (Jackson, 1:1000), Cy3 donkey anti mouse IgG

(Jackson, 1:1000), Cy3 donkey anti rabbit IgG (Jackson, 1:1000), Alexa Fluor 488 donkey anti goat (Jackson, 1:1000), Cy3 donkey anti goat IgG (Jackson, 1:1000), Alexa Fluor 647 donkey anti goat IgG (Jackson, 1:1000). To acquire low-resolution overview images, we used an Axioscan light microscope (Zeiss, 5x objective) and for higher resolution imaging, we used a FV1000 confocal microscope (Olympus) or a custom-made spinning disk microscope (Visitron Inc.).

### **Anatomical reconstructions**

Three-dimensional reconstructions of RM neurons stratified by projection target: To assess the spatial location, quantitative contributions and overlap between populations of RM neurons projecting to the contralateral latRM, ipsilateral MdV, ipsilateral MdD and spinal cord, 80 $\mu$ m thick coronal brainstem sections were acquired with the 20x objective of a FV1000 confocal microscope (Olympus), tiling mosaics of multiple fields of view (tile number was variable depending on section size at different rostro-caudal levels) in order to cover the full section (z-step: 4 $\mu$ m). Subsequent stitching and maximum intensity projection images were used as previously described<sup>4,21</sup>. Manual alignment using Amira (Thermo Fisher Scientific Inc.) preceded automatic cell body position assignment with customized image analysis workflows in Knime. Respective regions were assigned using the mouse brain atlas as described above (see also virus production and injection section). 2-D density plots were generated using 2d-kernel density estimate plotting 6 density lines covering the space of 20–100% of highest density equally using the MATLAB function kde2d (Botev Z.I., Grotowski J.F. and Kroese D.P., 2010).

Reconstructions of synaptic output of excitatory latRM neurons: To assess major output projections of excitatory latRM neurons, 80 $\mu$ m thick coronal brainstem sections or

transverse spinal cord sections were acquired with a 40x objective of a confocal microscope (FV 1000, Olympus) or a custom-made spinning disk microscope (Visitron Inc.), tiling mosaics of multiple fields of view (z-step = 2 $\mu$ m). Subsequent stitching and maximum intensity projection images were generated using custom-made macros in Fiji. Automatic synaptic spot detection was carried out in Imaris (v9.1.2. Oxford Instruments, Bitplane) and 2-D density plots were generated using 2d-kernel density estimate plotting 6 density lines covering the space of 10-100% of highest density equally using the MATLAB function kde2d. To assess the decrease of synapses derived from excitatory latRM neurons along the rostro-caudal axis in the spinal cord, the total number of detected synapses at C1 was used as a reference to calculate the decrease in synaptic numbers at C5 and C8 levels.

### **Behavioral experiments**

Open Field Assay: Mice were placed in a 35 x 35 cm square arena which they were allowed to explore freely for at least 10 min. For single-unit recording experiments, mice were exposed to tasks in a sequential manner, including the open field assay at the end. For loss-of-function and photometry experiments, open field sessions were carried out after the experimental days during which the pellet task was completed.

### Lever Task:

Mice were kept under water restriction and body weight was monitored to not drop below 85% of the original weight. We used a custom-made behavioral chamber allowing for high-speed videography from the two sides of an ultra-sensitive lever (2g sensitivity, MedAssociates Inc.) adapted from previous work (Jin and Costa, 2010). Water rewards (50 $\mu$ l) were delivered in the chamber at a spatially separate location from the lever in response to single lever presses using electrically controllable water pumps

(MedAssociates Inc.). Training consisted of exposure to the behavioral box during 3 training days for a maximum of 60 minutes or 5 (day 1), 10 (day 2) or 20 (day 3) rewards. Experiments with mice that did not achieve at least 20 rewards on the 4<sup>th</sup> training day were not continued. Selected mice were then trained to reliably achieve at least 20 rewards by pressing the lever during at least 4 more training sessions. The entire training did not exceed 2 weeks. For analysis, only first attempt forelimb lever presses (see behavioral analysis) were used. During experimental sessions, mice were allowed to press the lever for as long as they were engaged in the task to achieve a maximum number of successful trials for analysis. The protocol was applied in closed-loop using an Arduino Uno board (Arduino Inc.) coupled with TTL pulses recording lever press timepoints and triggering water rewards via the Arduino MATLAB extension package (The Mathworks Inc.). A synchronizing start TTL pulse was sent from the Arduino Uno board to the OmniPlex recording system to allow for correct alignment of behavioral with electrophysiological data.

#### Pellet Task:

Mice were kept under food restriction and body weight was monitored to not drop below 85% of the original weight. A custom-made chamber was designed as previously reported (Xu *et al.*, 2009; Esposito, Capelli and Arber, 2014), containing a slit through which mice are trained to reach for a food reward. Movies were taken using one camera from the front and one from the side (Pike, Allied Vision Inc., 200 fps) or only a side camera for photometry experiments (Plexon Inc, 60 fps). On the first day, mice were allowed to also obtain food pellets with their tongue. On following days, food pellets were placed at a marked, consistent position outside the slit further away, to not allow for tongue retrievals to enforce forelimb reaching trials. The position of the pellet was slightly moved to the side relative to the slit, depending on whether mice were right- or left-handed. Mice were trained for at least 8 days aiming for a success rate of > 30% and

with a goal of retrieving >15 pellets or 35 reaches. For loss-of-function experiments, mice with a baseline success rate of <30% were excluded. Following the baseline session, mice were injected intraperitoneally first with CNO (10 mg/kg body weight in PBS) and then with PBS, spaced by at least 24 hours from each other, followed by another analogous exposure paradigm. CNO or PBS injections occurred 40 minutes prior to initiation of the pellet task. For single-unit recordings, mice were exposed to other behavioral tasks consecutively and no success rate exclusion rate was applied. For photometry experiments, mice were exposed to the pellet task and subsequent food handling. For analysis, only successful, first attempt forelimb reaches (see behavioral analysis) were used. For the two-choice pellet reaching task and recordings along the dorso-ventral axis, mice were first trained the same way for 3 sessions with only one slightly shifted pellet position. From the 4<sup>th</sup> training session onward, a second pellet was placed exactly in the middle at the same distance, aligned with the slit. Mice were trained to reach for both positions to retrieve pellets for at least another 12 sessions before silicon probe implantation. During experimental sessions, mice were allowed to reach for as long as they were engaged in the task to achieve a maximum number of successful trials for analysis. For analysis along the dorso-ventral axis, medial and lateral reaches were pooled into one reaching category (see electrophysiological analysis section).

#### Handling Task:

Mice were kept under food restriction as described above (pellet task). During habituation, they were provided with short spaghetti sticks in the home cage and exposed to the testing chamber (10 min, once a day for 2 days). For loss of function experiments, the testing chamber was a 8.2cm by 7.1cm custom-made plexiglass box with transparent floor, mounted on a holder containing a 45° inclined mirror, allowing for a bottom view of the paws during pasta handling. Movies were taken using one camera from the front and one directed at the mirror (Pike, Allied Vision Inc., 200 fps). During behavioral testing (20

min session), spaghetti sticks (~2 cm length) were presented, upon which mice started bilateral handling as previously reported (Tennant *et al.*, 2010). For data analysis of electrophysiological data, additionally, successful trials in the pellet task resulted in the retrieval of food pellets, thereafter handled with both hands, resulting in qualitatively similar movements as during spaghetti handling. These trials were pooled for analysis.

Grip Strength Analysis: Forelimb grip strength of mice was tested as previously described (Esposito, Capelli and Arber, 2014).

#### Optogenetic Activation Experiments:

Optogenetic activation of RM neurons was performed using a PlexBright Optogenetic Stimulation System (Plexon Inc.) in combination with laser stimulation (Cobolt 06-MLD; 473nm; 100mW). The laser was triggered manually when mice were at rest. Unless otherwise specified, we used continuous light exposure at intensities of 5 or 10 mW. We measured the laser intensity at the beginning of every experimental session at the tip of an optic fiber of the same length as the one implanted to ensure precise and reliable stimulation strength with an optical power meter (Thorlabs Inc.). Mouse behaviors and responses were monitored simultaneously with two cameras (Pike, Allied Vision Inc.) at 200 frames/sec or a Sony alpha 7s camera (Sony Inc.) at 100 fps in an open field environment. For trajectory reconstructions with DeepLabCut (Mathis *et al.*, 2018; Nath *et al.*, 2019) (see behavioral analysis section) high-frame rate videos (uEyeCP, IDS Inc., 450 – 668 fps) were acquired to allow for successful tracking.

#### **Behavioral analysis, scripts and statistics**

### Open Field Assay:

To quantify basic locomotor parameters in the open field, videos acquired from above (Pike, Allied Vision Inc., 200 fps or an integrated camera for photometry, 60 fps, Plexon Inc.) were used. Mice were placed in a square arena (35 x 35 cm) within a noise-isolated chamber for 10 minutes. Center-of-mass body tracking was performed using the CinePlexStudio tracking function (CinePlexStudio v3.7.1. Plexon Inc.) and speed values were calculated from extracted coordinates on a frame-by-frame basis. Whole body and speed traces were clustered into defined locomotor bouts (>5cm/s for >200msec) and for analysis of loss-of-function experiments, maximum speed (highest single speed value during a locomotor bout), bout duration and bout distance parameters were calculated using custom-written MATLAB scripts. For electrophysiological recording and photometry experiments, locomotor bout start- and end-points were extracted and aligned with single-unit activity data, as detailed in the electrophysiology analysis section. To determine the timing of locomotion swing phase, we annotated ipsilateral forelimb footfalls during open field locomotion, and used the time window -0.1 sec prior to footfall for analysis. Since forelimbs were often not discernible on the recorded top-camera videos, we also used coincidence of diagonal hindlimb footfall data for annotation of forelimb data, a behavioral feature confirmed by video analysis using top and bottom cameras in another dataset.

### Lever Task:

Lever reaching behavior was recorded using high-speed videography from both sides of the lever (Pike, Allied Vision Inc., 200 fps). Video capture was triggered synchronized with electrophysiology measurements using commercially available software (OmniPlex, Plexon Inc.). Relevant behavioral timepoints were extracted manually using CinePlexEditor (v3.6.0, Plexon Inc.). Definition of the behavioral timepoints was as follows: Arrival: Timepoints when the mouse was present and attending in front of the

lever were defined as arrival. Reaching start: Video frame, in which the forepaw was first observed to lift off the ground or start to move towards the lever from an already slightly lifted position was defined as reaching start. Lever on and off: The first frame, in which the paw touched the lever was defined as the onset of the lever phase and the last frame, in which the paw was still observed on the lever as the offset. Retraction end: After retrieving the paw from the lever, the last video frame in which the paw was observed in a retraction movement before being placed on the ground or slightly stopped above in the air was defined as the end of retraction. For electrophysiological analysis, only first-attempt lever pressing sequences were analyzed. Secondary lever pressing sequences (i.e. the immediate initiation of another lever pressing sequence after the first attempt) were not used for electrophysiological analysis to ensure minimal trial-to-trial variability. These extracted timepoints were then used for analysis and alignment with electrophysiology data as detailed in the electrophysiology analysis section.

#### Pellet Task:

Movies taken from the front and side (Pike, Allied Vision Inc., 200 fps) were used for manual assignment of behavioral timepoints and for coordinate extraction using CinePlexEditor (v3.6.0, Plexon Inc.) or MATLAB (The Mathworks Inc.). Synchronization of movies with electrophysiological and fiber photometry data was achieved using commercially available software (Omniplex, Plexon Inc.). Movies for photometry experiments were acquired using a system-integrated camera from the side (Plexon Inc.) acquiring at 60fps allowing for precise alignment with calcium transients. For loss-of-function experiments assessing reaching behavior, success rate was defined as the fraction of successful trials of all reaching attempts when a pellet was presented. Single reaching attempts were defined as whenever the tip of the fingers exited and re-entered the slit opening of the pellet reaching box. Successful trials were defined as the complete successful behavioral sequence composed of reaching for, grasping and retrieving a

pellet to the inside of the pellet reaching box. We defined “miss trials” as trials during which the mouse missed to touch the pellet during reaching. To assess directionality defects, the spatial location of the hand at the most extended timepoint was registered in camera pixel coordinates from both the side and front camera and used for plotting and quantification of the endpoint variability and distance from the pellet using MATLAB. Pixel coordinates were first normalized to a defined spatial constant at the behavioral box and then to the pellet position itself to correct for any potential trial-to-trial effects in pellet or camera positioning. Variability was defined as the area of the ellipse with x and y-diameters defined as the average standard deviation of all endpoint coordinates in the x and y-direction in pixels respectively. Distance was defined as the average pixel distance of all the endpoints from the pellet position. For single-unit electrophysiology, behavioral timepoints were defined as follows: Reaching start: Video frame, in which the forepaw was first observed to lift off the ground or start to move towards the slit from an already slightly lifted position was defined as reaching start. Grasping: Timepoints when the fingers started to spread in anticipation of the grasping for the pellet were defined as the onset of the grasping movement. Timepoints during which the pellet is firmly grasped and the retraction sequence initiated were defined as the endpoints of grasping. This coincided often but not always with paw supination. Retraction end: After grasping the pellet, the hand is transported towards the mouth. Timepoints at which the pellet arrived at the mouth were defined as retraction endpoints. For electrophysiological and fiber photometry analysis, only first-attempt successful reaching sequences were analyzed. Unsuccessful or secondary, successful reaching sequences (i.e. the immediate initiation of another reaching sequence after an unsuccessful attempt) were not used for electrophysiological and fiber photometry analysis to ensure minimal trial-to-trial variability. Sessions during which mice achieved <4 successful reaching sequences as defined above were excluded. Further analysis was conducted as detailed in the electrophysiological or fiber photometry analysis section.

### Handling Task:

Handling episodes were recorded using high-speed videography (for electrophysiology, Pike, Allied Vision Inc., 200 fps for photometry, integrated camera, 60 fps, Plexon Inc.) and behavioral timepoints were defined using CinePlexEditor (v3.6.0, Plexon Inc.) or MATLAB (The Mathworks Inc.) as follows. Handling start was defined as the timepoint when both forelimbs arrived at the mouth before stereotypic, coordinated handling was initiated. The end of the handling was defined as the video frame when both forelimbs retrieve from the mouth and stop any subsequent food handling. Synchronization with electrophysiological and photometry data was achieved through commercially available software (Omniplex, for electrophysiology, CineLyzer for photometry, Plexon Inc.) and analyzed as detailed in the electrophysiological analysis section.

For loss-of-function experiments, handling sessions were recorded using high-speed videography (Pike, Allied Vision Inc., 200 fps). Based on previously reported data<sup>34</sup>, the following parameters were quantified: Number of pasta drops, percentage of time during which the preferred paw is used as guide paw, as well as probability distribution of pasta handling angle. Pasta drop rates were quantified manually, while all other quantifications were based on pose estimation performed with DeepLabCut (see Optogenetic Activation Experiments). The network was trained using at least 200 frames annotated on the following body parts: nose, forepaws and feet, as well as on the extremities and marks on the pasta pellet. Pasta Drops were defined as events where mice inadvertently released the pasta pellet from its forepaws, causing it to fall on the floor of the test chamber. Quantification of preferred paw usage as guide paw: The guide paw was defined as the one kept closer to the snout during handling (also see Fig. 5.4e). For each mouse, the preferred paw was defined as the one preferentially employed as guide paw during the control handling session. After pose estimation, the distance between each paw and the nose was computed over all handling episodes and the time where

“preferred-hand to nose” distance was shorter than “non-preferred-hand to nose” was calculated as percentage of the total handling time. Probability of distribution of pasta handling angle: for each handling frame, we quantified the angle comprised between the line fitting the tracked marks on the pasta pellet and the body midline. The body midline was calculated as the line connecting the nose and the midpoint between the feet (see also Fig. 5.6a). Probability was calculated based on the total number of handling frames, and relative handling angle values were offset from median angle value for each mouse during control sessions.

#### Optogenetic Activation Experiments:

For analysis of optogenetically-induced behaviors, quantification of the reliability to elicit the assessed behavior upon stimulation was performed manually, using high-speed videography (Pike, Allied Vision Inc., 200 fps, Sony alpha 7s, Sony Inc., 100 fps or uEyeCP, IDS Inc., 450 – 668 fps). For each mouse, a minimum of 30 optogenetic stimulation events were scored. Each stimulation event was analyzed frame by frame and whenever laser-induced movements were detected, assigned to the appropriate behavioral category. Reliability percentages for each behavioral category were calculated as the fraction of trials eliciting that specific behavior from all scored stimulation trials. Behavioral categories referred to in Fig. 5.12 were defined according to the following observed phenotypes. Reaching: Single event, unilateral lifting and extension of the forelimb accompanied only by spreading of individual fingers. Grasping: Unilateral lifting and extension of the forelimb in combination with flexing finger dynamics. Tapping: Repeated, unilateral lifting of the forepaw without flexing finger dynamics. Hand-to-mouth movement: Repeated, unilateral extensions of the forelimb with flexing finger dynamics directed towards the mouth. Grooming: Repeated, bilaterally coordinated lifting of the forelimbs and rhythmic swiping over facial areas. Locomotion: Coordinated full body movement involving the repetitive use of all four limbs to translocate the entire body in a coordinated manner. Head Turning: Horizontal head

rotation not involving forelimb movements. No behavior: Events were categorized as such when no discernible movement was elicited upon optogenetic stimulation. For analysis of forelimb trajectories during the various different forelimb behaviors elicited from the distinct subpopulations, the machine learning algorithm DeepLabCut was used in combination with high-speed videography to characterize behavioral phenotypes (uEyeCP, IDS Inc., 450-668 fps). We trained the network with an initial dataset for each kind of elicited behavior using at least 200 frames to annotate individual parts of the forelimb. Subsequent unsupervised training involved at least 600'000 iteration rounds, after which no improvement of the pose estimation reliability could be observed. Extracted pixel coordinates were plotted using customized MATLAB or Python scripts. For reaching analysis, trajectory coordinates were relative to the resting position of the paw before stimulation. Time coordinates were normalized using the time from movement onset to maximum extension (along the front-back axis) of the reach episode and discretized into equal bins. For tapping analysis, dorso-ventral coordinates were relative to the resting position of the paw before stimulation. Time coordinates were normalized by the time between motion onset and the maximum dorso-ventral position of the tap episode, discretized into equal bins and offset such that  $t=0$  occurs at the tapping peak. For grooming analysis, trajectory coordinates were relative to the resting position of the paws before stimulation. Time coordinates were normalized by the time between motion onset and completion of a grooming bout and discretized into equal bins. For EMG experiments, only reaching start timepoints with respect to the laser stimulation were assessed, aligned to the EMG traces and analyzed as detailed in the EMG analysis section.

#### Electrophysiology Analysis:

All spiking timepoints of single unit data were imported for further analysis to MATLAB from NeuroExplorer v5 (Plexon Inc.). We determined the distribution of average firing

rates for latRM neurons during behavior and found that most exhibited values below 20Hz, with only a minority displaying higher values (Fig. 5.2c). To determine how individual neurons contribute to changes in activity profiles, we aligned the relative mean-subtracted firing rates according to timing of peak changes. Spiking events were aligned with individual behavioral timepoints in a window of  $\pm 8$  sec and for individual behavioral sessions, average firing frequencies were calculated using 50ms binning. Baseline (BL) firing rates were determined during the time window between -6 to -2 sec for each behavior and are indicated separately in displayed raster plots throughout the presented Figures (scale: 0-100Hz). For analysis defining neuronal tuning to task, we used the reaching start as an alignment point in the pellet and lever task, and the start of locomotion in the open field task for locomotion. To illustrate single example neurons graphically, alignment was sometimes performed to different timepoints as indicated and the display of single trial raster plots was limited to a subset of 10 randomly selected trials. For tuning analysis to pellet or lever tasks, we included neurons for which the average firing rate reached 20Hz at least once during the task-relevant time window ( $\pm 2.5$ s; task-relevant neurons,  $n = 84$  for pellet task,  $n = 81$  for lever task;  $n = 48$  for locomotion). Task-tuned neurons were selected based on changes in firing rate  $>3$  standard deviations above baseline firing at least for one bin during the time window of -1.5s to +0.5s from onset of task as defined above ( $n=49$  for pellet task;  $n=43$  for lever task;  $n = 4$  for open field, see also Fig. 5.2). Average overall firing rates of neurons displayed in Fig. 5.2 were calculated from the  $\pm 8$  sec time period for the lever or pellet task individually. To assess task specificity to forelimb behaviors at the population level, we compared the baseline-subtracted firing rate of significantly task-tuned neurons in the pellet or lever task to the activity of the same neurons during open field locomotion or shuffled data (100x) in 250 msec bins (Fig. 5.1a, for statistical details see statistics section). Heat map plots (Fig. 5.1b, Fig. 5.7d and Fig. 5.4) were generated from mean-subtracted firing rates normalized for every neuron. 50 msec bins were assigned a color

in a 64-color range, over which the mean-subtracted firings rates were scaled. Baseline firing rates were calculated as average firing rates of individual neurons during the baseline period. The color scale for the baseline shown in the sidebar was generated by scaling the range of baseline firing rate values over a 64-color range displaying the 0-100Hz range. Average firing rates during behavior were calculated as average firing rates of individual neurons during the behavior period. Relative behavior firing rates were calculated as the difference between baseline and average behavior firing rates (see Fig. 5.2d). To determine behavioral phase tuning correlations, we selected neurons tuned to the behavioral phase of pellet reaching, lever reaching, handling or swing phase of locomotion. We determined the peak firing rate of individual neurons during the respective behavioral phases as defined below (each annotated on a trial-by-trial basis), from which the mean baseline firing rate was subtracted (50msec bins). Only trials with firing rate changes at least 3STD above baseline firing frequency, in the annotated time windows for the specific behavioral phase, were included in our analysis. We applied a reliability cut-off of 0.4 for neurons to be included into a behaviorally-tuned group. Reliability of a neuronal response was calculated from the number of trials for which the firing rate of the analyzed neuron crossed the 3STD threshold, divided by the total number of trials recorded. Additionally, to be included in the behaviorally-tuned group, a neuron must have reached an average firing rate of at least 10Hz during the task time window, and a maximum average firing rate that is greater during the behavioral phase than the baseline. The time window used for analysis of pellet or lever reaching was confined to -1.5 sec before reaching onset to the end of the reaching phase. For handling, the time window used for analysis was from the start of handling onset to the end of handling. Determined maximum trial-averaged firing rate values in the defined behavioral phase of the analyzed neurons subtracted by the maximum trial averaged baseline firing rates were plotted against each other and correlated to assess significance (see Fig. 5.3e, see Statistics section). For visualization purposes, 5 data points above 30Hz and 2 below -5Hz contributing to the regression line are not displayed

in top left panel of Fig. 5.3e. For recordings along the dorsoventral axis of latRM, we plotted the average baseline-subtracted peak firing rate of significantly behavior-tuned neurons in the two dorsal recording depths (Fig. 5.7c top; aligned to handling onset) and two ventral recording depths (Fig. 5.7c bottom; aligned to reaching onset). The activity of the reaching- and handling-tuned neurons in these recordings was compared to the activity of the same neurons, respectively, shuffled randomly (100x) in 250 msec bins (see Fig. 5.10b, for statistical details see statistics section). The four recorded depths are marked by color bars next to raster plots of individual neurons, with two shades of magenta indicating dorsal depths and two shades of cyan indicating ventral depths. For directionality analysis, task-tuned neurons in either direction were selected and relative average peak behavior firing rates (average peak behavior firing rate – average baseline firing rate) were calculated for both directions separately. The directionality index is the difference in average peak firing rates for the two directions in Hz. For plotting, we sorted the differential firing rates in ascending direction. We included a shadow depicting the standard deviations during the baseline of both directions for the corresponding neuron in the plot (see Fig. 5.5).

#### EMG Analysis:

For analysis of latencies and plotting of the EMG data (see Fig. 5.14) amplified and bandpass filtered raw signals were used for further analysis. A baseline period of 200 msec before the reaching start (see pellet reaching section) or the laser onset was used to calculate the average baseline activity and standard deviation. After mean subtraction, a threshold of 3 standard deviations of the baseline was used to derive latencies for the different muscles when the raw trace crossed this threshold for at least 4 consecutive frames. We analyzed at least 10 trials per mouse and condition. For the relative onset of muscle activity, average activation timepoints were normalized to time between the reaching start and the point of maximum forelimb extension (see pellet reaching section).

For the average plot, the raw trace was smoothed using a moving average window (29 frames for laser, 99 frames for pellet reaching).

#### Photometry Analysis:

Raw fluorescence and background fluorescent data were used to calculate  $\Delta F/F$  values based on a 3sec moving average window. Recording sessions in which the mean value of the 1000 maximum  $\Delta F/F$  single-frame peaks was either 50% higher or lower than on the first day of recording were excluded. Fluorescent traces were then aligned with individual behavioral events (reaching, handling or locomotion start) and normalized in between the maximum and minimum  $\Delta F/F$  values observed during all recording sessions. For shuffled data, the same number of random timepoints as pellet reaching events were generated from the pellet reaching experimental session. Average traces were plotted on a timescale from -1 to 5 sec around the respective behavior.

#### Plotting and programs:

All plots, scripts and analysis were generated or performed in MATLAB v2017b (The Mathworks Inc.), Python3 (Python.org) or GraphPadPrism7 (GraphPad Inc.) and Figures assembled using CorelDRAW X6 to X9 (Corel Inc). Mouse drawings were provided by E. Tyler and L. Kravitz through the SciDraw repository (scidraw.io) and adapted in Corel X6 or X8.

#### Statistics:

Significance levels indicated are as follows: \* $P < 0.05$ , \*\* $P < 0.01$ , \*\*\* $P < 0.001$ , unless otherwise specified. All data are presented as mean $\pm$ s.e.m, except where otherwise indicated. In all statistical comparisons, normality of the data was checked with quantile

plots and/or with D'Agostino & Pearson, Shapiro-Wilk and KS normality test in Prism. Non-normally distributed data were subsequently compared with non-parametric tests. The following statistical tests were used to assess significance when indicated. Firing specificity of latRM neurons according to task (Fig. 5.1a) was assessed by comparing the peak firing rates of 250 msec bins in the task window (defined by -1.5 to 0.5 sec) between all neuronal data pair-wise with the Wilcoxon signed rank test. The Bonferroni correction was applied to account for multiple comparisons and the significance levels were adjusted as  $*P < 0.0167$ ,  $**P < 0.0033$ ,  $***P < 0.00033$ . For shuffled data, the average p-value of all shuffles (100x) was used to assess significance (p-values: Pellet task vs. Shuffled:  $< 0.0001$ ; Pellet task vs. Locomotion:  $< 0.0001$ ; Locomotion vs. Shuffled: 0.245; Lever task vs. Shuffled:  $< 0.0001$ ; Lever task vs. Locomotion:  $< 0.0001$ ; Locomotion vs. Shuffled: 0.568). Similarly, the activity of neurons along the dorsoventral axis, specifically tuned to the behavioral time window of reaching or handling, was compared to the shuffled data (Figure 5.10b: Pellet Reach vs Shuffled:  $p < 0.0001$ ; Handling vs Shuffled:  $p = < 0.0001$ ). The same approach was used to probe the activity of the handling-tuned and lever reach-tuned latRM neurons during other behaviors, with a Bonferroni correction for 4 comparisons leading to adjusted significance levels of  $*P < 0.0125$ ,  $**P < 0.0025$ ,  $***P < 0.00025$  (Fig. 5.3a, b; time window was defined from 0 to 2 sec only for pellet reaching aligned activity for the handling tuned neurons since the onset of activity was delayed with respect to reaching start; p-values: Fig. 5.4a: Pellet Reaching vs Shuffled:  $p = < 0.0001$ ; Handling vs Shuffled:  $p = < 0.0001$ ; Lever reach vs Shuffled:  $p = 0.2281$ ; Locomotion vs Shuffled:  $p = 0.9523$ ; Figure 5.3b: Pellet Reaching vs Shuffled:  $p = 0.002548$ ; Handling vs Shuffled:  $p = 0.201408$ ; Lever reach vs Shuffled:  $p = < 0.0001$ ; Locomotion vs Shuffled:  $p = 0.700481$ ). To quantify action co-tuning between different behaviors (Fig. 5.2d) we used a Spearman's rank correlation test to assess significance (Spearman r- and p-values, upper left r: 0.43539, p: 0.00673; lower left r: -0.39194, p: 0.01495; upper right r: 0.39915, p: 0.02888; lower right r: -0.1315, p: 0.48852). All data shown in Fig. 5.4 and Fig. 5.5 were compared using the two-sided paired t-test unless

otherwise specified (p-values: Fig. 5.4b left experimental: <0.0001; Fig. 5.4b left control: 0.3539; Fig. 5.4b right, from left to right: < 0.0001, 0.0003, < 0.0001, < 0.0001; all other comparisons within CNO or within the PBS group did not result in significant changes; Fig. 5.4c: 0.0002; a Wilcoxon signed rank test was used for Fig. 5.4f : 0.007 and Fig. 5.4g: 0.006; Fig. 5.5b left: 0.5601; Fig. 5.5b middle: 0.6002; Fig. 5.5b right: 0.3892; Fig. 5.5c left: 0.0029; Fig. 5.5c middle: 0.0073; Fig. 5.5c right: 0.0034; Fig. 5.5e left: 0.0162; Fig. 5.5e middle: 0.0148; Fig. 5.5e right: 0.0095). Grip test analysis in Fig. 5.6b is shown as percentage on the PBS day using a Wilcoxon rank sum test (0.4237). Overlap ratios between distinct latRM or medRM subpopulations in triple injections are displayed as averages of all mice with respective subpopulation as a reference (see Fig 5.9b; latRM, left:  $19.2 \pm 5.5\%$  and  $17.2 \pm 5.1\%$ , middle:  $12.3 \pm 3.1\%$  and  $6.9 \pm 1.4\%$ , right:  $7.3 \pm 0.6\%$  and  $4.1 \pm 1.3\%$ ; Fig. 5.9c; medRM:  $70.9 \pm 18.7\%$  and  $53.8 \pm 13.2\%$ ). To compare spatial distributions of latRM subpopulations between the medial and lateral RM (Fig. 5.9c), we used a two-sided paired t-test (p-values: spinally-projecting: 0.0019; MdV-projecting: 0.0037; contra-projecting: 0.0058; MdD-projecting population: 0.0162). Reaching trajectory endpoints (Fig. 5.13b, right) were compared using the summed distance of individual endpoints to the centroid (grouped by animal, distance = 718px; all animals grouped together, distance = 1025px). A two-sided, unpaired t-test was used to compare EMG responses after light stimulation (see Fig. 5.14b; p-values: latency Biceps vs. Triceps: 0.0093; relative onset for Biceps vs. Triceps: 0.0383).

Code availability:

Custom-made scripts used in this manuscript are available in the GitHub repository:

<https://github.com/hk-2019-arber/ruder-et-al-2020>

Data availability:

Data sets included in this study are available from the corresponding author upon reasonable request.

## **5.6 Acknowledgements**

We are grateful to M. Sigrist, M. Mielich, P. Marini, M. Cases Escuté, P. Capelli and K. Fidelin for experimental help, K. Yamauchi for help with computational analysis of behavior, L. Gelman and J. Edlinger from the FMI imaging facility, N. Ehrenfeuchter from the Biozentrum Imaging facility for help and advice with image acquisition and analysis, J. Courtin (FMI) and members of the Moser laboratories (Trondheim) for advice and help with the acquisition and analysis of the single-unit recordings, P. Argast and P. Buchmann from the FMI mechanical workshop for building devices for behavioral experiments, M. Stadler for help with statistical analysis and to P. Caroni for discussions and comments on the manuscript. All authors were supported by funding from the European Research Council (ERC) under the European Union's Horizon 2020 research and innovation programme (Descent, grant agreement No 692617), the Swiss National Science Foundation, the Kanton Basel-Stadt and the Novartis Research Foundation.

## **5.7 Author Contributions**

All authors were involved in the design of experiments. L.R. together with C.P. carried out most experiments, acquired and analyzed data. R.S. was mainly involved in functional and anatomical experiments related to intra-brainstem interactions, fiber photometry experiments, and loss-of-function experiments. H.K. was involved in electrophysiology analysis and loss-of-function experiments. S.V.G. was involved in early experiments related to intra-brainstem interactions and anatomy. S.A. initiated the project, designed experiments, analyzed data and wrote the manuscript. All authors discussed the experiments and commented on the manuscript.

## **5.8 Author Information**

The authors declare no competing financial interests. Correspondence and requests for material should be addressed to S.A. ([silvia.arber@unibas.ch](mailto:silvia.arber@unibas.ch)).

# 6. Conclusions

## 6.1 Open questions and challenges

Movement is the defining quality of the animal kingdom and it can be expressed in an enormous variety of diverse actions, ranging from simple locomotion to extremely complex movements including the use of forelimbs and fingers. A fundamental question in circuit neuroscience is how such a varied assortment of activities is managed by motor centers in the brain, or in other words: how can a limited number of brain centers select, initiate, regulate and coordinate a virtually limitless array of movements.

As we describe in the introduction of this dissertation, in the past, the study of the brainstem and its motor areas has proven challenging due to its remote anatomic location and the absence of appropriate techniques to disentangle its intricate networks. In addition, although it has been known since a long time that the brainstem is a major source of input to the spinal cord, it has been challenging to associate definite sets of neurons to specific behaviors because of the impossibility to identify them.

Thanks to recent technological advances, these issues are rapidly being outpaced and it has become possible to target, record and influence the activity of specific sets of brainstem neurons in a precise manner (also see chapter 4). Recently, definite groups of brainstem neurons have been identified who are involved in the regulation of grasping (Esposito, Capelli and Arber, 2014), high-speed locomotion (Capelli *et al.*, 2017) and halting ongoing locomotor activity (Bouvier *et al.*, 2015).

The brainstem is a key structure for motor control as it holds a strategic position between the wide array of upstream motor centers important for planning, learning or selecting body actions and execution centers in the spinal cord. This intermediate position of motor centers of the brainstem is likely a crucial clue in the quest to understanding their function

and influence, suggesting a more active and integrative role in shaping the motor output than previously thought (Arber and Costa, 2018). However, through which mechanisms and to which extent brainstem neurons influence behavior is still an open question. In addition, understanding the connectivity between brainstem nuclei and mapping the inputs such areas receive from upstream motor centers is also a key question to address in order to fully understand the integrative role of the brainstem in motor control.

In this dissertation we have taken advantage of an array of state-of-the-art techniques to describe brainstem circuits driving diversification of skilled forelimb movements. We have unraveled the presence of intermingled intra-brainstem networks stratified by projection pattern, identified their specific contributions to the control of skilled actions, shedding light on the contributions of the brainstem to natural behavior.

Here, we will discuss our findings in the broader context of the motor systems networks and formulate hypothesis on how such a diverse array of supraspinal signals may be integrated to finally produce a coherent motor output.

## **6.1 Skilled forelimb movements: the brainstem and beyond**

Early investigations have proven that the brainstem is not just a relay center for motor commands (see chapter 1), and evidence from the present study strongly supports the notion that different populations of neurons in the brainstem can functionally contribute to skilled motor behaviors by encoding different phases of complex movements and recruiting relevant spinal effector circuits. However, how these neuronal ensembles are contacted and selected by upstream motor centers is an important question that is still open to investigation. Importantly, the areas encompassed by the LatRM were shown to

receive inputs from motor areas such as the motor cortex (Li *et al.*, 2015; Mercer Lindsay *et al.*, 2019), central amygdala (Han *et al.*, 2017), the Basal Ganglia as well as many others (Chronister *et al.*, 1988; Shammah-Lagnado, Costa and Ricardo, 1992). Some of these inputs have been shown to be functionally relevant; for example it was found that strong projections originate from the central nucleus of the amygdala (CeA) targeting PCRt, and artificially activating them through optogenetics elicited predatory movements such as capturing a prey using forelimbs and biting it to perform a kill (Han *et al.*, 2017). Such results are of great interest in the context of the present study as they highlight the strategic position of LatRM as possible integration center for a diverse array of movements including orofacial and forelimb actions (see also section 3.3 and 6.2 of this dissertation). Similarly, another study has highlighted an important connection between the anterior lateral motor cortex (ALM) and another LatRM subregion, the IRt (Li *et al.*, 2015). Here, pyramidal tract neurons projecting to IRt were shown to develop a directionally biased signal in the form of a ramping up of activity before the movement, suggesting encoding of preparatory activity, possibly subsequently transmitted to brainstem circuits. While it is known since a long time that the motor cortex has a role in dexterous movements, to this day it is not clear what the specific function is. A recent study has addressed this question in a novel way, by designing a behavioral task separating learning and generation of motor sequences (Kawai *et al.*, 2015). Importantly, it was found that lesions of the motor cortex have no effect on the execution of a previously learned motor sequence, but completely hinder the ability of naive rats to acquire the same behavioral sequence. These results were interpreted ascribing an instructive function to the motor cortex, suggesting it may tutor subcortical structures when learning and consolidating novel tasks (Kawai *et al.*, 2015). Such outcomes disagree with previous reports of rats being able to learn simple forelimb reaching tasks even after extensive motor cortex lesions (Gharbawie and Whishaw, 2006), a confound probably due to the particular complexity of the sequence rats had to learn. Another study found that optogenetically inhibiting the motor cortex before or during a pellet reaching

and grasping task resulted in a freezing of the movement which resumed once the cortex was disinhibited, without any additional sensory cue (J.-Z. Guo *et al.*, 2015) suggesting that the motor cortex is necessary to execute a skilled forelimb task.

Moreover, the LatRM receives input from the basal ganglia through the substantia nigra pars reticulata (SNr) (Chronister *et al.*, 1988; Shammah-Lagnado, Costa and Ricardo, 1992). The basal ganglia are a crucial structure in motor control, traditionally serving the role of promoting appropriate actions and inhibiting undesired movements. Over the last decades, new evidence emerged, which identified specific populations of neurons in the striatum, the input structure of the basal ganglia, encoding distinct movements such as locomotion, rearing or turning (Barbera *et al.*, 2016; Klaus *et al.*, 2017; Parker *et al.*, 2018). Similarly, the SNr, which receives input from the striatum shows segregate action coding (Jin, Tecuapetla and Costa, 2014; Tecuapetla *et al.*, 2016; Lee, Wang and Sabatini, 2020), leading to the interesting hypothesis that connectivity linking these subcortical circuits to the brainstem would follow the same principles and engage distinct neuronal ensembles in a movement specific manner (Arber and Costa, 2018; Ruder and Arber, 2019).

While the exact role of the motor cortex, basal ganglia and brainstem motor centers in generating and controlling movement is still a subject of intense debate, a model can be imagined where the motor cortex selects the appropriate action based on sensory stimuli and the evaluation of the internal state, broadcasting such information to many subcortical structures. In particular, this information would flow to the striatum and to premotor neurons in the brainstem, potentially “priming” them to perform a certain movement. However, the ultimate decision to perform an action may be computed by basal ganglia circuits, who relay commitment and action vigor information to the appropriate command centers in the brainstem. Brainstem nuclei, in turn, may manage the coordination of multiple motor units in the spinal cord, linking them in a coherent sequence in order to perform complex movements (Figure 6.1), (Arber and Costa, 2018;

Klaus, Alves da Silva and Costa, 2019). This simplistic model leaves out a number of important motor structures such as the cerebellum and superior colliculus, but a review of their roles and influences on the motor system goes beyond the scope of this dissertation.

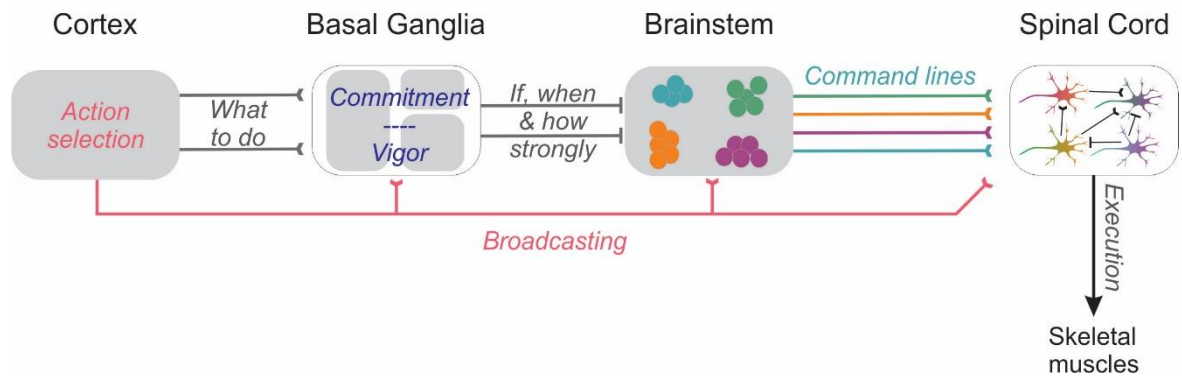


**Figure 6.1 Brain circuits for movement.** Schematic view of the current model for the function of brain centers regulating movement. The motor cortex selects the appropriate action according to sensory feedback and internal state, broadcasting the signal to all subcortical circuits, including the spinal cord. The basal ganglia are responsible for allowing an action to happen by disinhibiting lower motor centers, but also for modulating the appropriate vigor of execution. Brainstem centers act as integrators and execute the selected action by selecting and coordinating different motor neuronal pools in the spinal cord. Adapted from (Arber and Costa, 2018; Klaus, Alves da Silva and Costa, 2019)

Lastly, another important question that still remain open regards the function of inhibitory neurons in LatRM. Inhibition is an integral part of the normal physiology of the nervous system and has been the subject of intense studies in the last decades. However, this holds true only for the most prominently studied areas of the nervous system such as the cortex (Lim *et al.*, 2018). Here inhibitory neurons have been shown to act mainly locally serving multiple functions such as isolating cortical columns, providing

feedforward inhibition and normalizing network activity (Harris and Mrsic-Flogel, 2013). Conversely, in the brainstem, inhibitory neurons have been seldom studied and to date their role remains elusive, especially in the context of the motor system. Recent evidence showed that inhibitory neurons in the caudal medulla have a role in halting ongoing locomotion (Capelli *et al.*, 2017) and regulate vibrissa movements (Bellavance *et al.*, 2017). In addition, neuronal tracing carried out in our lab shows that inhibitory neurons of the brainstem project extensively to other brainstem areas (data not shown) and even to interneurons in the spinal cord (Esposito, Capelli and Arber, 2014). It can therefore be hypothesized that inhibitory neurons in the brainstem may serve different functions, exerting both inter- and intra-brainstem nuclei influence on the motor output, playing roles in gating or selecting behavioral programs and coordinating the flow of signals towards motor neurons. In the future, it would be desirable to determine a detailed map of the connectivity of brainstem inhibitory neurons and to study their activity in behaving animals carrying out different behavioral tasks. It will also be important to understand the influence of inhibitory neurons on interactions between different motor nuclei of the brainstem and ultimately discerning how and in which ways they can shape the motor output.

## **6.2 Skilled forelimb movements and other motor behaviors**

While it is convenient to treat individual motor behaviors as freely-standing, separate actions when studying them, this is hardly the case in nature. Skilled forelimb movements utilized for foraging or other aims are blended in an action space continuum together with a diverse assortment of motor actions such as locomotion, orofacial movements as well as self-centered activities such as grooming.

It is therefore important to highlight the open questions that arise from such considerations. In our study we have shown how subpopulations of glutamatergic neurons in the Lateral Rostral Medulla (LatRM) encode and regulate different motor programs in the forelimb action space. Of these, some are directed outwards (i.e. reaching, grasping) while others are self-centered (i.e. hand-to-mouth, grooming). As highlighted above, the forelimb motor syllables we have identified are part of ethologically relevant actions which also contain orofacial movements such as whisking, licking and chewing (Whishaw and Pellis, 1990). How such different actions are coordinated and concatenated into seamlessly smooth sequences, and which brain structures are involved in making this possible is currently still unknown.

Could the brainstem preside this complex task? One hint comes from connectivity: it is important to consider that both PCRt and MdV possess direct connections to cranial nerve nuclei such as the 5N (trigeminal), 7N (facial) and 12N (hypoglossal) which are themselves located in the brainstem and contain motor neurons directly controlling muscles of the jaw, face and tongue. Moreover, it is known that CPGs or neuronal oscillators for whisking, licking and chewing reside within the boundaries of the IRt nucleus, at a level caudal to that of LatRM (Figure 6.2) (Kleinfeld *et al.*, 2014b; Moore, Kleinfeld and Wang, 2014; McElvain *et al.*, 2018).

In this context it is possible to hypothesize that LatRM may be part of a much broader network of neighboring premotor and motor areas in the brainstem, connected to each other by means of excitatory or inhibitory projections, which have the potential to regulate complex sequences or forelimb and orofacial movements. In addition, upstream centers might play important roles in influencing these behaviors; a recent report has shown that cortex neurons projections to the brainstem are able to directly influence behavior modifying the activity of orofacial or forelimb muscles (Mercer Lindsay *et al.*, 2019).

In the future, it will be important to establish new methodologies and techniques allowing for the recording and analysis of neuronal activity during continuous natural behavior, composed of many different actions in a naturalistic setting. Studying circuit interactions within and beyond the brainstem has the potential to lead to a broader understanding of how complex movements come to be planned, regulated and executed.

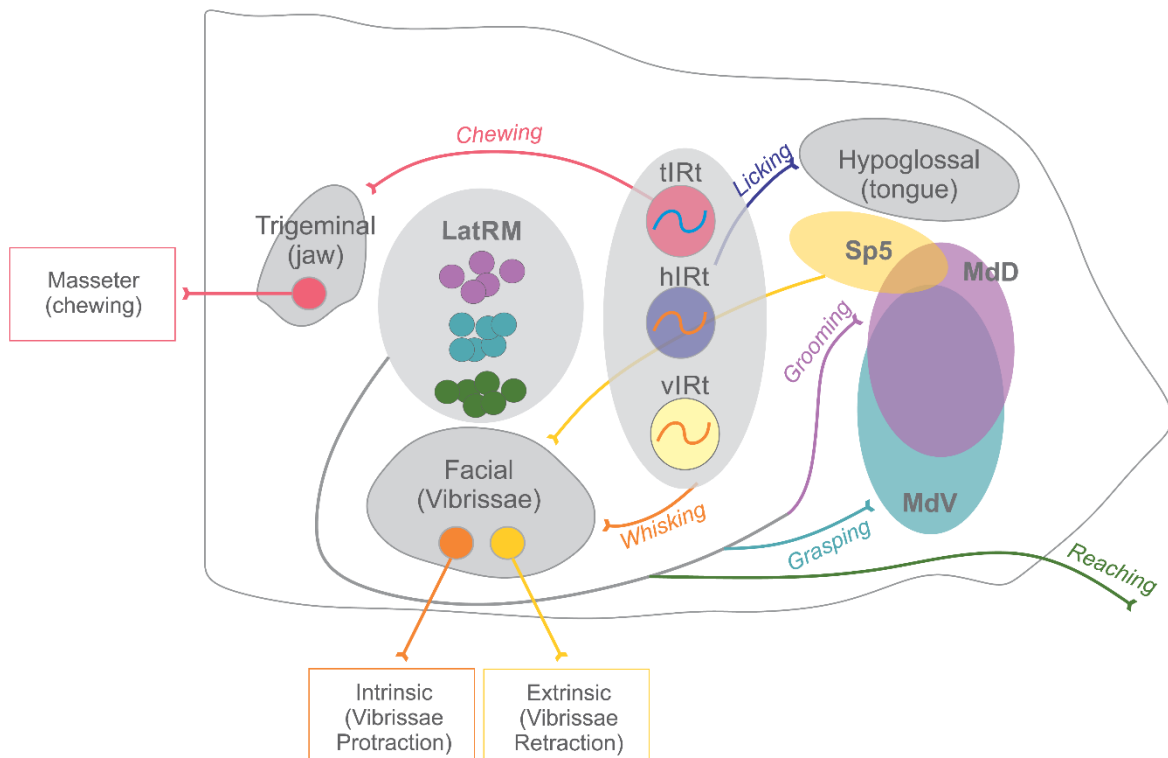


**Figure 6.2 Brainstem circuits involved in skilled forelimb and orofacial movements.** Side view of the brainstem, showing LatRM and its neuronal subpopulations in the context of the orofacial network. Note how the dorsoventral distribution populations in LatRM is paralleled by that of IRt oscillators. Abbreviations: vIRt, vibrissa IRt; hIRt, hypoglossal IRt; tIRt, trigeminal IRt; MdV, medullary reticular formation, ventral part; MdD, medullary reticular formation, dorsal part; Sp5, spinal trigeminal nucleus. (Nakamura and Katakura, 1995; Matyas *et al.*, 2010; Moore *et al.*, 2013; Moore, Kleinfeld and Wang, 2014; Deschênes *et al.*, 2016; McElvain *et al.*, 2018)

## 7. Acknowledgments

This work would not have been possible if not for the countless contributions of the many outstanding people I was lucky enough to meet in my journey.

First and foremost, my deepest gratitude goes to my PhD supervisor, Prof. Silvia Arber. Her inspiring passion for science, her expertise and knowledge of the nervous system were second only to her invaluable guidance in making my doctoral experience not just a successful, but an exceptionally enjoyable one.

Moreover, I would like to thank Prof. Pico Caroni and Prof. Botond Roska, the other members of my doctoral committee, for their time in reviewing this thesis and for being an inspiration to me in my scientific journey.

A heartfelt thank you goes to all present and past members of the Arber lab, and in particular to the colleagues who shared this monumental project with me: Ludwig Ruder, Sara Valencia Garcia, Harsh Kanodia and Chiara Pivetta. Thanks to all of you for teaching me what teamwork really means.

A special mention goes to the two people I looked up to the most over these years: Maria Soledad Esposito, who nurtured me during my first year and always found time to listen to me, even with a baby and a trans-continental moving on the way, and Eduardo Arteaga Bracho who supported me in difficult times and gave me the confidence I needed to get through them, always leading by example.

I want to personally thank Paolo Capelli, for always being there when I needed help, both inside and outside the lab, for his competent scientific advice and for sharing with me our common passions: hiking, cooking and photography.

At least some part of life happens outside the lab and this is the time and place to express my gratitude to the people that made it worth living:

To my lifelong friends Dario, Davide and Denis: thank you for keeping me sane with our Tuesday night games and for your constant, daily presence in my life.

To the good friends I met on this adventure, Giulia, Federica, Staci and Wuzhou: thank you for sharing this part of your journey with me.

To my parents: thank you for always supporting my passion for science and selflessly embracing my decision to move far away to follow it, even though it meant we would rarely see each other.

Finally, to my wife Elisa; I would not be writing this thesis if not for you. Thank you for being my best friend, my companion and partner in all endeavors and adventures. Thank you for making me want to give the best of myself and for being there for me, always.



## 8. References

- Akerboom, J. *et al.* (2012) 'Optimization of a GCaMP Calcium Indicator for Neural Activity Imaging', *Journal of Neuroscience*, 32(40), pp. 13819–13840. doi: 10.1523/JNEUROSCI.2601-12.2012.
- Alaverdashvili, M. and Whishaw, I. Q. (2008) 'Motor cortex stroke impairs individual digit movement in skilled reaching by the rat', *European Journal of Neuroscience*, 28(2), pp. 311–322. doi: 10.1111/j.1460-9568.2008.06315.x.
- Alexander, G. M. *et al.* (2009) 'Remote Control of Neuronal Activity in Transgenic Mice Expressing Evolved G Protein-Coupled Receptors', *Neuron*, 63(1), pp. 27–39. doi: 10.1016/j.neuron.2009.06.014.
- Alstermark, B. and Isa, T. (2012) 'Circuits for Skilled Reaching and Grasping', *Annual Review of Neuroscience*, 35(1), pp. 559–578. doi: 10.1146/annurev-neuro-062111-150527.
- Aravanis, A. M. *et al.* (2007) 'An optical neural interface: *in vivo* control of rodent motor cortex with integrated fiberoptic and optogenetic technology', *Journal of Neural Engineering*, 4(3), pp. S143–S156. doi: 10.1088/1741-2560/4/3/S02.
- Arber, S. and Costa, R. M. (2018) 'Connecting neuronal circuits for movement', *Science*, 360(6396), pp. 1403–1404. doi: 10.1126/science.aat5994.
- Arenkiel, B. R. *et al.* (2007) 'In Vivo Light-Induced Activation of Neural Circuitry in Transgenic Mice Expressing Channelrhodopsin-2', *Neuron*, 54(2), pp. 205–218. doi: 10.1016/j.neuron.2007.03.005.
- Armbruster, B. N. *et al.* (2007) 'Evolving the lock to fit the key to create a family of G protein-coupled receptors potently activated by an inert ligand', *Proceedings of the National Academy of Sciences*, 104(12), pp. 5163–5168. doi: 10.1073/pnas.0700293104.
- Atasoy, D. *et al.* (2012) 'Deconstruction of a neural circuit for hunger', *Nature*, 488(7410), pp. 172–177. doi: 10.1038/nature11270.
- Baker, S. N. *et al.* (2015) 'Chapter 18 - Pathways mediating functional recovery', in Dancause, N., Nadeau, S., and Rossignol, S. (eds) *Progress in Brain Research*. Elsevier (Sensorimotor Rehabilitation), pp. 389–412. doi: 10.1016/bs.pbr.2014.12.010.
- Bamberg, E., Tittor, J. and Oesterhelt, D. (1993) 'Light-driven proton or chloride pumping by halorhodopsin.', *Proceedings of the National Academy of Sciences*, 90(2), pp. 639–643. doi: 10.1073/pnas.90.2.639.
- Barbera, G. *et al.* (2016) 'Spatially Compact Neural Clusters in the Dorsal Striatum Encode Locomotion Relevant Information', *Neuron*, 92(1), pp. 202–213. doi: 10.1016/j.neuron.2016.08.037.
- Basaldella, E. *et al.* (2015) 'Multisensory Signaling Shapes Vestibulo-Motor Circuit Specificity', *Cell*, 163(2), pp. 301–312. doi: 10.1016/j.cell.2015.09.023.

- Bellavance, M.-A. *et al.* (2017) 'Parallel Inhibitory and Excitatory Trigemino-Facial Feedback Circuitry for Reflexive Vibrissa Movement', *Neuron*, 95(3), pp. 673-682.e4. doi: 10.1016/j.neuron.2017.06.045.
- Bender, D., Holschbach, M. and Stöcklin, G. (1994) 'Synthesis of n.c.a. carbon-11 labelled clozapine and its major metabolite clozapine-N-oxide and comparison of their biodistribution in mice', *Nuclear Medicine and Biology*, 21(7), pp. 921–925. doi: 10.1016/0969-8051(94)90080-9.
- Bentivoglio, M. *et al.* (1979) 'Fluorescent retrograde neuronal labeling in rat by means of substances binding specifically to adenine-thymine rich DNA', *Neuroscience Letters*, 12(2), pp. 235–240. doi: 10.1016/0304-3940(79)96068-3.
- Bernhard, C. G. (1954) 'CORTICAL REPRESENTATION AND FUNCTIONAL SIGNIFICANCE OF THE CORTICOMOTONEURONAL SYSTEM', *Archives of Neurology And Psychiatry*, 72(4), p. 473. doi: 10.1001/archneurpsyc.1954.02330040075006.
- Berntson, G. G. (1973) 'Attack, grooming, and threat elicited by stimulation of the pontine tegmentum in cats', *Physiology & Behavior*, 11(1), pp. 81–87. doi: 10.1016/0031-9384(73)90126-1.
- Berntson, G. G., Jang, J. F. and Ronca, A. E. (1988) 'Brainstem Systems and Grooming Behaviors', *Annals of the New York Academy of Sciences*, 525(1), pp. 350–362. doi: 10.1111/j.1749-6632.1988.tb38619.x.
- Berridge, K. C. (1989) 'Progressive degradation of serial grooming chains by descending decerebration', *Behavioural Brain Research*, 33(3), pp. 241–253. doi: 10.1016/S0166-4328(89)80119-6.
- Berridge, K. C. and Fentress, J. C. (1987) 'Disruption of natural grooming chains after striatopallidal lesions', *Psychobiology*, 15(4), pp. 336–342. doi: 10.3758/BF03327290.
- Berridge, K. C., Fentress, J. C. and Parr, H. (1987) 'Natural syntax rules control action sequence of rats', *Behavioural Brain Research*, 23(1), pp. 59–68. doi: 10.1016/0166-4328(87)90242-7.
- Berridge, K. C. and Whishaw, I. Q. (1992) 'Cortex, striatum and cerebellum: control of serial order in a grooming sequence', *Experimental Brain Research*, 90(2), pp. 275–290. doi: 10.1007/BF00227239.
- Biruté M. F. Galdikas (1989) 'Orangutan Tool Use', *Science, New Series*, Vol. 243(No. 4888), p. 152.
- Bjursten, L.-M., Norrsell, K. and Norrsell, U. (1976) 'Behavioural repertory of cats without cerebral cortex from infancy', *Experimental Brain Research*, 25(2). doi: 10.1007/BF00234897.
- Bolles, R. C. (1960) 'Grooming behavior in the rat.', *Journal of Comparative and Physiological Psychology*, 53(3), pp. 306–310. doi: 10.1037/h0045421.
- Botev Z.I., Grotowski J.F. and Kroese D.P. (2010) 'Kernel density estimation via diffusion', *Ann. Statist.*, 38, pp. 2916–2957.
- Bouvier, J. *et al.* (2015) 'Descending Command Neurons in the Brainstem that Halt Locomotion', *Cell*, 163(5), pp. 1191–1203. doi: 10.1016/j.cell.2015.10.074.

- Boyden, E. S. *et al.* (2005) 'Millisecond-timescale, genetically targeted optical control of neural activity', *Nature Neuroscience*, 8(9), pp. 1263–1268. doi: 10.1038/nn1525.
- Boyle, P. M., Karathanos, T. V. and Trayanova, N. A. (2018) 'Cardiac Optogenetics: 2018', *JACC: Clinical Electrophysiology*, 4(2), pp. 155–167. doi: 10.1016/j.jacep.2017.12.006.
- Brácha, V., Zhuravin, I. A. and Bureš, J. (1990) 'The reaching reaction in the rat: A part of the digging pattern?', *Behavioural Brain Research*, 36(1), pp. 53–64. doi: 10.1016/0166-4328(90)90159-C.
- Bräuer, J. and Call, J. (2015) 'Apes produce tools for future use', *American Journal of Primatology*, 77(3), pp. 254–263. doi: 10.1002/ajp.22341.
- Buzsáki, G. (2004) 'Large-scale recording of neuronal ensembles', *Nature Neuroscience*, 7(5), pp. 446–451. doi: 10.1038/nn1233.
- Caggiano, V. *et al.* (2018) 'Midbrain circuits that set locomotor speed and gait selection', *Nature*, 553(7689), pp. 455–460. doi: 10.1038/nature25448.
- Capelli, P. *et al.* (2017) 'Locomotor speed control circuits in the caudal brainstem', *Nature*, 551(7680), pp. 373–377. doi: 10.1038/nature24064.
- Cartmill (1974) 'Rethinking primate origins', *Science*, 184(4135), pp. 436–443.
- Chen, T.-W. *et al.* (2013) 'Ultrasensitive fluorescent proteins for imaging neuronal activity', *Nature*, 499(7458), pp. 295–300. doi: 10.1038/nature12354.
- Chronister, R. B. *et al.* (1988) 'Interconnections between substantia nigra reticulata and medullary reticular formation', *Brain Research Bulletin*, 21(2), pp. 313–317. doi: 10.1016/0361-9230(88)90246-8.
- Chuong, A. S. *et al.* (2014) 'Noninvasive optical inhibition with a red-shifted microbial rhodopsin', *Nature Neuroscience*, 17(8), pp. 1123–1129. doi: 10.1038/nn.3752.
- Ciabatti, E. *et al.* (2017) 'Life-Long Genetic and Functional Access to Neural Circuits Using Self-Inactivating Rabies Virus', *Cell*, 170(2), pp. 382–392.e14. doi: 10.1016/j.cell.2017.06.014.
- Cobbold, P. H. and Rink, T. J. (1987) 'Fluorescence and bioluminescence measurement of cytoplasmic free calcium', *Biochemical Journal*, 248(2), pp. 313–328. doi: 10.1042/bj2480313.
- Csicsvari, J. *et al.* (2003) 'Massively Parallel Recording of Unit and Local Field Potentials With Silicon-Based Electrodes', *Journal of Neurophysiology*, 90(2), pp. 1314–1323. doi: 10.1152/jn.00116.2003.
- Dana, H. *et al.* (2019) 'High-performance calcium sensors for imaging activity in neuronal populations and microcompartments', *Nature Methods*, 16(7), pp. 649–657. doi: 10.1038/s41592-019-0435-6.
- Del Negro, C. A., Funk, G. D. and Feldman, J. L. (2018) 'Breathing matters', *Nature Reviews Neuroscience*, 19(6), pp. 351–367. doi: 10.1038/s41583-018-0003-6.
- Deng, J. *et al.* (2009) 'ImageNet: A large-scale hierarchical image database', in *2009 IEEE Conference on Computer Vision and Pattern Recognition. 2009 IEEE Computer*

*Society Conference on Computer Vision and Pattern Recognition Workshops (CVPR Workshops)*, Miami, FL: IEEE, pp. 248–255. doi: 10.1109/CVPR.2009.5206848.

Deschênes, M. *et al.* (2016) 'Inhibition, Not Excitation, Drives Rhythmic Whisking', *Neuron*, 90(2), pp. 374–387. doi: 10.1016/j.neuron.2016.03.007.

Dombeck, D. A. *et al.* (2010) 'Functional imaging of hippocampal place cells at cellular resolution during virtual navigation', *Nature Neuroscience*, 13(11), pp. 1433–1440. doi: 10.1038/nn.2648.

Drew, T. and Rossignol, S. (1990) 'Functional organization within the medullary reticular formation of intact unanesthetized cat. I. Movements evoked by microstimulation', *Journal of Neurophysiology*, 64(3), pp. 767–781. doi: 10.1152/jn.1990.64.3.767.

Dunbar, Robin (1991) 'Functional Significance of Social Grooming in Primates', *Folia Primatologica*, 57, pp. 121–131.

Esposito, M. S., Capelli, P. and Arber, S. (2014) 'Brainstem nucleus MdV mediates skilled forelimb motor tasks', *Nature*, 508(7496), pp. 351–356. doi: 10.1038/nature13023.

Falótico, T., Siqueira, J. O. and Ottoni, E. B. (2017) 'Digging up food: excavation stone tool use by wild capuchin monkeys', *Scientific Reports*, 7(1), p. 6278. doi: 10.1038/s41598-017-06541-0.

Fayet, A. L., Hansen, E. S. and Biro, D. (2020) 'Evidence of tool use in a seabird', *Proceedings of the National Academy of Sciences of the United States of America*, 117(3), pp. 1277–1279. doi: 10.1073/pnas.1918060117.

Fenno, L. E. *et al.* (2014) 'Targeting cells with single vectors using multiple-feature Boolean logic', *Nature Methods*, 11(7), pp. 763–772. doi: 10.1038/nmeth.2996.

Fentress, J. C. (1973) 'Development of Grooming in Mice with Amputated Forelimbs', *Science*, 179(4074), pp. 704–705. doi: 10.1126/science.179.4074.704.

Ferguson, S. *et al.* (2011) 'Transient neuronal inhibition reveals opposing roles of indirect and direct pathways in sensitization', *Nature neuroscience*, 14(1), pp. 22–24. doi: 10.1038/nn.2703.

Ferreira-Pinto, M. J. *et al.* (2018) 'Connecting Circuits for Supraspinal Control of Locomotion', *Neuron*, 100(2), pp. 361–374. doi: 10.1016/j.neuron.2018.09.015.

Franklin K.B. and Paxinos G. (2007) *The Mouse Brain in Stereotaxic Coordinates*. 3rd edn. Elsevier.

Gail Richmond and Benjamin D. Sachs (1980) 'Grooming in Norway Rats: The Development and Adult Expression of a Complex Motor Pattern', *Behaviour*, 75(1), pp. 82–96.

Galiñanes, G. L., Bonardi, C. and Huber, D. (2018) 'Directional Reaching for Water as a Cortex-Dependent Behavioral Framework for Mice', *Cell Reports*, 22(10), pp. 2767–2783. doi: 10.1016/j.celrep.2018.02.042.

Garcia-Rill, E. and Skinner, R. D. (1987) 'The mesencephalic locomotor region. I. Activation of a medullary projection site', *Brain Research*, 411(1), pp. 1–12. doi: 10.1016/0006-8993(87)90675-5.

- Georgopoulos, A. *et al.* (1982) 'On the relations between the direction of two-dimensional arm movements and cell discharge in primate motor cortex', *The Journal of Neuroscience*, 2(11), pp. 1527–1537. doi: 10.1523/JNEUROSCI.02-11-01527.1982.
- Gerfin, C. R. and Sawchenko, P. E. (1985) 'A method for anterograde axonal tracing of chemically specified circuits in the central nervous system: combinedPhaseolus vulgaris-leucoagglutinin (PHA-L) tract tracing and immunohistochemistry', *Brain Research*, 343(1), pp. 144–150. doi: 10.1016/0006-8993(85)91168-0.
- Ghali, M. G. Z. (2017) 'The brainstem network controlling blood pressure: an important role for pressor sites in the caudal medulla and cervical spinal cord', *Journal of Hypertension*, 35(10), pp. 1938–1947. doi: 10.1097/HJH.0000000000001427.
- Gharbawie, O. A. and Whishaw, I. Q. (2006) 'Parallel stages of learning and recovery of skilled reaching after motor cortex stroke: "Oppositions" organize normal and compensatory movements', *Behavioural Brain Research*, 175(2), pp. 249–262. doi: 10.1016/j.bbr.2006.08.039.
- Gomez, J. L. *et al.* (2017) 'Chemogenetics revealed: DREADD occupancy and activation via converted clozapine', *Science*, 357(6350), pp. 503–507. doi: 10.1126/science.aan2475.
- Govorunova, E. G. *et al.* (2015) 'Natural light-gated anion channels: A family of microbial rhodopsins for advanced optogenetics', *Science*, 349(6248), pp. 647–650. doi: 10.1126/science.aaa7484.
- Gray, L. A., O'Reilly, J. C. and Nishikawa, K. C. (1997) 'Evolution of forelimb movement patterns for prey manipulation in anurans', *Journal of Experimental Zoology*, 277(6), pp. 417–424. doi: 10.1002/(SICI)1097-010X(19970415)277:6<417::AID-JEZ1>3.0.CO;2-R.
- Grillner, S. (2006) 'Biological Pattern Generation: The Cellular and Computational Logic of Networks in Motion', *Neuron*, 52(5), pp. 751–766. doi: 10.1016/j.neuron.2006.11.008.
- Grillner S., Georgopoulos A.P. and Jordan L.M. (1997) in. The MIT Press.
- Gunaydin, L. A. *et al.* (2010) 'Ultrafast optogenetic control', *Nature Neuroscience*, 13(3), pp. 387–392. doi: 10.1038/nn.2495.
- Gunaydin, L. A. *et al.* (2014) 'Natural Neural Projection Dynamics Underlying Social Behavior', *Cell*, 157(7), pp. 1535–1551. doi: 10.1016/j.cell.2014.05.017.
- Guo, J.-Z. *et al.* (2015) 'Cortex commands the performance of skilled movement', *eLife*. Edited by M. Hausser, 4, p. e10774. doi: 10.7554/eLife.10774.
- Guo, Q. *et al.* (2015) 'Multi-channel fiber photometry for population neuronal activity recording', *Biomedical Optics Express*, 6(10), pp. 3919–3931. doi: 10.1364/BOE.6.003919.
- Hafting, T. *et al.* (2005) 'Microstructure of a spatial map in the entorhinal cortex', *Nature*, 436(7052), pp. 801–806. doi: 10.1038/nature03721.
- Hall, K. R. L. and Schaller, G. B. (1964) 'Tool-Using Behavior of the California Sea Otter', *Journal of Mammalogy*, 45(2), pp. 287–298. doi: 10.2307/1376994.
- Han, W. *et al.* (2017) 'Integrated Control of Predatory Hunting by the Central Nucleus of the Amygdala', *Cell*, 168(1), pp. 311–324.e18. doi: 10.1016/j.cell.2016.12.027.

- Han, X. *et al.* (2011) 'A High-Light Sensitivity Optical Neural Silencer: Development and Application to Optogenetic Control of Non-Human Primate Cortex', *Frontiers in Systems Neuroscience*, 5. doi: 10.3389/fnsys.2011.00018.
- Harris, K. D. and Mrsic-Flogel, T. D. (2013) 'Cortical connectivity and sensory coding', *Nature*, 503(7474), pp. 51–58. doi: 10.1038/nature12654.
- Heffner, R. S. (1983) 'The Role of the Corticospinal Tract in the Evolution of Human Digital Dexterity', *Brain, Behavior and Evolution*, 23, pp. 165–183.
- Hubel, D. H. (1957) 'Tungsten Microelectrode for Recording from Single Units', *Science, New Series*, 125(3247), pp. 549–550.
- Hunt, G. R. (1996) 'Manufacture and use of hook-tools by New Caledonian crows', *Nature*, 379(6562), pp. 249–251. doi: 10.1038/379249a0.
- Insafutdinov, E. *et al.* (2016) 'DeeperCut: A Deeper, Stronger, and Faster Multi-Person Pose Estimation Model', in. *14th European Conference on Computer Vision*, Springer, pp. 34–50. doi: 10.1007/978-3-319-46466-4\_3.
- Isa, T. *et al.* (2007) 'Direct and Indirect Cortico-Motoneuronal Pathways and Control of Hand/Arm Movements', *Physiology*, 22(2), pp. 145–152. doi: 10.1152/physiol.00045.2006.
- Iwaniuk, A. N. and Whishaw, I. Q. (2000) 'On the origin of skilled forelimb movements', *Trends in Neurosciences*, 23(8), pp. 372–376. doi: 10.1016/S0166-2236(00)01618-0.
- Iwasaki, Y. and Clark, H. F. (1975) 'Cell to cell transmission of virus in the central nervous system. II. Experimental rabies in mouse', *Laboratory Investigation; a Journal of Technical Methods and Pathology*, 33(4), pp. 391–399.
- James W. Woods (1964) 'Behavior of chronic decerebrate cats', *Journal of Neurophysiology*.
- Jin, X. and Costa, R. M. (2010) 'Start/stop signals emerge in nigrostriatal circuits during sequence learning', *Nature*, 466(7305), pp. 457–462. doi: 10.1038/nature09263.
- Jin, X., Tecuapetla, F. and Costa, R. M. (2014) 'Basal ganglia subcircuits distinctively encode the parsing and concatenation of action sequences', *Nature Neuroscience*, 17(3), pp. 423–430. doi: 10.1038/nn.3632.
- Johansson, G. (1975) 'VISUAL MOTION PERCEPTION', *SCIENTIFIC AMERICAN*, p. 15.
- Jun, J. J. *et al.* (2017) 'Fully integrated silicon probes for high-density recording of neural activity', *Nature*, 551(7679), pp. 232–236. doi: 10.1038/nature24636.
- Kalueff, A. V. *et al.* (2016) 'Neurobiology of rodent self-grooming and its value for translational neuroscience', *Nature Reviews Neuroscience*, 17(1), pp. 45–59. doi: 10.1038/nrn.2015.8.
- Kane, G. *et al.* (2020) 'Real-time, low-latency closed-loop feedback using markerless posture tracking', *bioRxiv*, p. 2020.08.04.236422. doi: 10.1101/2020.08.04.236422.
- Kawai, R. *et al.* (2015) 'Motor Cortex Is Required for Learning but Not for Executing a Motor Skill', *Neuron*, 86(3), pp. 800–812. doi: 10.1016/j.neuron.2015.03.024.

- Kelly, R. M. and Strick, P. L. (2000) 'Rabies as a transneuronal tracer of circuits in the central nervous system', *Journal of Neuroscience Methods*, 103(1), pp. 63–71. doi: 10.1016/S0165-0270(00)00296-X.
- Kennedy, P. R. (1990) 'Corticospinal, rubrospinal and rubro-olivary projections: a unifying hypothesis', *Trends in Neurosciences*, 13(12), pp. 474–479. doi: 10.1016/0166-2236(90)90079-P.
- Kent C. Berridge (1990) 'Comparative Fine Structure of Action: Rules of Form and Sequence in the Grooming Patterns of Six Rodent Species', *Behavior*, 1(113), pp. 21–56.
- Kim, C. K. *et al.* (2016) 'Simultaneous fast measurement of circuit dynamics at multiple sites across the mammalian brain', *Nature Methods*, 13(4), pp. 325–328. doi: 10.1038/nmeth.3770.
- Kim, L. H. *et al.* (2017) 'Integration of Descending Command Systems for the Generation of Context-Specific Locomotor Behaviors', *Frontiers in Neuroscience*, 11. doi: 10.3389/fnins.2017.00581.
- Klapoetke, N. C. *et al.* (2014) 'Independent optical excitation of distinct neural populations', *Nature Methods*, 11(3), pp. 338–346. doi: 10.1038/nmeth.2836.
- Klaus, A. *et al.* (2017) 'The Spatiotemporal Organization of the Striatum Encodes Action Space', *Neuron*, 95(5), pp. 1171–1180.e7. doi: 10.1016/j.neuron.2017.08.015.
- Klaus, A., Alves da Silva, J. and Costa, R. M. (2019) 'What, If, and When to Move: Basal Ganglia Circuits and Self-Paced Action Initiation', *Annual Review of Neuroscience*, 42(1), pp. 459–483. doi: 10.1146/annurev-neuro-072116-031033.
- Kleinfeld, D. *et al.* (2014a) 'The Brainstem Oscillator for Whisking and the Case for Breathing as the Master Clock for Orofacial Motor Actions', *Cold Spring Harbor Symposia on Quantitative Biology*, 79, pp. 29–39. doi: 10.1101/sqb.2014.79.024794.
- Kleinfeld, D. *et al.* (2014b) 'The Brainstem Oscillator for Whisking and the Case for Breathing as the Master Clock for Orofacial Motor Actions', *Cold Spring Harbor Symposia on Quantitative Biology*, 79, pp. 29–39. doi: 10.1101/sqb.2014.79.024794.
- Kleinlogel, S. *et al.* (2011) 'Ultra light-sensitive and fast neuronal activation with the Ca<sup>2+</sup>-permeable channelrhodopsin CatCh', *Nature Neuroscience*, 14(4), pp. 513–518. doi: 10.1038/nn.2776.
- Kristensson, K., Ghetti, B. and Wiśniewski, H. M. (1974) 'Study on the propagation of Herpes simplex virus (type 2) into the brain after intraocular injection', *Brain Research*, 69(2), pp. 189–201. doi: 10.1016/0006-8993(74)90001-8.
- Kristensson, K. and Olsson, Y. (1971) 'Uptake and retrograde axonal transport of peroxidase in hypoglossal neurones', *Acta Neuropathologica*, 19(1), pp. 1–9. doi: 10.1007/BF00690948.
- Küchler, M. *et al.* (2002) 'Red nucleus projections to distinct motor neuron pools in the rat spinal cord', *Journal of Comparative Neurology*, 448(4), pp. 349–359. doi: 10.1002/cne.10259.

- Kudo, Y. *et al.* (1992) 'A single optical fiber fluorometric device for measurement of intracellular Ca<sup>2+</sup> concentration: Its application to hippocampal neurons in vitro and in vivo', *Neuroscience*, 50(3), pp. 619–625. doi: 10.1016/0306-4522(92)90451-7.
- Kurnikova, A. *et al.* (2017) 'Coordination of Orofacial Motor Actions into Exploratory Behavior by Rat', *Current Biology*, 27(5), pp. 688–696. doi: 10.1016/j.cub.2017.01.013.
- Kurnikova, A., Deschênes, M. and Kleinfeld, D. (2019) 'Functional brain stem circuits for control of nose motion', *Journal of Neurophysiology*, 121(1), pp. 205–217. doi: 10.1152/jn.00608.2018.
- Kuypers, H. G. J. M. and Brinkman, J. (1970) 'Precentral projections to different parts of the spinal intermediate zone in the rhesus monkey', *Brain Research*, 24(1), pp. 29–48. doi: 10.1016/0006-8993(70)90272-6.
- Kuypers HGJM (1981) 'Anatomy of the descending pathways', in *Handbook of physiology*. Vernon & Mountcastle, pp. 597–666.
- Lanciego, J. L. and Wouterlood, F. G. (2020) 'Neuroanatomical tract-tracing techniques that did go viral', *Brain Structure and Function*, 225(4), pp. 1193–1224. doi: 10.1007/s00429-020-02041-6.
- Lavail, J. H. and Lavail, M. M. (1972) 'Retrograde Axonal Transport in the Central Nervous System', *Science*, 176(4042), pp. 1416–1417. doi: 10.1126/science.176.4042.1416.
- Lawrence, D. G. and Kuypers, H. G. J. M. (1968a) 'THE FUNCTIONAL ORGANIZATION OF THE MOTOR SYSTEM IN THE MONKEYI. THE EFFECTS OF BILATERAL PYRAMIDAL LESIONS', *Brain*, 91(1), pp. 1–14. doi: 10.1093/brain/91.1.1.
- Lawrence, D. G. and Kuypers, H. G. J. M. (1968b) 'THE FUNCTIONAL ORGANIZATION OF THE MOTOR SYSTEM IN THE MONKEYII. THE EFFECTS OF LESIONS OF THE DESCENDING BRAIN-STEM PATHWAYS', *Brain*, 91(1), pp. 15–36. doi: 10.1093/brain/91.1.15.
- Lee, J., Wang, W. and Sabatini, B. L. (2020) 'Anatomically segregated basal ganglia pathways allow parallel behavioral modulation', *Nature Neuroscience*, pp. 1–11. doi: 10.1038/s41593-020-00712-5.
- Lemon, R. N. *et al.* (2004) 'Direct and indirect pathways for corticospinal control of upper limb motoneurons in the primate', in *Progress in Brain Research*. Elsevier (Brain Mechanisms for the Integration of Posture and Movement), pp. 263–279. doi: 10.1016/S0079-6123(03)43026-4.
- Lemon, R. N. (2008) 'Descending Pathways in Motor Control', *Annual Review of Neuroscience*, 31(1), pp. 195–218. doi: 10.1146/annurev.neuro.31.060407.125547.
- Lemon, R. N. *et al.* (2012) 'Lawrence and Kuypers (1968a, b) revisited: copies of the original filmed material from their classic papers in Brain', *Brain*, 135(7), pp. 2290–2295. doi: 10.1093/brain/aws037.
- Li, C. and Samulski, R. J. (2020) 'Engineering adeno-associated virus vectors for gene therapy', *Nature Reviews Genetics*, 21(4), pp. 255–272. doi: 10.1038/s41576-019-0205-4.

- Li, N. *et al.* (2015) 'A motor cortex circuit for motor planning and movement', *Nature*, 519(7541), pp. 51–56. doi: 10.1038/nature14178.
- Lim, L. *et al.* (2018) 'Development and Functional Diversification of Cortical Interneurons', *Neuron*, 100(2), pp. 294–313. doi: 10.1016/j.neuron.2018.10.009.
- Lin, J. Y. *et al.* (2009) 'Characterization of Engineered Channelrhodopsin Variants with Improved Properties and Kinetics', *Biophysical Journal*, 96(5), pp. 1803–1814. doi: 10.1016/j.bpj.2008.11.034.
- Lin, J. Y. *et al.* (2013) 'ReaChR: a red-shifted variant of channelrhodopsin enables deep transcranial optogenetic excitation', *Nature Neuroscience*, 16(10), pp. 1499–1508. doi: 10.1038/nn.3502.
- Litjens, G. *et al.* (2017) 'A survey on deep learning in medical image analysis', *Medical Image Analysis*, 42, pp. 60–88. doi: 10.1016/j.media.2017.07.005.
- M. W. Jann, Y. W. Lam, W. H. Chang (1994) 'Rapid formation of clozapine in guinea-pigs and man following clozapine-N-oxide administration', *Arch. Int. Pharmacodyn. Ther.*, 328, pp. 243–250.
- Magnus, C. J. *et al.* (2011) 'Chemical and Genetic Engineering of Selective Ion Channel–Ligand Interactions', *Science*, 333(6047), pp. 1292–1296. doi: 10.1126/science.1206606.
- Magnus, C. J. *et al.* (2019) 'Ultrapotent chemogenetics for research and potential clinical applications', *Science*, 364(6436). doi: 10.1126/science.aav5282.
- Mann, J. *et al.* (2008) 'Why Do Dolphins Carry Sponges?', *PLoS ONE*, 3(12). doi: 10.1371/journal.pone.0003868.
- Mathew Wilson, Bruce McNaughton, C. M. G., Pedro E. Maldonado (1995) 'Tetrodes markedly improve the reliability and yield of multiple single-unit isolation from multi-unit recordings in cat striate cortex', *Journal of Neuroscience Methods*, 63, pp. 43–54.
- Mathis, A. *et al.* (2018) 'DeepLabCut: markerless pose estimation of user-defined body parts with deep learning', *Nature Neuroscience*, 21(9), pp. 1281–1289. doi: 10.1038/s41593-018-0209-y.
- Matsuno-Yagi, A. and Mukohata, Y. (1977) 'Two possible roles of bacteriorhodopsin; a comparative study of strains of *Halobacterium halobium* differing in pigmentation', *Biochemical and Biophysical Research Communications*, 78(1), pp. 237–243. doi: 10.1016/0006-291X(77)91245-1.
- Matyas, F. *et al.* (2010) 'Motor Control by Sensory Cortex', *Science*, 330(6008), pp. 1240–1243. doi: 10.1126/science.1195797.
- McElvain, L. E. *et al.* (2018) 'Circuits in the Rodent Brainstem that Control Whisking in Concert with Other Orofacial Motor Actions', *Neuroscience*, 368, pp. 152–170. doi: 10.1016/j.neuroscience.2017.08.034.
- McNaughton, B. L., O'Keefe, J. and Barnes, C. A. (1983) 'The stereotrode: A new technique for simultaneous isolation of several single units in the central nervous system from multiple unit records', *Journal of Neuroscience Methods*, 8(4), pp. 391–397. doi: 10.1016/0165-0270(83)90097-3.

McNeillage, P.F (1990) 'In Vision and Action: The Control of Grasping', in *Grasping in modern primates: the evolutionary context*. Goodale, M.A., ed, pp. 1–13.

Mercer Lindsay, N. *et al.* (2019) 'Orofacial Movements Involve Parallel Corticobulbar Projections from Motor Cortex to Trigeminal Premotor Nuclei', *Neuron*, 104(4), pp. 765–780.e3. doi: 10.1016/j.neuron.2019.08.032.

Mesulam M-M (1982) *Tracing neural connections with horseradish peroxidase*. (Handbook series: methods in the neurosciences). Available at: [https://scholar.google.com/scholar\\_lookup?title=Tracing%20neural%20connections%20with%20horseradish%20peroxidase.%20Handbook%20series%3A%20methods%20in%20the%20neurosciences&publication\\_year=1982&author=Mesulam%2CM-M](https://scholar.google.com/scholar_lookup?title=Tracing%20neural%20connections%20with%20horseradish%20peroxidase.%20Handbook%20series%3A%20methods%20in%20the%20neurosciences&publication_year=1982&author=Mesulam%2CM-M) (Accessed: 22 September 2020).

Miri, A. *et al.* (2017) 'Behaviorally Selective Engagement of Short-Latency Effector Pathways by Motor Cortex', *Neuron*, 95(3), pp. 683–696.e11. doi: 10.1016/j.neuron.2017.06.042.

Moore, J. D. *et al.* (2013) 'Hierarchy of orofacial rhythms revealed through whisking and breathing', *Nature*, 497(7448), pp. 205–210. doi: 10.1038/nature12076.

Moore, J. D., Kleinfeld, D. and Wang, F. (2014) 'How the brainstem controls orofacial behaviors comprised of rhythmic actions', *Trends in Neurosciences*, 37(7), pp. 370–380. doi: 10.1016/j.tins.2014.05.001.

Morris, R. *et al.* (2011) 'Impaired Arpeggio Movement in Skilled Reaching by Rubrospinal Tract Lesions in the Rat: A Behavioral/Anatomical Fractionation', *Journal of Neurotrauma*, 28(12), pp. 2439–2451. doi: 10.1089/neu.2010.1708.

Mosberger, A. C. *et al.* (2017) 'Axotomized Corticospinal Neurons Increase Supra-Lesional Innervation and Remain Crucial for Skilled Reaching after Bilateral Pyramidotomy', *Cerebral Cortex*, p. cercor;bhw405v1. doi: 10.1093/cercor/bhw405.

Murlidharan, G., Samulski, R. J. and Asokan, A. (2014) 'Biology of adeno-associated viral vectors in the central nervous system', *Frontiers in Molecular Neuroscience*, 7. doi: 10.3389/fnmol.2014.00076.

Muybridge, E. (1887) *Animal Locomotion: An Electro-photographic Investigation of Consecutive Phases of Animal Movements*. Univ. of Pennsylvania, Philadelphia.

Nagano, A. and Aoyama, K. (2017) 'Tool-use by rats (*Rattus norvegicus*): tool-choice based on tool features', *Animal Cognition*, 20(2), pp. 199–213. doi: 10.1007/s10071-016-1039-5.

Nagel, G. (2002) 'Channelrhodopsin-1: A Light-Gated Proton Channel in Green Algae', *Science*, 296(5577), pp. 2395–2398. doi: 10.1126/science.1072068.

Nagel, G. *et al.* (2003) 'Channelrhodopsin-2, a directly light-gated cation-selective membrane channel', *Proceedings of the National Academy of Sciences of the United States of America*, 100(24), pp. 13940–13945. doi: 10.1073/pnas.1936192100.

Naghizadeh, M., Mohajerani, M. H. and Whishaw, I. Q. (2020) 'Mouse Arm and hand movements in grooming are reaching movements: Evolution of reaching, handedness, and the thumbnail', *Behavioural Brain Research*, 393, p. 112732. doi: 10.1016/j.bbr.2020.112732.

- Nakai, J., Ohkura, M. and Imoto, K. (2001) 'A high signal-to-noise Ca<sup>2+</sup> probe composed of a single green fluorescent protein', *Nature Biotechnology*, 19(2), pp. 137–141. doi: 10.1038/84397.
- Nakamura, T. *et al.* (2016) 'A Markerless 3D Computerized Motion Capture System Incorporating a Skeleton Model for Monkeys', *PLOS ONE*, 11(11), p. e0166154. doi: 10.1371/journal.pone.0166154.
- Nakamura, Y. and Katakura, N. (1995) 'Generation of masticatory rhythm in the brainstem', *Neuroscience Research*, 23(1), pp. 1–19. doi: 10.1016/0168-0102(95)90003-9.
- Nassi, J. J. *et al.* (2015) 'Neuroanatomy goes viral!', *Frontiers in Neuroanatomy*, 9. doi: 10.3389/fnana.2015.00080.
- Nath, T. *et al.* (2019) 'Using DeepLabCut for 3D markerless pose estimation across species and behaviors', *Nature Protocols*, 14(7), pp. 2152–2176. doi: 10.1038/s41596-019-0176-0.
- Nauta, W. J. H. and Gyax, P. A. (1951) 'Silver impregnation of degenerating axon terminals in the central nervous system: (1) Technic. (2) Chemical notes', *Stain Technology*, 26(1), pp. 5–11. doi: 10.3109/10520295109113170.
- Nishida, T. and Hiraiwa, M. (1982) 'Natural history of a tool-using behavior by wild chimpanzees in feeding upon wood-boring ants', *Journal of Human Evolution*, 11(1), pp. 73–99. doi: 10.1016/S0047-2484(82)80033-X.
- de Noordhout, A. M. *et al.* (1999) 'Corticomotoneuronal synaptic connections in normal man', *Brain*, 122(7), pp. 1327–1340. doi: 10.1093/brain/122.7.1327.
- Norlin, P. *et al.* (2002) 'A 32-site neural recording probe fabricated by DRIE of SOI substrates', *Journal of Micromechanics and Microengineering*, 12(4), pp. 414–419. doi: 10.1088/0960-1317/12/4/312.
- Northcutt, R. G. (2002) 'Understanding Vertebrate Brain Evolution', *Integrative and Comparative Biology*, 42(4), pp. 743–756. doi: 10.1093/icb/42.4.743.
- O'Connor, D. H. *et al.* (2010) 'Neural Activity in Barrel Cortex Underlying Vibrissa-Based Object Localization in Mice', *Neuron*, 67(6), pp. 1048–1061. doi: 10.1016/j.neuron.2010.08.026.
- Oesterhelt, D. and Stoeckenius, W. (1971) 'Rhodopsin-like Protein from the Purple Membrane of Halobacterium halobium', *Nature New Biology*, 233(39), pp. 149–152. doi: 10.1038/newbio233149a0.
- O'Keefe, J. and Recce, M. L. (1993) 'Phase relationship between hippocampal place units and the EEG theta rhythm', *Hippocampus*, 3(3), pp. 317–330. doi: 10.1002/hipo.450030307.
- Orlovsky G.N., Deliagina T.G. and Grillner S. (1999) *Neuronal control of locomotion: from mollusc to man*. Oxford: Oxford University Press.
- Palmer, E. and Ashby, P. (1992) 'Corticospinal projections to upper limb motoneurons in humans.', *The Journal of Physiology*, 448(1), pp. 397–412. doi: 10.1113/jphysiol.1992.sp019048.

- Parker, J. G. *et al.* (2018) 'Diametric neural ensemble dynamics in parkinsonian and dyskinetic states', *Nature*, 557(7704), pp. 177–182. doi: 10.1038/s41586-018-0090-6.
- Peters, A. J., Liu, H. and Komiyama, T. (2017) 'Learning in the Rodent Motor Cortex', *Annual Review of Neuroscience*, 40(1), pp. 77–97. doi: 10.1146/annurev-neuro-072116-031407.
- Petersen, C. C. H. (2019) 'Sensorimotor processing in the rodent barrel cortex', *Nature Reviews Neuroscience*, 20(9), pp. 533–546. doi: 10.1038/s41583-019-0200-y.
- Pivetta, C. *et al.* (2014) 'Motor-Circuit Communication Matrix from Spinal Cord to Brainstem Neurons Revealed by Developmental Origin', *Cell*, 156(3), pp. 537–548. doi: 10.1016/j.cell.2013.12.014.
- Raper, J. *et al.* (2017) 'Metabolism and Distribution of Clozapine-N-oxide: Implications for Nonhuman Primate Chemogenetics', *ACS Chemical Neuroscience*, 8(7), pp. 1570–1576. doi: 10.1021/acscchemneuro.7b00079.
- Redfern, C. H. *et al.* (1999) 'Conditional expression and signaling of a specifically designed G<sub>i</sub>-coupled receptor in transgenic mice', *Nature Biotechnology*, 17(2), pp. 165–169. doi: 10.1038/6165.
- Roh, J., Cheung, V. C. K. and Bizzi, E. (2011) 'Modules in the brain stem and spinal cord underlying motor behaviors', *Journal of Neurophysiology*, 106(3), pp. 1363–1378. doi: 10.1152/jn.00842.2010.
- Roseberry, T. K. *et al.* (2016) 'Cell-Type-Specific Control of Brainstem Locomotor Circuits by Basal Ganglia', *Cell*, 164(3), pp. 526–537. doi: 10.1016/j.cell.2015.12.037.
- Ross, G. and Sinnamon, H. (1984) 'Forelimb and hindlimb stepping by the anesthetized rat elicited by electrical stimulation of the pons and medulla☆', *Physiology & Behavior*, 33(2), pp. 201–208. doi: 10.1016/0031-9384(84)90100-8.
- Roth, B. L. (2016) 'DREADDs for Neuroscientists', *Neuron*, 89(4), pp. 683–694. doi: 10.1016/j.neuron.2016.01.040.
- Ruder, L. and Arber, S. (2019) 'Brainstem Circuits Controlling Action Diversification', *Annual Review of Neuroscience*, 42(1), pp. 485–504. doi: 10.1146/annurev-neuro-070918-050201.
- Sacrey, L.-A. R., Alaverdashvili, M. and Whishaw, I. Q. (2009) 'Similar hand shaping in reaching-for-food (skilled reaching) in rats and humans provides evidence of homology in release, collection, and manipulation movements', *Behavioural Brain Research*, 204(1), pp. 153–161. doi: 10.1016/j.bbr.2009.05.035.
- Saito, Y. *et al.* (2003) 'Activity of neurons in ventrolateral respiratory groups during swallowing in decerebrate rats', *Brain and Development*, 25(5), pp. 338–345. doi: 10.1016/S0387-7604(03)00008-1.
- van Schaik, C. P., Fox, E. A. and Sitompul, A. F. (1996) 'Manufacture and use of tools in wild Sumatran orangutans', *Naturwissenschaften*, 83(4), pp. 186–188. doi: 10.1007/BF01143062.
- Schepens, B. and Drew, T. (2004) 'Independent and Convergent Signals From the Pontomedullary Reticular Formation Contribute to the Control of Posture and Movement

- During Reaching in the Cat', *Journal of Neurophysiology*, 92(4), pp. 2217–2238. doi: 10.1152/jn.01189.2003.
- Schepens, B. and Drew, T. (2006) 'Descending Signals From the Pontomedullary Reticular Formation Are Bilateral, Asymmetric, and Gated During Reaching Movements in the Cat', *Journal of Neurophysiology*, 96(5), pp. 2229–2252. doi: 10.1152/jn.00342.2006.
- Schepens, B., Stapley, P. and Drew, T. (2008) 'Neurons in the Pontomedullary Reticular Formation Signal Posture and Movement Both as an Integrated Behavior and Independently', *Journal of Neurophysiology*, 100(4), pp. 2235–2253. doi: 10.1152/jn.01381.2007.
- Schmued, L. C. and Fallon, J. H. (1986) 'Fluoro-gold: a new fluorescent retrograde axonal tracer with numerous unique properties', *Brain Research*, 377(1), pp. 147–154. doi: 10.1016/0006-8993(86)91199-6.
- Semba, K. and Komisaruk, B. R. (1984) 'Neural substrates of two different rhythmical vibrissal movements in the rat', *Neuroscience*, 12(3), pp. 761–774. doi: 10.1016/0306-4522(84)90168-4.
- Serre, T. (2019) 'Deep Learning: The Good, the Bad, and the Ugly', *Annual Review of Vision Science*, 5(1), pp. 399–426. doi: 10.1146/annurev-vision-091718-014951.
- Shammah-Lagnado, S. J., Costa, M. S. M. O. and Ricardo-Ribeiro, J. A. (1992) 'Afferent connections of the parvocellular reticular formation: A horseradish peroxidase study in the rat', *Neuroscience*, 50(2), pp. 403–425. doi: 10.1016/0306-4522(92)90433-3.
- Shefchyk, S. J., Jell, R. M. and Jordan, L. M. (1984) 'Reversible cooling of the brainstem reveals areas required for mesencephalic locomotor region evoked treadmill locomotion', *Experimental Brain Research*, 56(2), pp. 257–262. doi: 10.1007/BF00236281.
- Shik, M. L. and Orlovsky, G. N. (1976) 'Neurophysiology of locomotor automatism', 56, p. 37.
- Shuster, G. and Sherman, P. W. (1998) 'Tool use by naked mole-rats', *Animal Cognition*, 1(1), pp. 71–74. doi: 10.1007/s100710050009.
- Smith, J. C. *et al.* (1991) 'Pre-Botzinger complex: a brainstem region that may generate respiratory rhythm in mammals', *Science*, 254(5032), pp. 726–729. doi: 10.1126/science.1683005.
- Soteropoulos, D. S., Williams, E. R. and Baker, S. N. (2012) 'Cells in the monkey pontomedullary reticular formation modulate their activity with slow finger movements', *The Journal of Physiology*, 590(16), pp. 4011–4027. doi: 10.1113/jphysiol.2011.225169.
- Stachniak, T. J., Ghosh, A. and Sternson, S. M. (2014) 'Chemogenetic Synaptic Silencing of Neural Circuits Localizes a Hypothalamus→Midbrain Pathway for Feeding Behavior', *Neuron*, 82(4), pp. 797–808. doi: 10.1016/j.neuron.2014.04.008.
- Stevenson, I. H. and Kording, K. P. (2011) 'How advances in neural recording affect data analysis', *Nature Neuroscience*, 14(2), pp. 139–142. doi: 10.1038/nn.2731.
- Strader, C. D. *et al.* (1991) 'Allele-specific activation of genetically engineered receptors.', *Journal of Biological Chemistry*, 266(1), pp. 5–8.

- Sun, S. and Schaffer, D. V. (2018) 'Engineered viral vectors for functional interrogation, deconvolution, and manipulation of neural circuits', *Current Opinion in Neurobiology*, 50, pp. 163–170. doi: 10.1016/j.conb.2017.12.011.
- Sustaita, D. *et al.* (2013) 'Getting a grip on tetrapod grasping: form, function, and evolution', *Biological Reviews*, 88(2), pp. 380–405. doi: 10.1111/brv.12010.
- Svoboda, K. and Li, N. (2018) 'Neural mechanisms of movement planning: motor cortex and beyond', *Current Opinion in Neurobiology*, 49, pp. 33–41. doi: 10.1016/j.conb.2017.10.023.
- Sych, Y. *et al.* (2019) 'High-density multi-fiber photometry for studying large-scale brain circuit dynamics', *Nature Methods*, 16(6), pp. 553–560. doi: 10.1038/s41592-019-0400-4.
- Takakusaki, K. *et al.* (2016) 'Brainstem control of locomotion and muscle tone with special reference to the role of the mesopontine tegmentum and medullary reticulospinal systems', *Journal of Neural Transmission*, 123(7), pp. 695–729. doi: 10.1007/s00702-015-1475-4.
- Takeoka, A. *et al.* (2014) 'Muscle Spindle Feedback Directs Locomotor Recovery and Circuit Reorganization after Spinal Cord Injury', *Cell*, 159(7), pp. 1626–1639. doi: 10.1016/j.cell.2014.11.019.
- Tallini, Y. N. *et al.* (2006) 'Imaging cellular signals in the heart in vivo: Cardiac expression of the high-signal Ca<sup>2+</sup> indicator GCaMP2', *Proceedings of the National Academy of Sciences*, 103(12), pp. 4753–4758. doi: 10.1073/pnas.0509378103.
- Tan, W. *et al.* (2008) 'Silencing preBötzing Complex somatostatin-expressing neurons induces persistent apnea in awake rat', *Nature Neuroscience*, 11(5), pp. 538–540. doi: 10.1038/nn.2104.
- Tecuapetla, F. *et al.* (2016) 'Complementary Contributions of Striatal Projection Pathways to Action Initiation and Execution', *Cell*, 166(3), pp. 703–715. doi: 10.1016/j.cell.2016.06.032.
- Tennant, K. A. *et al.* (2010) 'The Vermicelli and Capellini Handling Tests: Simple quantitative measures of dexterous forepaw function in rats and mice', *JoVE (Journal of Visualized Experiments)*, (41), p. e2076. doi: 10.3791/2076.
- Tervo, D. G. R. *et al.* (2016) 'A Designer AAV Variant Permits Efficient Retrograde Access to Projection Neurons', *Neuron*, 92(2), pp. 372–382. doi: 10.1016/j.neuron.2016.09.021.
- Tian, L. *et al.* (2009) 'Imaging neural activity in worms, flies and mice with improved GCaMP calcium indicators', *Nature Methods*, 6(12), pp. 875–881. doi: 10.1038/nmeth.1398.
- Tovote, P. *et al.* (2016) 'Midbrain circuits for defensive behaviour', *Nature*, 534(7606), pp. 206–212. doi: 10.1038/nature17996.
- Travers, J. B., Dinardo, L. A. and Karimnamazi, H. (1997) 'Motor and Premotor Mechanisms of Licking', *Neuroscience & Biobehavioral Reviews*, 21(5), pp. 631–647. doi: 10.1016/S0149-7634(96)00045-0.

- Travers, J., DiNardo, L. and Karimnamazi, H. (2000) 'Medullary reticular formation activity during ingestion and rejection in the awake rat', *Experimental Brain Research*, 130(1), pp. 78–92. doi: 10.1007/s002219900223.
- Ugolini, G. (1995) 'Specificity of rabies virus as a transneuronal tracer of motor networks: Transfer from hypoglossal motoneurons to connected second-order and higher order central nervous system cell groups', *Journal of Comparative Neurology*, 356(3), pp. 457–480. doi: 10.1002/cne.903560312.
- Ugolini, G., Kuypers, H. and Strick, P. (1989) 'Transneuronal transfer of herpes virus from peripheral nerves to cortex and brainstem', *Science*, 243(4887), pp. 89–91. doi: 10.1126/science.2536188.
- Vetere, G. *et al.* (2019) 'Memory formation in the absence of experience', *Nature Neuroscience*, 22(6), pp. 933–940. doi: 10.1038/s41593-019-0389-0.
- Vong, L. *et al.* (2011) 'Leptin Action on GABAergic Neurons Prevents Obesity and Reduces Inhibitory Tone to POMC Neurons', *Neuron*, 71(1), pp. 142–154. doi: 10.1016/j.neuron.2011.05.028.
- Wang, X. *et al.* (2017) 'Deconstruction of Corticospinal Circuits for Goal-Directed Motor Skills', *Cell*, 171(2), pp. 440–455.e14. doi: 10.1016/j.cell.2017.08.014.
- Weber, F. and Dan, Y. (2016) 'Circuit-based interrogation of sleep control', *Nature*, 538(7623), pp. 51–59. doi: 10.1038/nature19773.
- Wenthur, C. J. and Lindsley, C. W. (2013) 'Classics in Chemical Neuroscience: Clozapine', *ACS Chemical Neuroscience*, 4(7), pp. 1018–1025. doi: 10.1021/cn400121z.
- Whishaw, I. Q. *et al.* (2017) 'The syntactic organization of pasta-eating and the structure of reach movements in the head-fixed mouse', *Scientific Reports*, 7(1), p. 10987. doi: 10.1038/s41598-017-10796-y.
- Whishaw, I. Q., Gorny, B. and Sarna, J. (1998) 'Paw and limb use in skilled and spontaneous reaching after pyramidal tract, red nucleus and combined lesions in the rat: behavioral and anatomical dissociations', *Behavioural Brain Research*, 93(1–2), pp. 167–183. doi: 10.1016/S0166-4328(97)00152-6.
- Whishaw, I. Q. and Pellis, S. M. (1990) 'The structure of skilled forelimb reaching in the rat: A proximally driven movement with a single distal rotatory component', *Behavioural Brain Research*, 41(1), pp. 49–59. doi: 10.1016/0166-4328(90)90053-H.
- Wickersham, Ian R. *et al.* (2007) 'Monosynaptic Restriction of Transsynaptic Tracing from Single, Genetically Targeted Neurons', *Neuron*, 53(5), pp. 639–647. doi: 10.1016/j.neuron.2007.01.033.
- Wickersham, Ian R *et al.* (2007) 'Retrograde neuronal tracing with a deletion-mutant rabies virus', *Nature Methods*, 4(1), pp. 47–49. doi: 10.1038/nmeth999.
- Wilson, M. A. and McNaughton, B. L. (1993) 'Dynamics of the hippocampal ensemble code for space', *Science*, 261(5124), pp. 1055–1058. doi: 10.1126/science.8351520.
- Wu, Z., Asokan, A. and Samulski, R. J. (2006) 'Adeno-associated Virus Serotypes: Vector Toolkit for Human Gene Therapy', *Molecular Therapy*, 14(3), pp. 316–327. doi: 10.1016/j.yymthe.2006.05.009.

Xu, T. *et al.* (2009) 'Rapid formation and selective stabilization of synapses for enduring motor memories', *Nature*, 462(7275), pp. 915–919. doi: 10.1038/nature08389.

Yakovenko, S., Krouchev, N. and Drew, T. (2011) 'Sequential Activation of Motor Cortical Neurons Contributes to Intralimb Coordination During Reaching in the Cat by Modulating Muscle Synergies', *Journal of Neurophysiology*, 105(1), pp. 388–409. doi: 10.1152/jn.00469.2010.

Yasuda, R. *et al.* (2004) 'Imaging Calcium Concentration Dynamics in Small Neuronal Compartments', *Science's STKE*, 2004(219), pp. pl5–pl5. doi: 10.1126/stke.2192004pl5.

Zhang, F. *et al.* (2007) 'Multimodal fast optical interrogation of neural circuitry', *Nature*, 446(7136), pp. 633–639. doi: 10.1038/nature05744.

Zhang, Z. *et al.* (2018) 'Closed-loop all-optical interrogation of neural circuits in vivo', *Nature Methods*, 15(12), pp. 1037–1040. doi: 10.1038/s41592-018-0183-z.

# Riccardo Schina

**Date and place of birth:** 30.03.1990, Torino, Italy

**Address:** Amerbachstrasse 22, 4057, Basel

**E-mail:** [riccardo.schina@unibas.ch](mailto:riccardo.schina@unibas.ch)

**Phone:** +41/767372304

---

## Education

- 2015-2020 (expected) PhD Neurobiology, University of Basel
- 2013-2015 MSc Molecular Biotechnology, University of Torino
- 2009-2012 BSc Biotechnology, University of Torino

## Research

- 2015-2020 PhD research aimed at identifying and characterizing brainstem nuclei and neuronal subpopulations essential for skilled forelimb movements (Supervisor Prof. Silvia Arber, University of Basel)
- 2014 MSc research project on the broad physiological effects of the lack of MeCP2 from cortical circuits (Supervisor Prof. Lucas Pozzo-Miller, University of Alabama at Birmingham)
- 2013-2015 MSc research project on the effect of MeCP2 loss on the anatomy and physiology of inhibitory neurons in the somatosensory cortex (Supervisor Prof Maurizio Giustetto, University of Torino)
- 2011-2012 BSc research project on the role of sensory cortices in memory formation (Supervisor Prof. Benedetto Sacchetti, University of Torino)

## Publications

- A functional map for diverse forelimb actions within brainstem circuitry, 2020  
*(accepted)*
- Loss of Mecp2 Causes Atypical Synaptic and Molecular Plasticity of Parvalbumin-Expressing Interneurons Reflecting Rett Syndrome-Like Sensorimotor Defects, *eNeuro*, 2018

## Honors & Awards

- 2015: **Fellowship for Excellence** awarded from the Werner-Siemens foundation for three consecutive years